1. Referee comments

1.1. Thomas Prisner

This manuscript tries to tackle experimentally the question how the pump efficiency of broadband microwave pulses influences the quality of DEER data. Broadband mw pulses become available for pulsed EPR experiments by fast arbitrary waveform generators recently, allowing to adopt broadband excitation pulses known since a long time in the field of NMR for EPR experiments. For DEER experiments it has been shown that broadband pulses achieve larger modulation depth of the dipolar coupled bi-radical sample. On the other hand the larger pump efficiency also leads to a stronger de-cay arising from intermolecular interactions to the other spin labeled molecules in the sample. In this manuscript the interplay of modulation depth and decay arising from a series of broadband pulses (sech/tanh, WURST, linear chirp with rectangular amplitude shape) have been compared to excitation by rectangular or Gaussian monochromatic pulses. The experimental work performed at a commercial Q-band spectrometer is of good quality and compares the effect of different pump pulses with respect to a MNR(modulation to noise ratio) merit function. This function is defined as the ratio of the modulation depth to the over the time trace averaged noise level. The later part of this function depends on the length of the observer time window, because the noise which is constant per time in the original time trace, increases by the division procedure usually used to remove the intermolecular part. This problem has already been discussed in a recent paper by Fábregas et al., where other procedures to obtain distance distributions from the original data were proposed. Nevertheless, because these other simulations methods are not standard so far, the approach discussed here to optimize the experimental time traces is important and worthwhile to be published after several issues are addressed. 1) For me it is not perfectly clear if the merit function defined here (MNR) is really the most important point. Usually the distance information is encoded in the first part of the time trace and the longer times are only necessary to fit well the intermolecular background function – a necessary procedure to obtain reliable distance information. The question is how large the increasing noise at the end of the time trace is important for this purpose. This point should be discussed and clarified.2) The manuscript talks about the intermolecular background function but for the larger spin concentration, where most of the experiments are performed and most of the conclusions are taken from, the original time traces including this background function are not shown! This has to be included! It is not enough to show the background density k as in Figure S11. 3) In Figure S10 an unexpected large suppression of the echo intensity by longer broadband pump pulses is shown. This is totally unexpected for the given bandwidth of these pulses and contrary to own experiences, where longer pulses show better frequency shapes! If the pulses are generated by the Bruker soft-ware some care has to be taken to use the right amplitude setting, especially when the frequency runs over the carrier frequency (from minus offsets to plus offsets). The pulse profiles shown in Figure S7 are probably only calculated pulses and not really measured ones? Experimentally recording them including the resonator profile (which also seems somewhat suspicious to me) might give some hints on what is going on here! This issue is rather important for the conclusions drawn here from the shaped pulses! 4) The concentration dependence of the behavior is only discussed in a rather trivial and non-quantitative manner, despite the fact that it showed to be the major parameter influencing the improvement by the broadband pulses (comparison Figure6 and 7). That lower concentrations of spins are advantageous, especially for larger distances or broader distance distributions is well known in the community. Because broadband pulses might be especially interesting for these kind of systems, this should be discussed more quantitatively! The discussion in the SI including Figure S13 and the text after it is only very qualitative and rather trivial. 5) Minor point: In the supporting information equation (2) is wrong. After that there is a spelling error (ration).

1.2 Referee 2

This work investigates in detail the dependence of DEER signal-to-noise ratio on many experimental parameters (pulse shapes, pulse lengths, pump-observer separation, concentration, truncation).This work does not introduce any new method. Hyperbolic-secant pump pulses and Gaussian observer pulses are already commonly used in 4-pulse DEER, and many of the optimizations and explorations presented are routinely done by spectroscopists. Although not innovative for this reason, this manuscript demonstrates explicitly that it can be beneficial to spend time to optimize experimental parameters carefully. Novices to the field will find this manuscript particularly instructing as a tutorial. I recommend publication in Magnetic

Resonance, after the comments below are ad-dressed.[1] In section 3.3 (background decay), examine in detail how the type of shaped pulse affects the MNR if the recently published superior background correction method (kernel inclusion) is used. It is crucial to include this in this work.[2] Discuss in more detail whether and how the findings in this work are applicable to other samples (different distance distributions, different concentrations) and spectrometers (different resonator profiles, different Tx fidelity). From the current manuscript, itis unclear whether the findings are generalizable. This is important, since it appears to be the purpose of the manuscript to make some general statements about experimental settings in DEER.[3] - Eq.(3): Specify that the time axis is defined such that t=0 at the center of the pulse.- Eq.(11): (k*|t|)^(d/3) instead of k*t^(d/3) - Eq.(12): A factor of 2 might be missing. -8.13: "i.e. a chirp pulse" - 12.18: Here, it is not clear how the numbers for the minimum detectable distance limit are obtained. - Kupce needs a grave accent on the c. Bohlen needs an umlaut on the o. - SI Eq.(2): t_truncation instead of tau_2

2. Response to Referee comments

2.1 Response to Thomas Prisner

Dear Thomas,

Thank you very much for your effort reading our manuscript so carefully and for your valuable advices. We strongly believe that the suggested changes and additions improved the manuscript a lot. Please find below a point-by-point reply to all your recommendations (in blue).

1) For me it is not perfectly clear if the merit function defined here (MNR) is really the most important point. Usually the distance information is en-coded in the first part of the time trace and the longer times are only necessary to fit well the intermolecular background function – a necessary procedure to obtain reliable distance information. The question is how large the increasing noise at the end of the time trace is important for this purpose. This point should be discussed and clarified.

We have added an additional chapter in the SI where we discuss the MNR as a function of merit and up to which point of the DEER trace it has to been taken into account.

S2 The MNR as the function of merit

Here, we want to discuss whether the MNR is a suitable function of merit for the determination of distance distributions and up to which time point in the DEER trace, the MNR needs to be evaluated to serve this purpose. Therefore, we performed simulations with a model distance distribution p_0 that is based on the narrow distance distribution of the model system used in this study. We approximated the experimentally obtained distance distribution with a Gaussian with a mean at 5.08 nm and a standard deviation of 0.08 nm. We varied the background density in ten steps from k = 0.01 1/µs to k = 0.3 1/µs in combination with a low, medium and high noise level (noise σ_0 = 0.02, 0.05 and 0.1) that was added to the DEER trace. The background dimension was set to d = 3 and a modulation depth of 0.5 was used. The DEER traces were simulated in the time domain up to 8 µs. For each parameter set we generated ten different traces. To compare the background correction by division (Jeschke et al., 2006) with the kernel inclusion approach as described in (Fábregas Ibáñez and Jeschke, 2020) we analysed all simulated DEER traces with both methods. We did not fit the background but used the true background function. The regularisation parameter was chosen according to the generalised cross-validation method. The quality of the resulting distance distributions p was estimated by the Euclidian distance D from the true distance p_0:

$$D(p, p_0) = \|p - p_0\|_2 \quad (1)$$

The MNR of the form factor F was calculated as described in the main text up to a limit of 7 µs according to equation (13) of the main text.

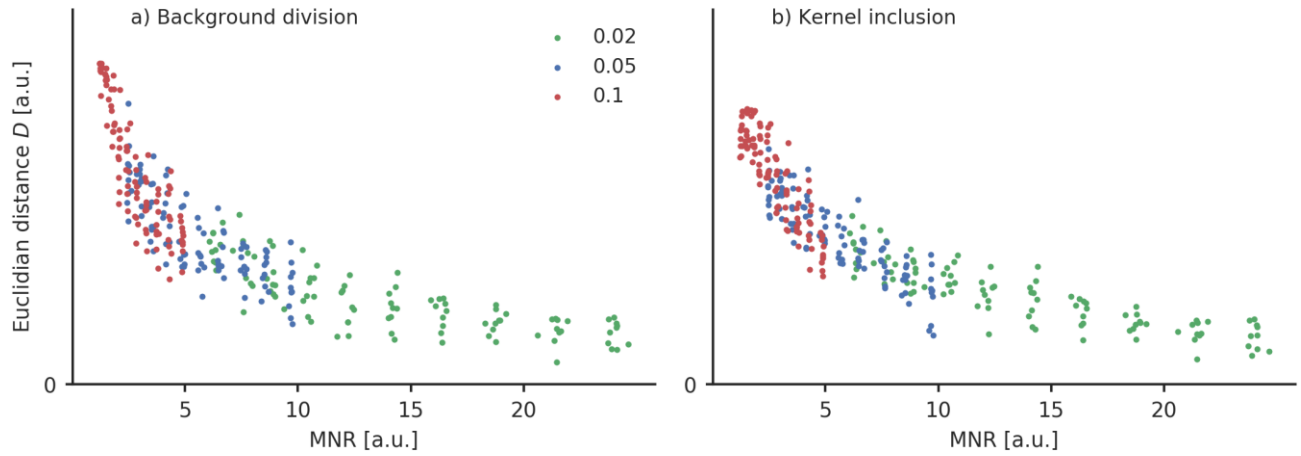

Figure S2: The Euclidian distance D of the real and calculated distance distribution as defined in equation (1) is plotted as a function of the MNR. Each dot represents a simulated DEER trace with either low (σ_0 = 0.02, green), medium (σ_0 = 0.05, blue) and high (σ_0 = 0.1, red) noise. The background correction was performed by (a) dividing the DEER trace by the background and (b) including the background in the kernel.

In Fig. S2, the quality of the determined distance distribution was plotted as a function of the determined MNR for both a background correction by division (Fig. S2a) and a kernel inclusion approach (Fig. S2b). For each noise level the MNR only depends on the density of the background as all other parameters are kept constant and only the background density is varied. So a lower MNR corresponds to a higher background density rate and vice versa. For the low noise level (σ_0 = 0.02), the quality of the determined distance distributions only varies a little for different background density rates. For medium (σ_0 = 0.05) and high (σ_0 = 0.1) noise levels, however, the dependency of the quality of the determined distance distribution decreases significantly with a decreasing MNR. If the MNR is only evaluated up to an early point of the form factor, the information of the background decay rate is lost in this case and is not properly included in the MNR as the MNR would then depend nearly exclusively on the given noise level.

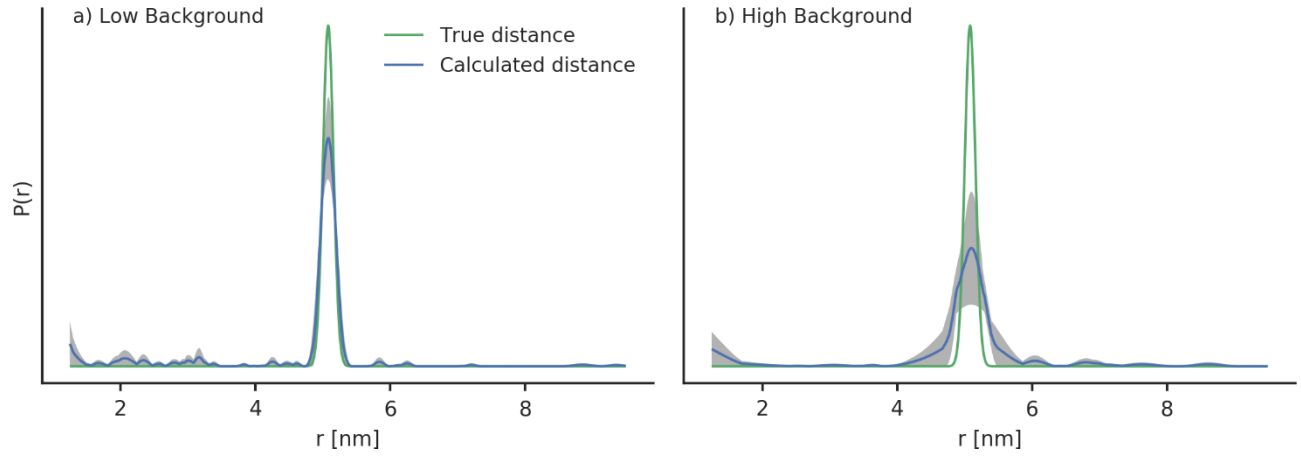

Figure S3: An exemplary distance distribution obtained for a medium noise level (σ_0 = 0.02) with (a) a low background density (k = 0.01 MHz) and (b) a high background density (k = 0.3 MHz). The grey area shows the area that is covered by the calculated distance distribution for ten exemplary DEER traces. The mean of the shaded area is drawn in blue and the true distance is drawn in green.

A closer inspection reveals that whereas the obtained distance distributions for high background densities reproduce the mean of the distance distribution correctly, they overestimate the width of the distribution and the distance appears to be broader as it is (see Fig. S3 for an exemplary data set). Depending on the information that shall be obtained by the DEER measurements, the mean of the distance distribution might suffice. However, if high resolution distance distributions shall be obtained, it seems to be important to optimise the MNR up to the limit which is given by equation (13) of the main text. The comparison of both background correction methods shows that the kernel inclusion gives better results particularly for a high noise and a high background decay. It should therefore be considered as the superior method. However, the correlation between the quality of the determined distance distribution and the MNR is still valid. This is why, we consider the MNR as a proper function of merit, even if the kernel inclusion approach is used.

For a more comprehensive study, the effect of the MNR on the quality of the obtained distance distribution could also be tested for distance distributions with different distance ranges and widths. Such a detailed study was, however, beyond the scope of the this manuscript.

2) The manuscript talks about the intermolecular background function but for the larger spin concentration, where most of the experiments are performed and most of the conclusions are taken from, the original time traces including this background function are not shown! This has to be included! It is not enough to show the background density k as in Figure S11.

We have added a new figure S17 with full DEER traces and background functions of both samples for rectangular and Gaussian pulses.

S20 Background decay of the DEER traces

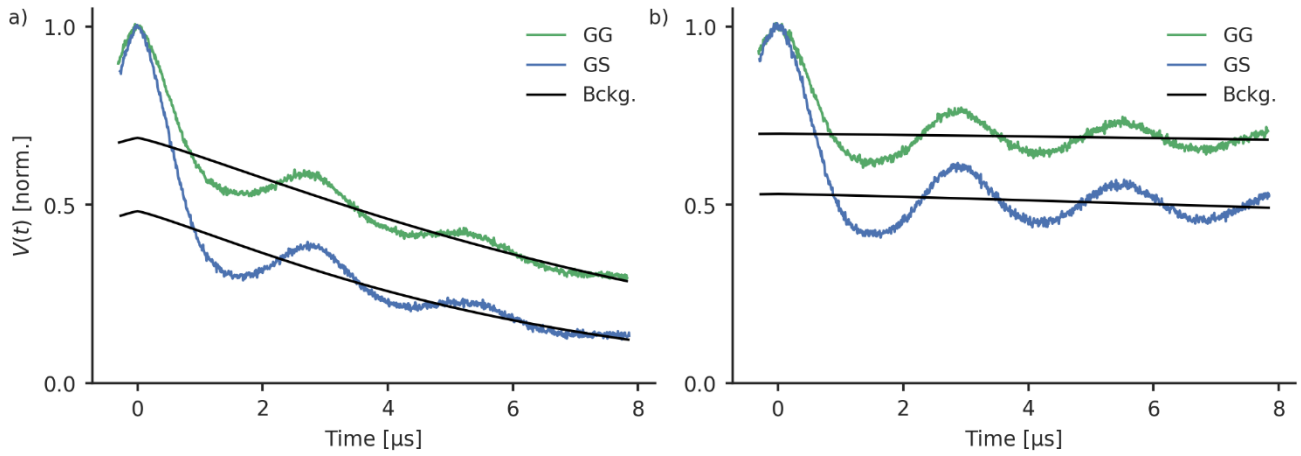

Figure S17: The (normalised) experimental raw data of the sample with a 80 µM (a) and 30 µM (b) ligand concentration. The settings for GG (green) were performed with a 100 %pulse amplitude and a 70 MHz offset. For GS (blue), the observer pulses were at a frequency of 70 MHz offset from the centre of the resonator. The pump pulses were HS{1,1} pulses, with the parameters $\beta = 8/t_p$, $t_p = 100$ ns, $\Delta f = 110$ MHz and an offset from the observer pulse of 90 MHz. Note that the acquisition time for the sample with lower concentration was longer in order to reach a similar noise level for both cases. The corresponding form factors are depicted in Fig. S11.

3) In Figure S10 an unexpected large suppression of the echo intensity by longer broadband pump pulses is shown. This is totally unexpected for the given bandwidth of these pulses and contrary to own experiences, where longer pulses show better frequency shapes! If the pulses are generated by the Bruker soft-ware some care has to be taken to use the right amplitude setting, especially the frequency runs over the carrier frequency (from minus offsets to plus offsets). The pulse profiles shown in Figure S7 are probably only calculated pulses and not really measured ones? Experimentally recording them including the resonator profile (which also seems somewhat suspicious to me) might give some hints on what is going on here! This issue is rather important for the conclusions drawn here from the shaped pulses!

We thank Thomas Prisner for this hint. We have redone the experiments and added measured inversion profiles of the pulses. We also want to note that the frequency of the calculated pump pulses does not run over the carrier frequency of the spectrometer because the pulse offset to the observer frequency (carrier frequency) is included. The resonator profile looks unusual (increase at the lower frequency end) because the used resonator is a dual mode resonator. In the figure below the resonator profile recorded over a larger range can be seen. Note that this was recorded with Gd and a different microwave power, hence the different values for the nutation frequency.

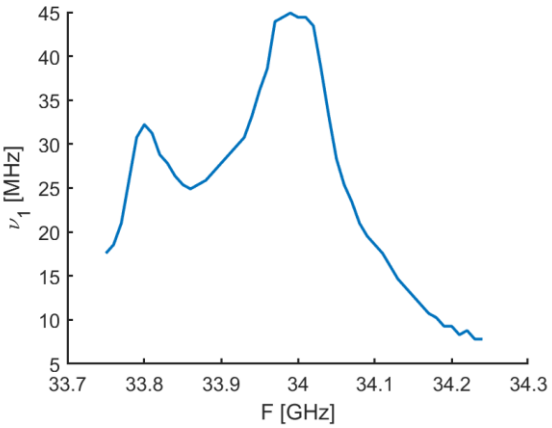

However, it was not feasible to use the second mode for the DEER measurements because of the limited width of the nitroxide EDFS spectrum. In order to discuss the issue with the 200 ns and 400 ns pump pulses, we have replaced S12 and S13 with the following new chapter, where we have also included measured inversion profiles of the broadband shaped pump pulses.

S13 The influence of the length of broadband shaped pump pulses

Tests with broadband shaped pump pulses with pulse lengths of 200 ns and 400 ns showed that they do not lead to an overall performance increase. This is shown here exemplary by comparing the performance of HS{1,1} pump pulses and Gaussian observer pulses (Fig. S12). There are indeed some pump pulses (for example a HS{1,1} pulse with $\beta = 10/t_p$ and $\Delta f =$ 110 MHz) that show an improvement with a longer pulse length, however there is no overall gain by using a pump pulse length of 200 ns.

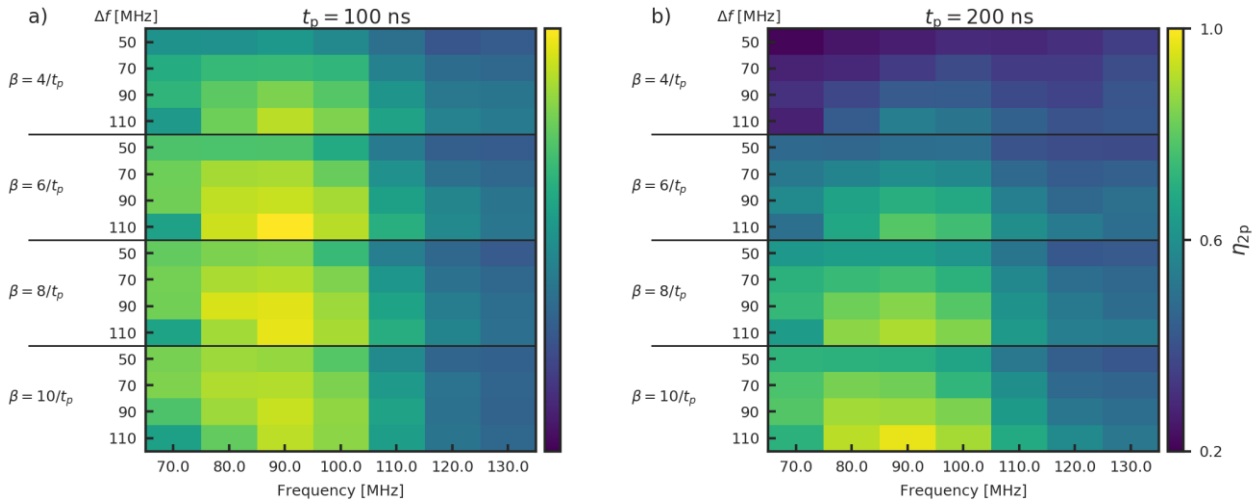

Figure S12: HS{1,1} pump pulses of (a) 100 ns and (b) 200 ns length. The observer pulses were Gaussian pulses with 100 % intensity at an observer position with a 90 MHz offset from the centre of the resonator profile and a pulse length of 56 ns for the π pulse. The colour bars are normalised to the same value so that both heat maps are comparable.

We noticed that a major problem with longer broadband shaped pump pulses is that the intensity of the echo can be reduced (Fig. S13a). For a pump pulse offset of 90 MHz, the echo intensity at the zero time of the DEER trace is reduced significantly when increasing the pump pulse lengths from 100 ns over 200 ns to 400 ns.

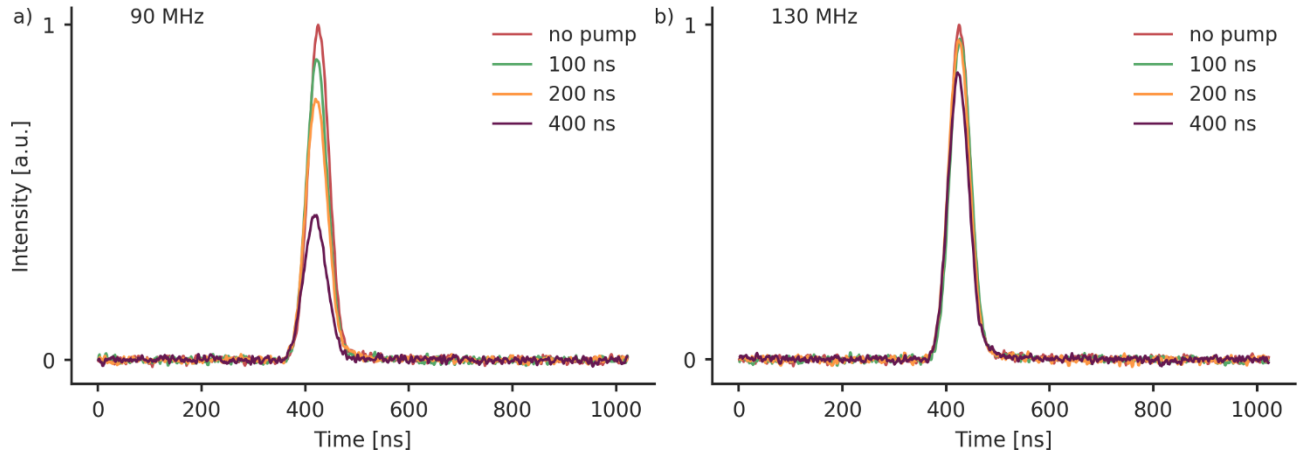

Figure S13: The echo at the zero time of the DEER trace. The observer pulses were Gaussian pulses with 100 % intensity at an observer position with a 70 MHz offset from the centre of the resonator profile and a pulse length of 56 ns for the π pulse. The pump pulses were HS{1,1} pulses with $\beta = 8/t_p$ and $\Delta f = 110$ MHz. The offset between the pulses is (a) 90 MHz and (b) 130 MHz.

A comparison of the calculated inversion profiles of the respective pulses (Fig. S14a-c) shows that, whereas the 100 ns pulse should lead to an incomplete inversion, a nearly complete inversion can be expected for the longer pulses. Furthermore, the longer pulses should have slightly steeper excitation flanks. Those trends can indeed be found for the measured inversion profiles. There are some deviations of the measured and calculated inversion profiles. The measured inversion profile of the 100 ns pulse shows an increased frequency width compared to the calculated profile. Furthermore, there is bump in the centre of the frequency sweep. The measured inversion profiles of the longer pulses show the expected steep frequency flanks that can also be seen in the simulation. The inversion profiles of the 200 ns and the 400 ns pulses show a small asymmetry around the centre of the frequency sweep. We assign these deviations to instrumental pulse distortions caused by the spectrometer.

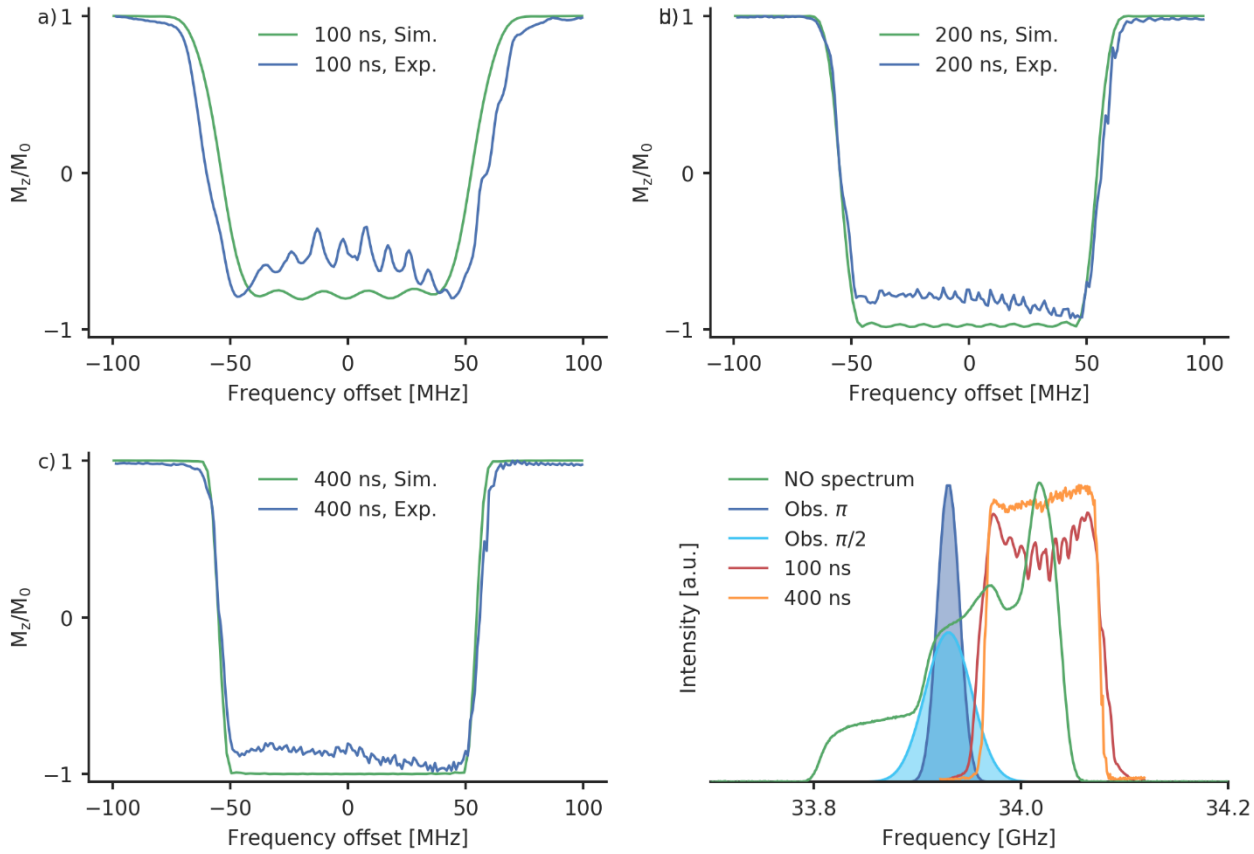

Figure S14: Calculated and measured inversion profiles of a HS{1,1} pulse with $\beta = 8/t_p$ and $\Delta f = 110$ MHz and a pulse length of (a) 100 ns, (b) 200 ns and (c) 400 ns. A 400 ns calculated pump excitation profiles next to the observer pulse excitation profiles is shown in (d).

It is expected that steeper excitation flanks lead to a smaller overlap with the observer pulses and therefore a smaller effect on the echo intensity. Despite this is the case here as well (Fig. 14d), the overlap is not reduced completely and 400 ns pulse still has some remaining spectral overlap with the observer pulses. We assume that the contradictive findings concerning the echo intensity here are caused by this remaining small overlap. It could become more perturbing for longer pulses as the overall energy of the pulses increases with the pulse length and therefore potential disturbances might be enhanced. A measurement with an larger offset between the pulses at 130 MHz shows that the echo decrease is indeed reduced (Fig. S13b) when the overlap gets smaller. Despite leading to a higher echo intensity, such a high offset is not favourable for nitroxode-nitroxide DEER, because of the limited width of the nitroxide spectrum.

4) The concentration dependence of the behavior is only discussed in a rather trivial and non-quantitative manner, despite the fact that it showed to be the major parameter influencing the improvement by the broadband pulses (comparison Figure6 and 7). That lower concentrations of spins are advantageous, especially for larger distances or broader distance distributions is well known in the community. Because broadband pulses might be especially interesting for these kind of systems, this should be discussed more quantitatively! The discussion in the SI including Figure S13 and the text after it is only very qualitative and rather trivial.

We have replaced the discussion in the SI with this section

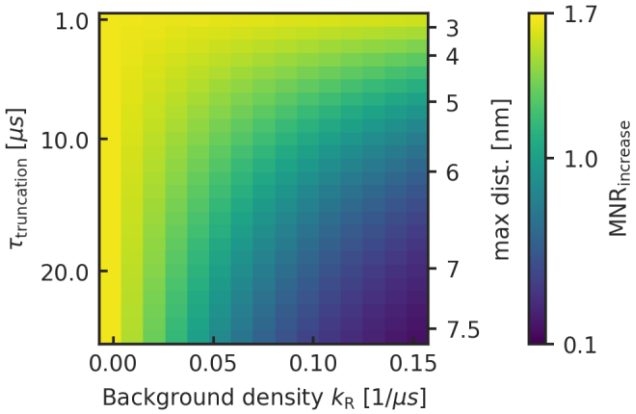

Figure S18: The MNR-ratio of adiabatic and rectangular pulses as a function of the background density (with rectangular pulses) and the $\tau_{truncation}$-time. The corresponding maximum distance according to equation (13) of the main text is also depicted. As the background density reflects the concentration the x-axis is a measure for the concentration of the spin centres. In our sample with 80 µM, we had a background density k_R of 0.1 with rectangular pulses.

Figure S18 shows that the performance of shaped pulses can heavily depend on the circumstances of the measurement. For a maximum distance below 4 nm ($\tau_{truncation} \approx 5$ µs), a MNR increase can be expected for all realistic concentration ranges. This is not the case if a longer distance shall be detected. For maximum distances around 5 nm, the MNR increase goes to 1 for high background densities of $k_R = 0.15$ 1/µs, which corresponds to very high concentrations > 100 µM. Typical concentrations for DEER measurements are around 50 µM, which here corresponds to a $k_R \approx 0.06$ 1/µs. For this concentration, a significant increase in the MNR can only be expected up to a truncation time of $\tau_{truncation} = 10$ µs, which is equal to a maximum distance of approximately 6 nm.

As broadband shaped pulses are particularly interesting for long distances, the calculations were performed up to a rather long truncation time of 25 µs (maximum distance of approximately 7.5 nm). For distances in the range > 6 nm, only with concentrations in the range of 10-30 µM ($k_R \approx 0.01$-0.04 1/µs) a significant increase in the MNR due to broadband shaped pump pulses can be expected. The MNR increase drops quickly when higher concentrations are used. For a maximum distance of 7.5 nm and for concentrations over approximately 40 µM no increase can be expected any more due to broadband shaped pulses. If a concentration of 80 µM is used, the MNR is about to decrease to roughly 40 % when switching to broadband shaped pulses. It is known that diluting the sample is favourable if long distances shall be detected because it increases the phase memory time of the echo (Schmidt et al., 2016). When broadband shaped pump pulses, the higher background decay

adds an additional point for carefully choosing the concentration of the sample and it seems to be advisable to avoid high concentrations.

5) Minor point: In the supporting information equation (2) is wrong. After that there is a spelling error (ration).

We thank Thomas Prisner for this remark. We have corrected the spelling mistakes.

2.2 Response to Referee 2

Dear Reviewer,

We thank you much for your effort reading our manuscript so carefully and for your valuable advices. We strongly believe that the suggested changes and additions improved the manuscript a lot. Please find below a point-by-point reply to all your recommendations (in blue).

[1] In section 3.3 (background decay), examine in detail how the type of shaped pulse affects the MNR if the recently published superior background correction method (kernel inclusion) is used. It is crucial to include this in this work.

We agree with the reviewer that the novel approach including the background into the Kernel is a very efficient and convincing approach. We have added a new section in the main text where we clarified why we think that the MNR as we used it is the most feasible parameter for optimising settings for DEER.

As stated by equation (10) the measured raw data does not only consist of the desired form factor but includes a background contribution emerging from intermolecular interactions. A common way to deal with this, is to fit the background according to equation (11) and divide the raw data by the fit to obtain the form factor that can then be transformed into a distance distribution (Jeschke, 2012; Jeschke et al., 2006). When measuring DEER traces, a precise distance determination is desired. Since for an experimental parameter optimisation, the true underlying distance distribution is unknown, a metric is needed that is based on the recorded data. The MNR of the form factor is a suitable for this case as it increases with an increasing modulation depth and an increasing echo intensity. As the noise of the form factor increases towards its end due to the division by the background, the MNR goes down with a stronger background decay. It can therefore capture the fact that a larger background decay leads to less reliable distance distributions as has recently be investigated by [Fabregas, et. Al., 2020] in a detailed study. In their paper they also suggest a different method for background correction that treats the background by directly including it in the kernel that is needed to calculate the distance distribution from the DEER trace. As this methods renders the calculation of a form factor redundant, a MNR cannot be directly obtained by it. Even though this new method has shown itself to give more reliable distance distributions in the case of large background decays its performance still drops with an increasing background. Therefore, we consider the MNR that is obtained by the background correction by division still as the best measure to optimise settings for a DEER measurements experimentally.

We have also added a chapter in the SI to discuss the suitability of the MNR as a merit function if the background correction by kernel inclusion is used:

S2 The MNR as the function of merit

Here, we want to discuss whether the MNR is a suitable function of merit for the determination of distance distributions and up to which time point in the DEER trace, the MNR needs to be evaluated to serve this purpose. Therefore, we performed simulations with a model distance distribution p_0 that is based on the narrow distance distribution of the model system used in this study. We approximated the experimentally obtained distance distribution with a Gaussian with a mean at 5.08 nm and a standard deviation of 0.08 nm. We varied the background density in ten steps from k = 0.01 1/µs to k = 0.3 1/µs in combination with a low, medium and high noise level (noise σ_0 = 0.02, 0.05 and 0.1) that was added to the DEER trace. The background dimension was set to d = 3 and a modulation depth of 0.5 was used. The DEER traces were simulated in the time domain up to 8 µs. For each parameter set we generated ten different traces. To compare the background correction by division (Jeschke et al., 2006) with the kernel inclusion approach as described in (Fábregas Ibáñez and Jeschke, 2020) we analysed all simulated DEER traces with both methods. We did not fit the background but used the true background function. The regularisation parameter was chosen according to the generalised cross-validation method. The quality of the resulting distance distributions p was estimated by the Euclidian distance D from the true distance p_0:

$$D(p, p_0) = \|p - p_0\|_2 \tag{1}$$

The MNR of the form factor F was calculated as described in the main text up to a limit of 7 µs according to equation (13) of the main text.

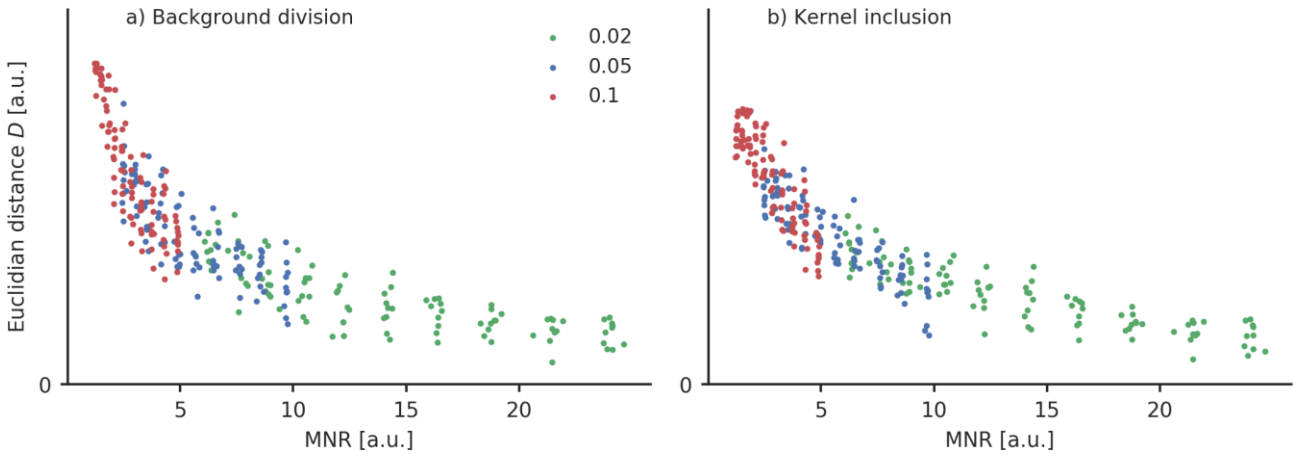

Figure S2: The Euclidian distance D of the real and calculated distance distribution as defined in equation (1) is plotted as a function of the MNR. Each dot represents a simulated DEER trace with either low (σ_0 = 0.02, green), medium (σ_0 = 0.05, blue) and high (σ_0 = 0.1, red) noise. The background correction was performed by (a) dividing the DEER trace by the background and (b) including the background in the kernel.

In Fig. S2, the quality of the determined distance distribution was plotted as a function of the determined MNR for both a background correction by division (Fig. S2a) and a kernel inclusion approach (Fig. S2b). For each noise level the MNR only depends on the density of the background as all other parameters are kept constant and only the background density is varied. So a lower MNR corresponds to a higher background density rate and vice versa. For the low noise level (σ_0 = 0.02), the quality of the determined distance distributions only varies a little for different background density rates. For medium (σ_0 = 0.05) and high (σ_0 = 0.1) noise levels, however, the dependency of the quality of the determined distance distribution decreases significantly with a decreasing MNR. If the MNR is only evaluated up to an early point of the form factor, the

information of the background decay rate is lost in this case and is not properly included in the MNR as the MNR would then depend nearly exclusively on the given noise level.

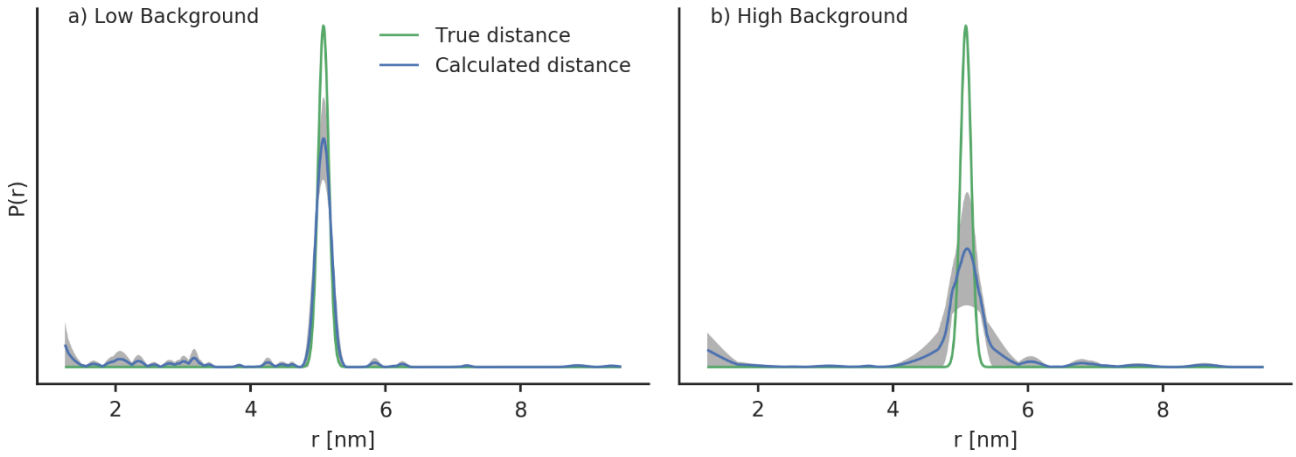

Figure S3: An exemplary distance distribution obtained for a medium noise level (σ_0 = 0.02) with (a) a low background density (k = 0.01 MHz) and (b) a high background density (k = 0.3 MHz). The grey area shows the area that is covered by the calculated distance distribution for ten exemplary DEER traces. The mean of the shaded area is drawn in blue and the true distance is drawn in green.

A closer inspection reveals that whereas the obtained distance distributions for high background densities reproduce the mean of the distance distribution correctly, they overestimate the width of the distribution and the distance appears to be broader as it is (see Fig. S3 for an exemplary data set). Depending on the information that shall be obtained by the DEER measurements, the mean of the distance distribution might suffice. However, if high resolution distance distributions shall be obtained, it seems to be important to optimise the MNR up to the limit which is given by equation (13) of the main text. The comparison of both background correction methods shows that the kernel inclusion gives better results particularly for a high noise and a high background decay. It should therefore be considered as the superior method. However, the correlation between the quality of the determined distance distribution and the MNR is still valid. This is why, we consider the MNR as a proper function of merit, even if the kernel inclusion approach is used.

For a more comprehensive study, the effect of the MNR on the quality of the obtained distance distribution could also be tested for distance distributions with different distance ranges and widths. Such a detailed study was, however, beyond the scope of the this manuscript.

[2] Discuss in more detail whether and how the findings in this work are applicable to other samples (different distance distributions, different concentrations) and spectrometers (different resonator profiles, different Tx fidelity). From the current manuscript, itis unclear whether the findings are generalizable. This is important,

since it appears to be the purpose of the manuscript to make some general statements about experimental settings in DEER.

We have added a section in the main text to discuss the effect of different resonator profiles

Depending on the resonator and the microwave amplifier, different B_1 field strengths are available on different spectrometers. However, as the inversion efficiency of broadband shaped pulses is less dependent on the B_1 field strength as is the case for rectangular and Gaussian pulses, who always require a proper adjustment of the pulse length, we assume the findings here to be rather generalisable. In order to discuss this more quantitatively we simulated inversion profiles of the best performing pulses from Table 3 for B_1 field strengths.

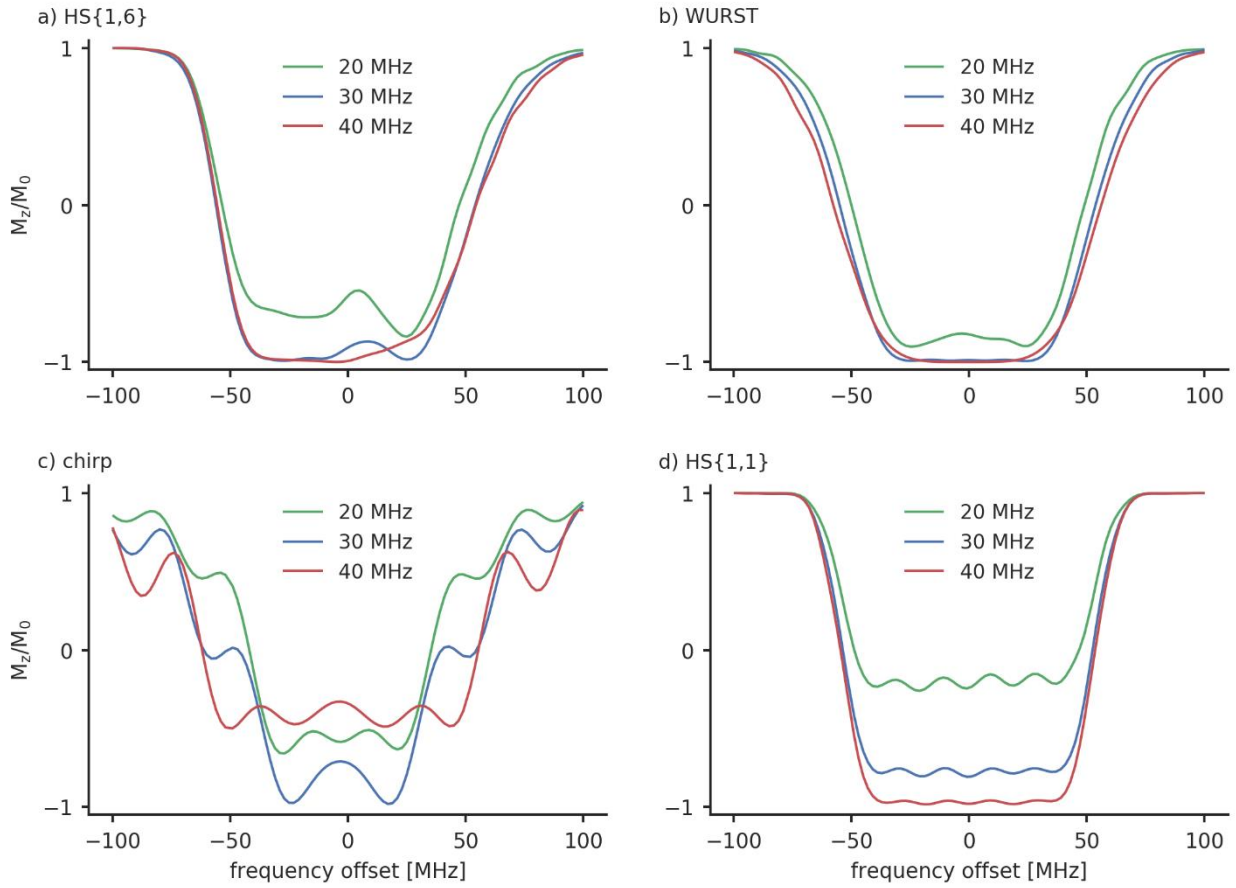

Figure 6: The inversion profiles of the best performing (a) HS{1,6}, (b) WURST, (c) chirp and (d) HS{1,1} pulses with the parameters from Table 3. They were simulated with a B_1 field strength of 20 MHZ (green), 30 MHz (blue) and 40 MHz (red). These field strengths correspond to a π-pulse lengths of 25.0 ns, 16.7 ns (which approximately correspond our setup) and 12.5 ns. The B_1 field here is depicted as the Rabi frequency.

We compare the pulse profiles with B_1 = 30 MHz, which corresponds our setup, with the cases where a lower (B_1 = 20 MHz) or higher (B_1 = 40 MHz) B_1 field strengths arereached. Figure 6 shows how the different pulses behave, when different B_1 field strengths are used. The WURST pulse (Fig. 6b) shows the least variation for different B_1 field strengths. As expected the inversion efficiency drops a little bit for B_1 = 20 MHz. But this drop seems to be rather insignificant and good modulation depths can still be expected. The decrease in inversion efficiency is a bit more significant for the HS{1,6} pulse so that a small reduction in the modulation depth is possible here. Both pulse profiles do not show significant changes when a higher B_1 field strength is used. The HS{1,1} pulse has a massive drop in inversion efficiency when going to lower B_1 field strengths. This

comes not as a surprise as the inversion efficiency is already incomplete at B_1 = 30 MHz. Here, it might be advantageous to reduce the β parameter of the HS{1,1} pulse. As it has been stated earlier this will increase the inversion efficiency. For a higher B_1 field strength of B_1 = 40 MHz the inversion efficiency of this HS{1,1} will increase. Therefore, a higher modulation depth comparable to the HS{1,1} pulse is expected. As this will also increase the background decay, a higher MNR is not guaranteed. The chirp pulse also shows a rather strong decrease in the inversion efficiency for a B_1 = 20 MHz. However, the inversion efficiency also decreased for a higher B_1 field strength of B_1 = 40 MHz. This rather unexpected behaviour is probably caused by an insufficient smoothing of the edges of the chirp pulse. With higher B_1 field strength the initial effective magnetic field vector in the accelerated frame becomes less aligned with the z-axis. Therefore, smoothing becomes more important. In Fig. S10, we compared the inversion profiles of 36 ns and 100 ns chirp pulses with and without quarter sine smoothing. When quarter sine smoothing is applied, chirp pulses can with a length of 36 ns indeed reach a high inversion efficiency with B_1 = 40 MHz. (Fig. S10b). As the width of the inversion profile of this chirp pulse drops significantly for smaller B_1 field strengths, it is only advisable to implement a quarter sine smoothing with chirp pulses of a length of 36 ns when enough microwave power is available. The situation looks different for chirp pulses with a pulse length of 100 ns. Here, the inversion profile looks very similar for all tested B_1 field strengths. Particularly for smaller B_1 field strengths we expect 100 ns chirp pulses to outperform chirp pulses with a length of 36 ns.

Another crucial parameter for DEER measurements that can vary from setup to setup is the width of the resonator profile. Here, we have a FWHM of approximately 200 MHz. Larger widths do not seem to be necessary because they would exceed the width of the spectrum of the nitroxide. If only a smaller width is available, the offset between pump and observer pulses might need to be reduced. This would increase the overlap between the observer and pump pulses. This problem could be overcome by either using longer pump pulses or reducing the frequency width of the broadband shaped pulses. As a narrower resonator profile is also necessarily steeper, it might also be necessary to perform a resonator bandwidth compensation as suggested by (Doll et al., 2013). Performing a resonator bandwidth compensation with our setup does not give a significant advantage in the η_{2p} value (see S15). This is probably due to the rather flat resonator profile in the region with maximum sensitivity where the pump pulse is applied.

We have also added the following two sections to discuss different distances ranges and concentrations:

For a concentration of 80 µM, a high MNR improvement can be achieved if the maximum distance of interest is below 4 nm with pulse that achieves a high modulation depth. This would correspond to the HS{1,6} and WURST pulse in this case. If longer distances up to 5 nm shall be detected, it seems to be advantageous to use pulses that might not give the highest modulation depth in order to reduce the background decay. An extrapolation for higher truncation times shows that if even longer distances are of interest, broadband shaped pulses will not give a better MNR compared to rectangular pulses. Here, it is necessary to reduce the background decay by using lower concentrations.

When the MNR shall be increased by using broadband shaped pulses to detect long distances > 5 nm, lower concentrations are preferable as they reduce the enhancement of the background decay. Here, switching to a concentration of 30 µM of the doubly labelled ligand was enough the significantly reduce the influence of the background. In S19 we performed analytical calculations to estimate the potential MNR increase that can be achieved by switching to broadband shaped pulses for different

concentrations and distance ranges. For maximum distances below 4 nm an increase of the MNR can be expected for all concentrations up to approximately 100 µM. The situation is different if distances over 6 nm shall be detected. A significant gain can only be expected for smaller concentrations in the range between 10-30 µM. For higher concentrations the MNR gain drops quickly. For higher concentrations in the range of 80 µM a MNR decrease has to be expected in this distance regime. This is discussed in more detail in S21.

3] - Eq.(3): Specify that the time axis is defined such that t=0 at the center of the pulse.- Eq.(11): (k*|t|)ˆ(d/3) instead of k*tˆ(d/3) - Eq.(12): A factor of 2 might be missing. -8.13: "i.e. a chirp pulse" - 12.18: Here, it is not clear how the numbers for the minimum detectable distance limit are obtained. - Kupce needs a grave accent on the c. Bohlen needs an umlaut on the o. - SI Eq.(2): t_truncation instead of tau_2

We thank the referee for these remarks and corrected and clarified these points.

3. List of major changes

We have made the following major changes in the manuscript. For clarity reasons we have not included the full sections here. They are marked as changes in the revised manuscript which starts on the next page.

1. In the introduction we have clarified the objective of this manuscript.
2. We have exchanged Fig.1 because we noticed a minor error in a sugar moiety of the tetravalent ligand.
3. A section where we discuss the suitability of the MNR as the function of merit, particularly when different background techniques are used, i.e. including the background in the kernel was added.
4. We added a section where we have discussed the pulse performance for different resonators based on simulated inversion profiles.
5. In the section “Background behaviour” and “Concentration dependence” we have added two section with a more quantitative discussion.

In the SI we have made the following changes:

1. The suitability of the MNR as merit function is discussed in a new section S2.
2. A new section S11 was added to discuss discrepancies from experimental and simulated inversion profiles of the broadband shaped pulses.
3. The former section S12 and S13 have been replaced by a new section S13 where we discuss the influence of the length of the broadband shaped pump pulses in more detail. Therefore, we have added experimentally recorded pulse inversion profiles for 100 ns, 200 ns and 400 ns broadband shaped pulses.
4. The full DEER traces of the sample with the high and low concentration are shown in anew section S20.
5. Major changes were made in the new section S21 to add a quantitative discussion of different concentration and distance ranges for the performance of broadband shaped pump pulses.

Optimising broadband pulses for DEER depends on concentration and distance range of interest

Andreas Scherer, Sonja Tischlik, Sabrina Weickert, Valentin Wittmann, Malte Drescher

Department of Chemistry and Konstanz Research School Chemical Biology, University of Konstanz, Konstanz, Germany
Correspondence to: Malte Drescher (malte.drescher@uni–konstanz.de)

Abstract. EPR distance determination in the nanometre region has become an important tool for studying the structure and interaction of macromolecules. Arbitrary waveform generators (AWGs), which have recently become commercially available for EPR spectrometers, have the potential to increase the sensitivity of the most common technique double electron-electron resonance (DEER, also called PELDOR), as they allow the generation of broadband pulses. There are several families of broadband pulses, which are different in general pulse shape and the parameters that define them. Here, we compare the most common broadband pulses. When broadband pulses lead to a larger modulation depth they also increase the background decay of the DEER trace. Depending on the dipolar evolution time this can significantly increase the noise level towards the end of the form factor and limit the potential increase of the modulation–to–noise ratio (MNR). We found asymmetric hyperbolic secant (HS{1,6}) pulses to perform best for short DEER traces leading to a MNR improvement of up to 86 % compared to rectangular pulses. For longer traces we found symmetric hyperbolic secant (HS{1,1}) pulses to perform best, however, the increase compared to rectangular pulses goes down to 43 %.

1 Introduction

In the last years DEER (double electron-electron resonance) has developed into an important technique for the determination of distances in the nanometre range (Jeschke, 2012, p.2; Milov et al., 1984; Salkhon, K.M. Milov, A.D., Shchirov, M.D., 1981) and in particular into a suitable tool for studying biological macromolecules (e.g. proteins (Jeschke, 2012; Robotta Marta et al., 2014) or RNA/DNA (Grytz et al., 2017; Kuzhelev et al., 2018)). As many bio-macromolecules do not contain paramagnetic centres, for many DEER experiments spin labels are introduced with the help of site-directed spin labelling (Hubbell et al., 1998). Although many different types of spin labels have been introduced in the last years ranging from trityl (Abdullin et al., 2015; Jassoy et al., 2018), Gd(III) (Collauto et al., 2016; Dalaloyan et al., 2015; Mahawaththa et al., 2018), Copper(II) (Wort et al., 2019) to photoexcitable spin labels (Di Valentin et al., 2014; Hintze et al., 2016), just to mention a few examples, nitroxide labels are still amongst the most widely used tags.

Increasing the sensitivity of DEER spectroscopy is an active field of research (Borbat et al., 2013; Breitgoff et al., 2017; Doll et al., 2015; Jeschke et al., 2004; Lovett et al., 2012; Milikisiyants et al., 2019; Polyhach et al., 2012; Tait and Stoll, 2016; Teucher and Bordignon, 2018). A very elegant approach to increasing DEER sensitivity has been made possible by the availability of arbitrary waveform generators with time resolution in the nanosecond region as they allow the generation of broadband microwave pulses (Doll et al., 2013; Doll and Jeschke, 2017; Spindler et al., 2017).

Here, we compare nitroxide-nitroxide DEER performance for different types of ~~broadband shaped pulses and identify the best parameters for each pulse type as well as the best pulse for different measurement and sample conditions. We show that the performance of the broadband pulses can depend on the required length of the DEER trace as well as the spin concentration. A calculation shows what performance of shaped pulses can be expected for different trace lengths and spin concentrations.~~

pulses and different sample conditions. The manuscript is organized as follows: In Sect. 1 we will give a brief overview over the pulse shapes that are compared in this manuscript. In Sect. 2, we will describe the experimental details and the compounds

that have been used in this study. In Sect. 3, we will present and discuss the experimental results. ~~We will first compare rectangular and Gaussian pulses for DEER spectroscopy and show that Gaussian pulses can yield a higher sensitivity than rectangular pulses. We will then compare broadband pulses with rectangular and Gaussian pulses. After an optimisation of the parameters for broadband pulses, we will show that HS{1,1} and HS{1,6} have the highest sensitivity for nitroxide-nitroxide DEER. Finally, it will be shown that the performance of the pulses is dependent on the spin concentration as well as on the measured distance~~We will compare rectangular, Gaussian and different types of broadband shaped pulses on a commercial spectrometer. In order to give them a fair comparison, the parameters for each pulse family will be optimised. In doing so, we will provide a step-by-step guidance how an experimental optimisation for DEER can be performed. The larger inversion efficiency of broadband shaped pump pulses that leads to a higher modulation depth will also lead to a higher background decay and therefore potentially limit the signal gain that is promised by broadband shaped pump pulses. We set out to examine this effect for the presented pulse families in detail and show that different types of broadband shaped pulses are ideal for different spin concentrations and distance ranges.

In magnetic resonance experiments, a pulse is generated by a time-dependent field B_1 that is applied perpendicular to the B_0 field which defines the z-direction. All pulses in this paper can be described in terms of an amplitude function $A(t)$ and a frequency function $\omega(t)$.

The resulting B_1 field in the rotating frame is:

$$B_{1,x}(t) = A(t)\cos\big(\rho(t)\big), \tag{1}$$

$$B_{1,y}(t) = A(t)\sin\big(\rho(t)\big). \tag{2}$$

Where the phase $\rho(t)$ is defined as $\rho(t) = \int_0^t \omega(\mathrm{t}')\mathrm{dt}'$. Rectangular pulses are described by $\omega(t) = 0$ and $A(t) = B_1$ during the pulse, i.e. by a B_1 field with a constant phase and intensity. The sidebands of the sinc-shaped excitation profile of rectangular pulses increase the overlap of the observer and pump pulse in DEER, resulting in so called '2+1' artefacts at the end of the DEER trace. It has recently been shown that those artefacts can be reduced by replacing the rectangular pulses with Gaussian pulses (Teucher and Bordignon, 2018). Gaussian pulses also have a frequency function of $\omega(t) = 0$ but an amplitude function:

$$A(t) = \exp\left(-\frac{4\ln(2)t^2}{\mathrm{FWHM}^2}\right), \tag{3}$$

FWHM describes the full width at half maximum of the pulse in the time domain (Teucher and Bordignon, 2018). Here and in the following equations the time axis is defined such that $t = 0$ lies in the centre of the pulses. During a rectangular or Gaussian pulse the magnetisation vector is rotated around the B_1 field with an angle that is independent of the initial orientation of the magnetisation vector. Such pulses are therefore called uniform rotation pulses (Kobzar et al., 2012). As rectangular and Gaussian pulses have a fixed frequency, they are also referred to as monochromatic pulses.

One of the most significant challenges in EPR spectroscopy is the limited excitation bandwidth of rectangular and also Gaussian pulses compared to the width of many EPR spectra. In the case of nitroxide-nitroxide DEER, a significant part of the EPR spectrum does neither contribute to observing nor to pumping when using rectangular pulses.

Using broadband shaped pulses, the excitation bandwidth can be increased (Doll et al., 2013). Broadband shaped pulses distinguish from- rectangular and Gaussian pulses mainly in that they do not have a constant frequency, but the frequency is swept over a given range during the pulse, which allows increasing the excitation bandwidth. In an accelerated frame, which rotates with the instantaneous excitation frequency of the pulse, the effective field rotates from the +z to the –z direction (Baum et al., 1985; Deschamps et al., 2008; Garwood and DelaBarre, 2001; Kupce and Freeman, 1996). Under adiabatic conditions the magnetisation follows the effective field on its way from +z to –z (Baum et al., 1985; Doll et al., 2013a). Pulses that induce

this kind of spin flip behaviour are called point-to-point rotation pulses. This approach allows the generation of pulses that have a large excitation bandwidth and that are, above a certain threshold, more insensitive to the resonator profile than rectangular pulses (Baum et al., 1985). Their ability to flip spins from the +z to the –z-axis makes such broadband shaped pulses perfect candidates for the pump pulse in the DEER pulse sequence. Their larger excitation profile has the potential to result in a larger modulation depth and therefore a larger sensitivity (Bahrenberg et al., 2017; Doll et al., 2015; Spindler Philipp E. et al., 2013; Tait and Stoll, 2016).

Intuitively, a high adiabaticity means that the effective magnetic field moves more slowly from +z to –z, making it easier for the spins to follow, thus resulting in a higher inversion efficiency.

The adiabaticity Q is formally defined as (Kupce and Freeman, 1996):

$$Q = \frac{2\pi\nu_1}{|\mathrm{d}\theta/\mathrm{d}t|}. \tag{4}$$

Here, ν_1 is the strength of the effective magnetic field and θ is its polar angle in the accelerated frame. The pulses have a good inversion efficiency, if $Q \gg 1$ (Deschamps et al., 2008). In general, the adiabaticity changes during the duration of the pulse and is different for spins with different frequency offsets. Adiabatic pulses are typically quantified by their minimum adiabaticity Q_{min}.

Chirp pulses have a constant amplitude function and a linear frequency function $\omega(t) = f_{\mathrm{start}} + pt$, where $p = \frac{\Delta f}{t_p}$ is a sweep constant, t_p is the pulse length and $\Delta f = f_{\mathrm{end}} - f_{\mathrm{start}}$. f_{start} and f_{end} are the start and end frequencies of the frequency sweep. The minimum adiabaticity Q_{min} is reached when a spin is on resonance with the pulse frequency (Doll et al., 2013a):

$$Q_{\mathrm{min}} = \frac{2\pi\nu_1^2 t_p}{\Delta f}, \tag{5}$$

Q_{min} increases with the pulse length but decreases with the sweep width. The frequency width for a pump pulse should be chosen such that a large part of the spectrum is excited without having significant spectral overlap with the pulses at the observer frequency. The steep flanks at the beginning and the end of the rectangular amplitude profile lead to distortions in the excitation profiles of chirp pulses~~.~~, because the initial effective magnetic field is not aligned with the z-axis. Smoothing both ends of the pulses with a quarter sine-wave can reduce theses distortions (Bohlen and Bodenhausen, 1993). The smoothing can be adapted by changing the rising time t_{rise}. Following the logic so far, the pulse length should be chosen as long as possible to enable a very high adiabaticity. However, a broadband shaped pulse flips spins with different offsets at different times. When used as a pump pulse in DEER, this results in a shift of the dipolar oscillations and an artificial broadening of smaller distances in the distance distribution. Therefore, the pulse length should be chosen such that (Breitgoff et al., 2019):

$$t_p < \frac{T_{dd}}{4}, \tag{6}$$

with the dipolar evolution time T_{dd} of the shortest expected distance.

In addition to chirp pulses there are more elaborate pulses employing more elaborate frequency and amplitude functions. The most common ones are WURST (wideband, uniform, smooth truncation) and HS (hyperbolic secant) pulses. The trends discussed so far are valid for them as well. However, they feature additional parameters that can be used to tune the steepness of the corresponding excitation profiles.

WURST pulses have a linear frequency sweep as well but a different amplitude function than chirp pulses ~~(Kupce and Freeman, 1995b; Spindler et al., 2017)~~(Kupče and Freeman, 1995b; Spindler et al., 2017):

$$A(t) = A_{\mathrm{max}}\left(1 - \left|\sin\left(\frac{\pi t}{t_p}\right)\right|^n\right), \tag{7}$$

The effect of the parameter n determining the steepness of the amplitude function will be discussed below.

HS pulses have non-linear frequency sweeps and are described by the following amplitude and frequency functions:

$$A(t) = \mathrm{sech}\left(\beta 2^{h-1}\left(\frac{t}{t_p}\right)^h\right), \tag{8}$$

$$\omega(t) = \frac{\Delta f}{2}\tanh\left(\frac{\beta}{2}\right)^{-1} \tanh\left(\frac{\beta t}{t_p}\right), \tag{9}$$

with order parameter h and truncation parameter β. The effects of β will be discussed below. A common choice for h is to set $h = 1$. These pulses have an offset-independent adiabaticity and a rather rectangular excitation profile (Baum et al., 1985; Tannús and Garwood, 1996). Increasing the order h of an HS pulse will lead to a higher adiabaticity at the maximum of the excitation profile but less steeper flanks (Breitgoff et al., 2019). A compromise can be found by using an asymmetric HS pulse where the flank close to the observer is made steep by an order of 1 and where the other flank has a higher order for a higher adiabaticity (Doll et al., 2016). Symmetric pulses with an order parameter of $h = 1$ will be referred to as HS{1,1}, asymmetric pulses where the first part of the pulse has on order parameter of $h = 1$ and the second half has $h = 6$, as suggested by Doll et al. (2016) are referred to as HS{1,6} (Doll et al., 2016).

The measured DEER-trace $V(t)$ is the product of the form factor $F(t)$ that contains the required intramolecular distance information and a background-function $B(t)$ (Jeschke, 2012):

$$V(t) = F(t) \cdot B(t), \tag{10}$$

The background decay is caused by the intermolecular interactions of the observer spin with pump spins of surrounding molecules. ~~Assuming that the spins are homogenously distributed the background decay can be described by an exponential decay:~~Assuming that the spins are homogenously distributed the background decay can be described by an exponential decay (Jeschke, 2007a):

$$B(t) = \text{~~}\exp(-kt^{d/3}\text{~~}\exp(-(k|t|)^{d/3}), \tag{11}$$

~~where d is a dimensionality constant and the decay constant k is described by the following equation (Pannier et al., 2000):~~

~~$k = \frac{N_a \pi \mu_0}{9\sqrt{3}\hbar}$~~where d is a dimensionality constant and the decay constant k is described by the following equation (Hu and Hartmann, 1974; Pannier et al., 2000):

$$k = \frac{2N_a \pi \mu_0}{9\sqrt{3}\hbar} g^2 \mu_e^2 f c, \tag{12}$$

Here, c is the spin concentration, f the inversion efficiency of the pump pulse, μ_e the Bohr-magneton, μ_0 the magnetic field constant, N_a the Avogadro number and g the isotropic g-factor of the nitroxide.

2 Materials and Methods

2.1 Sample preparation

Wheat germ agglutinin (WGA) was purchased from Sigma-Aldrich (article-no.: L9640) as lyophilized powder and used without further purification. The doubly spin-labelled tetravalent ligand (1) was synthesised in the lab of Valentin Wittmann. Details of synthesis and characterisation will be published elsewhere. For the WGA-ligand samples investigated in this study solutions of WGA and the tetravalent ligand were prepared separately in deionised water. The protein concentration of the WGA solution was determined spectrophotometrically.

WGA-ligand samples were prepared by mixing WGA and ligand solutions resulting in a 2:1 molar excess of WGA compared to the ligand referring to the final sample volume. The 2-fold excess on protein was chosen to prevent free, unbound ligand in solution. The sample solution was lyophilised and the resulting powder was dissolved in D_2O (Magnisolv, Cas-no.: 7789200, article: S571556621) and 20 % (v/v) deuterated glycerin (Sigma-Aldrich, lot-no. MBBB5255, article: 447498-1G) as cryoprotectant. Unless stated otherwise we used a sample concentration of 160 µM WGA and 80 µM ligand. 60 µL of solution were filled into 3 mm outer diameter quartz sample tubes (ER 221 TUB/2, Part No. E221003), shock-frozen in liquid nitrogen before measurement and placed in the probe head precooled to 50 K. Samples were stored at -80 °C with unfreezing avoided.

2.2 EPR experiments

All experiments have been performed on a Bruker Elexsys E580 spectrometer at Q-band (34 GHz). The spectrometer is equipped with a SpinJet-AWG unit (Bruker) and a 150 W pulsed travelling-wave tube (TWT). All samples were measured in 3 mm outer diameter sample tubes in an overcoupled ER5106QT-2 resonator (Bruker). The quality factor Q of the overcoupled resonator is approximately 200.

The samples were cooled to 50 K with a Flexline helium recirculation system (CE-FLEX-4K-0110, Bruker Biospin, ColdEdge Technologies) comprising a cold head (expander, SRDK-408D2) and a F-70H compressor (both SHI cryogenics, Tokyo, Japan), controlled by an Oxford Instruments Mercury ITC.

DEER measurements were recorded with the standard four pulse DEER sequence (Pannier et al., 2000), an 8-step phase cycle (Tait and Stoll, 2016) and nuclear modulation averaging (Jeschke, 2012). The dipolar evolution time was set to 8 µs and the time step to 8 ns.

We analysed the DEER traces with DeerAnalysis2019 (Jeschke et al., 2006). We performed a background correction resulting in a background function with a dimension of $d = 3.5$. The form factor was analysed with Tikhonov ~~regularization~~regularisation and a ~~regularization~~regularisation parameter chosen by the generalised cross-validation criterion (Edwards and Stoll, 2018).

A crucial parameter for pulsed dipolar spectroscopy is the modulation-to-noise parameter $\mathrm{MNR} = \frac{\lambda}{n}$, with the modulation depth λ and the noise level n. We calculated the noise similarly to published procedures by the standard error from a fit with a smoothing spline (Bahrenberg et al., 2017; Breitgoff et al., 2019; Mentink-Vigier et al., 2013). We excluded the first 10 datapoints from the form factor because the spline typically showed some deviations at the start of the trace. Unless stated otherwise the upper limit for the noise calculation was 7 µs.

We used the η_{2P}-parameter which has been suggested by (Doll et al., 2015) and already been used by other authors (Doll et al., 2015; Spindler Philipp E. et al., 2013; Tait and Stoll, 2016). The η_{2p} value is defined as the difference between two distinct time points in the DEER trace, and therefore does not require the measurement of full DEER traces. We recorded short DEER traces with 8 data points only and calculated η_{2P} as the difference of the phase corrected DEER trace at the zero time $V(0)$ minus the first minimum of the DEER trace $V(t_{\min})$.

For a more detailed description of materials and methods see ~~the Supporting Information~~S1.

3 Results and Discussion

In order to study the performance of DEER using different pulses, we used the doubly nitroxide-labelled tetravalent ligand bound to wheat germ agglutinin dimer (WGA) as a model system (Fig. 1). The ligand binds with a very high affinity to WGA and features a narrow distance distribution (FWHM = 0.2 nm) at 5.1 nm (to be published elsewhere). We performed DEER experiments with different combinations of pulses. In the following, we will refer to a combination of rectangular observer and pump pulses as RR, to a combination of Gaussian observer and pump pulses as GG for, to a combination of rectangular observer and broadband shaped pump pulses as RS and to a combination of Gaussian observer and broadband shaped pump pulses as GS for. ~~The preferred parameter for assessing the sensitivity of individual DEER measurements is the modulation to noise ratio (MNR) as defined previously.~~

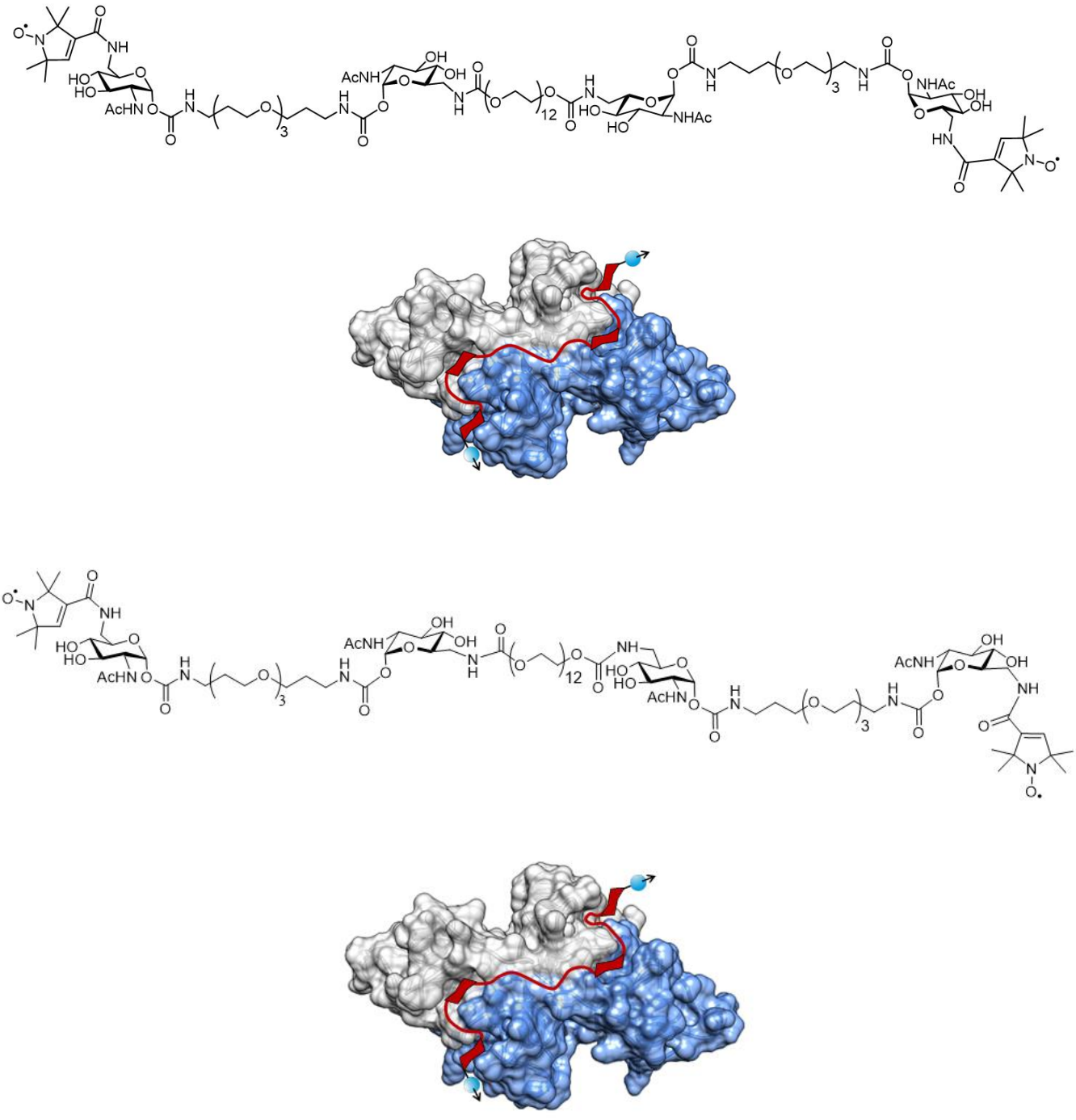

Figure 1: The structure of the tetravalent ligand with its two spin-(2,2,5,5-tetramethyl-3-pyrrolin-1-yloxycarbonyl)-labels and the ligand bound to WGA. The visualisation of the dimeric WGA with the subunits coloured in grey and blue is based on the crystal structure (PDB entry 2X52 *(Schwefel et al., 2010)*). In red, a schematic representation of the ligand is overlaid to the crystal structure. The ligand is suggested to bind with its four GlcNAc moieties to the primary binding sites of WGA. Blue balls and arrows indicate nitroxide spin labels.

As stated by equation (10) the measured raw data does not only consist of the desired form factor but includes a background contribution emerging from intermolecular interactions. A common way to deal with this, is to fit the background according to equation (11) and divide the raw data by the fit to obtain the form factor that can then be transformed into a distance distribution (Jeschke, 2012; Jeschke et al., 2006). When measuring DEER traces, a precise distance determination is desired. Since for an experimental parameter optimisation, the true underlying distance distribution is unknown, a metric is needed that is based on the recorded data. The MNR of the form factor is a suitable for this case as it increases with an increasing modulation depth and an increasing echo intensity. As the noise of the form factor increases towards its end due to the division by the background, the MNR goes down with a stronger background decay. It can therefore capture the fact that a larger background decay leads to less reliable distance distributions as has recently be investigated by (Fábregas Ibáñez and Jeschke, 2020) in a detailed study. In their paper they also suggest a different method for background correction that treats the background by directly including it in the kernel that is needed to calculate the distance distribution from the DEER trace. As this methods renders the calculation of a form factor redundant, a MNR cannot be directly obtained by it. Even though this new method has shown itself to give more reliable distance distributions in the case of large background decays its performance still drops with an increasing background. Therefore, we consider the MNR that is obtained by the background correction by division still as the best measure to optimise settings for a DEER measurements experimentally.

The evaluation of the noise of the entire DEER trace is not always feasible. It depends on the maximum distance r_{max} that shall be detected up to which part the form factor is of interest. Here, we truncated the form factor for the calculation of the MNR at three times of the oscillation period of the maximum distance that is of interest (Edwards and Stoll, 2018):

$$\tau_{\mathrm{truncation}} = 3\frac{\left(\frac{r_{\mathrm{max}}}{\mathrm{nm}}\right)^3}{52\ \mathrm{MHz}}. \qquad (13)$$

This corresponds to roughly three dipolar oscillations in the form factor. In this case of a distance at 5.1 nm this is equivalent to a truncation time $\tau_{\mathrm{truncation}} \approx 7\ \mu\mathrm{s}$. A simulation with a model distance reveals that in order to obtain the correct width of the distance distribution, a good MNR up to this time point can be necessary and a good MNR of only the first part of the form factor is not as reliable when the credibility of the obtained distance distribution is to be estimated. The details of this study can be found in S2.

3.1 Performance comparison for rectangular and Gaussian pulses

The pump pulse frequency was set to 34.00 GHz which is the maximum of the resonator profile (Fig. 2a). The magnetic field was set such that we pumped on the maximum of the nitroxide spectrum (Fig. 2b). To optimise the settings for RR and GG we tested observer pulses with a frequency offset of 90 MHz and 70 MHz between the pump and observer pulse, respectively. To check for different excitation profile widths of the observer pulse, we tested settings with an observer pulse amplitude of 100 % and 60 %. The pulse length was always adjusted to get $\pi/2$ and π pulses. The observer pulse lengths for both tested frequency offsets were identical in all experiments owing to the similar values of the resonator profile at both observer frequencies (33.91 GHz and 33.93 GHz, Fig. 2a). For rectangular observer pulses the pulse lengths were 28 ns and 32 ns, for Gaussian observer pulses, they were 56 ns and 74 ns. For the pump pulse we kept the amplitude fixed at 100 %, which resulted in pulse lengths of 16 ns for rectangular and 34 ns for Gaussian pulses. As we used Gaussian pulses that were generated by Xepr, the

FWHM of the Gaussian pulses was automatically defined by the software as FWHM $= \frac{t_p}{2\sqrt{2\ln(2)}}$ and we did not optimise this parameter. An overview over all observer pulse settings can be found in Table S1 and S2.

For optimum observation of the spin echo modulation in DEER traces, it has been suggested to record the echo in transient mode and then perform a digital integration over a product of the recorded echo with a Gaussian filter (Pribitzer et al., 2017). This procedure is not ideal for commercial spectrometers as the transient recording of the echo drastically increases the spectrometer overhead time. Therefore, we performed a direct integration of the spin echo. We optimised the integration window for each parameter set for a maximum MNR by recording a series of Hahn echoes. ~~Compared with commonly used integration lengths equal to the π pulse length for rectangular pulses (Jeschke, 2007)~~Compared with commonly used integration lengths equal to the π-pulse length for rectangular pulses (Jeschke, 2007b), we find settings where a 14 % increase in the SNR can be achieved by choosing a larger integration window. For Gaussian pulses, we find that it is typically preferable to choose integration windows that are shorter than the π-pulse length. More details can be found in ~~SI 2~~S2.

Table 1: The rectangular and Gaussian pulses with the best performance.

Pulse Type	Offset [MHz]	Obs. Amp. [%]	MNR	Mod depth λ
RR	70	60	35	0.31
GG	70	100	41	0.31

The best MNR for the setting RR was found to be 35 (Table 1). It was achieved for an offset of 70 MHz and 60 % intensity. The best MNR for GG was 41 at an offset of 70 MHz as well and a pulse amplitude of 100 % (Table 1). This corresponds to a 17 % increase in the MNR of Gaussian pulses compared to rectangular pulses. This is in contrast to the findings of (Teucher and Bordignon, 2018), who found that Gaussian observer pulses have a slightly lower MNR that rectangular pulses. The exact reason for the deviating results is not entirely clear to us, we assume that this is due to their different setup with a homebuilt-resonator that that has slightly different properties as our commercial one.

As expected, the missing sidebands of the Gaussian pulses allow the usage of higher pulse amplitudes. This hints that for the chosen parameters the pulse overlap is indeed a limiting factor for rectangular pulses. The modulation depth for RR and GG is approximately 30 % in both cases, but Gaussian pulses seem to have the advantage of a higher echo intensity, probably due to a lower pulse overlap. For RR and GG, the small offset of 70 MHz performed better than a larger offset of 90 MHz most likely due to the different echo intensities at the corresponding positions in the EPR spectrum (Fig. 2b). The results for all RR and GG setting can be found in the tables S3 and S4.

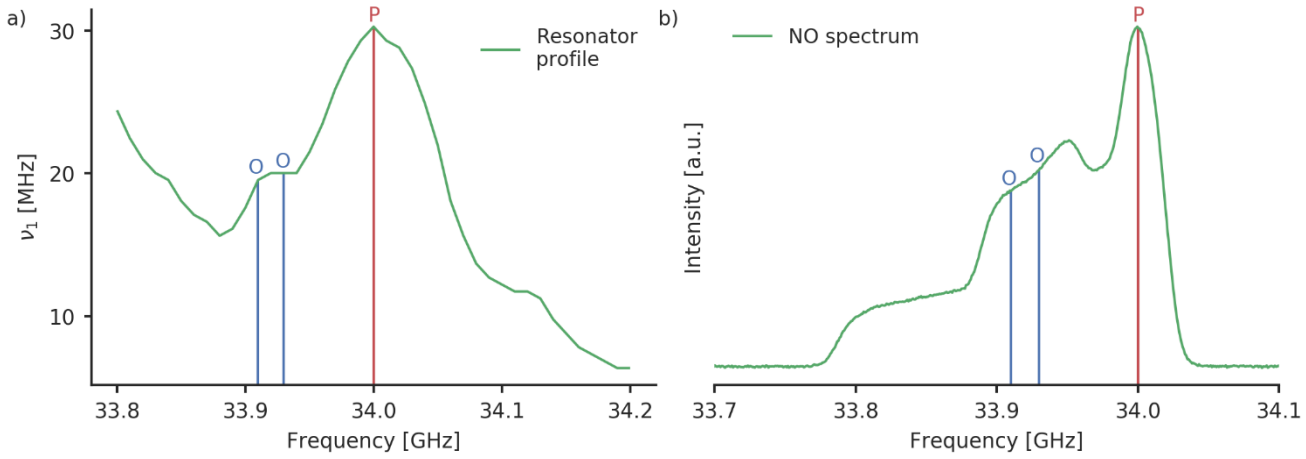

Figure 2: (a) Resonator profile with both tested observer frequencies (blue) and the pump (red) frequencies for the rectangular pulses and (b) the nitroxide spectrum with the positions of the two tested observer frequencies and the pump frequency.

3.2 Broadband shaped pulses

We set out to investigate several broadband shaped pulses, i.e. chirp, WURST, HS{1,1} and HS{1,6} pulses for the settings RS and GS. Unless specified otherwise we used pump pulse lengths of 100 ns. According to Eq. (6), the pulse length of 100 ns corresponds to a minimum accessible distance of $r_{\mathrm{min}} = 2.75$ nm. For the determination of shorter distances we also tested chirp pulses with a length of 36 ns (referred to as short chirp pulses below), which corresponds to a distance of $r_{\mathrm{min}} = 1.96$ nm. Such a distance limit should be suitable for most practical applications. ~~Furthermore, the spins~~Despite the fact that longer broadband shaped pump pulses should give higher inversion efficiencies, we found that they do not result in a better performance for DEER. As the minimum accessible distance also increases when longer pump pulses are used, we did not test pump pulses longer than 100 ns. This is discussed in more detail in S13.

Spins are not flipped within the whole pulse duration but only a smaller fraction of it (Spindler Philipp E. et al., 2013). Simulations with an HS{1,1} pulse with a length of $t_p = 100$ ns, a frequency sweep width of $\Delta f = 110$ MHz and $\beta = 8/t_p$ show distances up to $r_{\mathrm{min}} = 2.32$ nm could be detectable (~~SI 6~~see S7). It is, however, hard to generalise this effect as the spin trajectories for different broadband pulses are not necessarily the same.

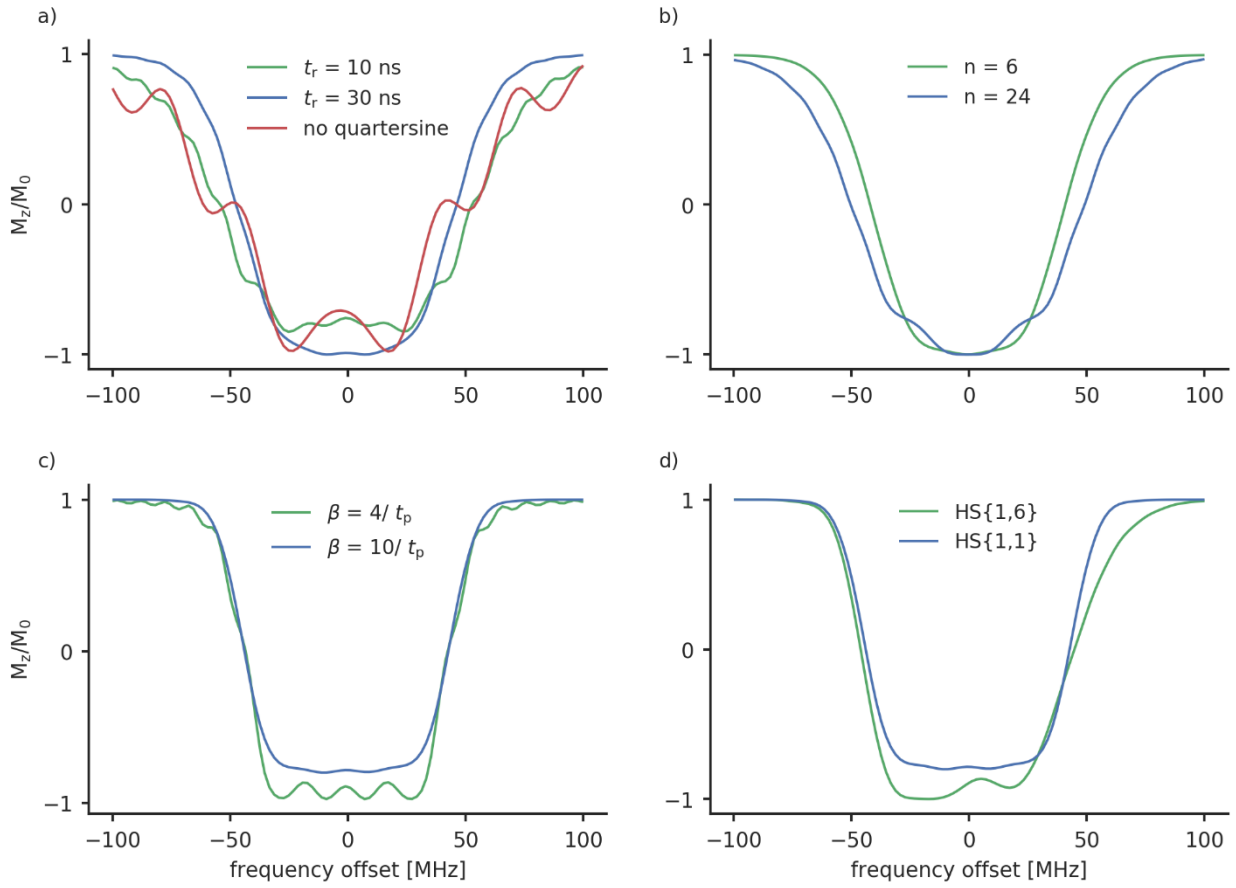

Figure 3: Calculated inversion profiles of broadband pulses normalised to ν_1 = 30 MHz, which corresponds to the maximum of the measured resonator profile. a) Chirp pulses with a frequency width of 120 MHz, a length of 100 ns and a rising time of 10 ns (green), a rising time of 30 ns (blue), a length of 36 ns and no quarter- sine smoothing (red). b) WURST pulses with a frequency width of 120 MHz, a pulse length of 100 ns and a value for n of 6 (green) and 24 (blue). c) HS{1,1} pulses with a frequency width of 90 MHz and a truncation parameter of 4 (green) and 10 (blue). d) An HS{1,6} (green) and HS{1,1} (blue) pulse with a width of 90 MHz and a pulse length of 100 ns. The truncation parameter was 10 in both cases.

Figure 3 shows the calculated excitation profiles of some of the tested pulses. The calculated excitation profiles are normalised to a ν_1 field strength of 30 MHz, which we achieved with our setup at the maximum of the resonator profile. Under such conditions, the long chirp pulses have an adiabaticity of around 5, i.e. ~~A~~a chirp pulse with a length of 100 ns, a sweep width of 120 MHz and a ν_1 strength of 30 MHz has a calculated adiabaticity of 4.7. A short chirp pulse with a length of 36 ns (and otherwise unchanged parameters) has an adiabaticity of 1.7 due to the higher frequency sweep rate. Although this value is rather low, the calculations show that short chirp pulses achieve a nearly complete inversion efficiency around the maximum of the excitation profile (Fig. 3a). On the other hand, the excitation profile is rather broad with many sidebands. The finite length of the pulses creates an additional distortion. By smoothing the edge with a quarter sine, this disturbance can be reduced (Fig. 3a). A higher rising time will lead to a more properly defined excitation profile with fewer sidebands but the overall width of the excitation profile is reduced (see Fig. 3a).

WURST pulses (Fig. 3b) are characterised by an additional parameter n. A high value of n results in a more rectangular shape of the pulse and leads to distortions in the excitation profile around the maximum ~~(Kupce and Freeman, 1995b, 1995a; O'Dell, 2013)~~(Kupce and Freeman, 1995b, 1995a; O'Dell, 2013). Small values of n lead to excitation profiles with very steep and well defined side flanks. However, for small n very long pulse durations are needed to achieve a high inversion efficiency. As long

pulses are not feasible, because they limit the minimum distances that can be resolved, we chose to stick to 100 ns pulses and test the values for n of 6, 12 and 24, for which a reasonable excitation profile can be expected (Fig. 3b).

In Fig. 3c we show the comparison of the excitation profile of HS{1,1} pulses for a truncation parameter of $\beta = 4/t_p$ and $\beta = 10/t_p$. For $\beta = 10/t_p$ the inversion efficiency is smaller than for $\beta = 4/t_p$, however, the excitation profile is well defined and does not show the sideband oscillations that can be seen for the latter.

Owing to their higher adiabaticity, HS{1,6} pulses feature higher inversion efficiency than HS{1,1} pulses with otherwise equal parameters (Fig. 3d), while maintaining the steep frequency flank towards the observer profile at the lower frequency end.

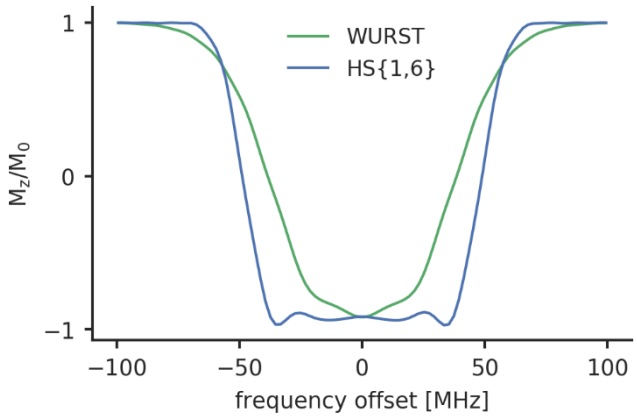

Figure 4: Calculated inversion profiles of a WURST (n = 12, green) and a HS{1,6} (truncation parameter of $6/t_p$, blue) pulse with a pulse length of 100 ns and a sweep width of 100 MHz normalised to ν_1 = 30 MHz, which corresponds to the maximum of the measured resonator profile.

For HS{1,1} and HS{1,6} pulses a frequency sweep width of 50 MHz to 110 MHz were tested. WURST and chirp pulses tend to have a narrower excitation profiles for a given frequency sweep width at the tested parameters (see Fig 4). We therefore chose to use higher frequency sweep widths for WURST than for HS pulses to achieve a similar excitation bandwidth.

As the bandwidth of the resonator and the width of the spectrum is limited, there is an optimum offset between the two pulses that minimises the overlap but is not too large for the resonator bandwidth. We tested offsets from a range of 70 MHz to 130 MHz. The offset is defined as the difference between the observer frequency and the centre of the frequency sweep of the broadband shaped pulses. For the optimisation measurements, the frequency of the observer channel was fixed and the frequency of the pump pulse was changed stepwise. We shifted the magnetic field with the pump pulse so that we always pumped on the maximum of the spectrum (see ~~SI-1~~S1). During the increase of the offset, the position of the observer pulses in the spectrum will change as the spectrum is shifted with the pump pulse resulting in a decrease of the echo for higher offsets. Table 2 shows an overview over all tested pump pulse parameter sets.

Table 2: The parameters for the broadband shaped pump pulses.

Pulse type	Length [ns]	Frequency width [MHz]	Offset [MHz]	additional parameter
chirp	100	80, 120, 160 200	70-130	$t_r = \frac{t_p}{4}$, 10 ns, 30 ns
short chirp	36	80, 120,160, 200	70-130	$t_r = \frac{t_p}{4}$, 10 ns, 30 ns and without quarter sine smoothing
WURST	100	80, 120, 160, 200	70-130	$n = 6, 12, 24$
HS{1,1}	100	50, 70, 90, 110	70-130	$\beta = 4/t_p, 6/t_p, 8/t_p, 10/t_p$
HS{1,6}	100	50, 70, 90, 110	70-130	$\beta = 4/t_p, 6/t_p, 8/t_p, 10/t_p$

We used the same parameters for the observer pulses as before, meaning that we tried rectangular and Gaussian observer pulses at a microwave frequency of 33.91 GHz and 33.93 GHz at 100 % and 60 % amplitude, respectively, (see Tables S1 and S2) and combined them with all the broadband shaped pulses from Table 2. This results in 504 different settings (Table 2) for the pump pulse and 8 different settings for the observer pulses, which gives a total of 4032 different DEER settings. As the measurement of full DEER traces and subsequent determination of the MNR would be very time consuming we used the η_{2P} parameter as an estimation for the MNR. This was suggested by (Doll et al., 2015) and already used by other authors (Spindler Philipp E. et al., 2013; Tait and Stoll, 2016). As it requires only two points of the DEER trace, the measurement time can be drastically reduced. However, it has the disadvantage that artefacts, e.g. echo crossing artefacts or nuclear modulation might remain undetected. Therefore, we decided to additionally perform phase cycling and nuclear modulation averaging. For different observer pulse settings, the η_{2P} parameters are not necessarily comparable, because η_{2P} assumes a constant absolute noise level. However, this noise level could change with different integration windows. Hence, we identified the best chirp, WURST, HS{1,1} and HS{1,6} pulse for each observer pulse setting and recorded full DEER traces of them, giving a total number of 16 traces of the type RS and GS each.

Exemplary heat maps showing the η_{2p} for Gaussian observer pulses and 100 ns pump pulses can be found in Fig. 5. We could identify several trends that were true for all observer pulse settings. HS{1,1} and HS{1,6} pulses have higher maximum η_{2p} values than chirp and WURST pulses. HS{1,1} and HS{1,6} have their highest η_{2p} values for smaller offsets than chirp and WURST pulses. This fits to the steeper flanks in their excitation profiles and a resulting smaller overlap with the observer frequency. Nonetheless, the overall range of reasonable offsets for all pulses is rather small and within a range of 80 MHz and 100 MHz, meaning that for nitroxide-nitroxide DEER and our setup the width of the spectrum and the resonator profile has a more crucial influence in choosing the right offset than the excitation profiles of the different pump pulses. HS{1,1} and HS{1,6} pulses have smaller ideal frequency widths of 90 MHz and 110 MHz, whereas for chirp and WURST pulses the frequency widths seem to be ideal at 120 MHz and 160 MHz. This fits to the already mentioned observation, that WURST pulses have smaller excitation profiles for a given sweep width with the used parameters than HS{1,1} and HS{1,6} pulses (see Fig. 4). Interestingly, despite their lower adiabaticity the short chirp pulses with a length of 36 ns had a larger η_{2p} value than the chirps with a length of 100 ns for all observer pulse settings. ~~Generally, we noticed that longer pump pulses lead to a reduction in the echo intensity (see also SI 13).~~ Quarter sine smoothing does not necessarily lead to a better performance of the short chirp pulses. For the WURST pulses, a value of $n = 6$ gives the best performance with all observer pulses. For different observer pulses, we find that the best performance of HS{1,1} and HS{1,6} pulses can be achieved with β parameters ranging from $6/t_p$ to $10/t_p$.

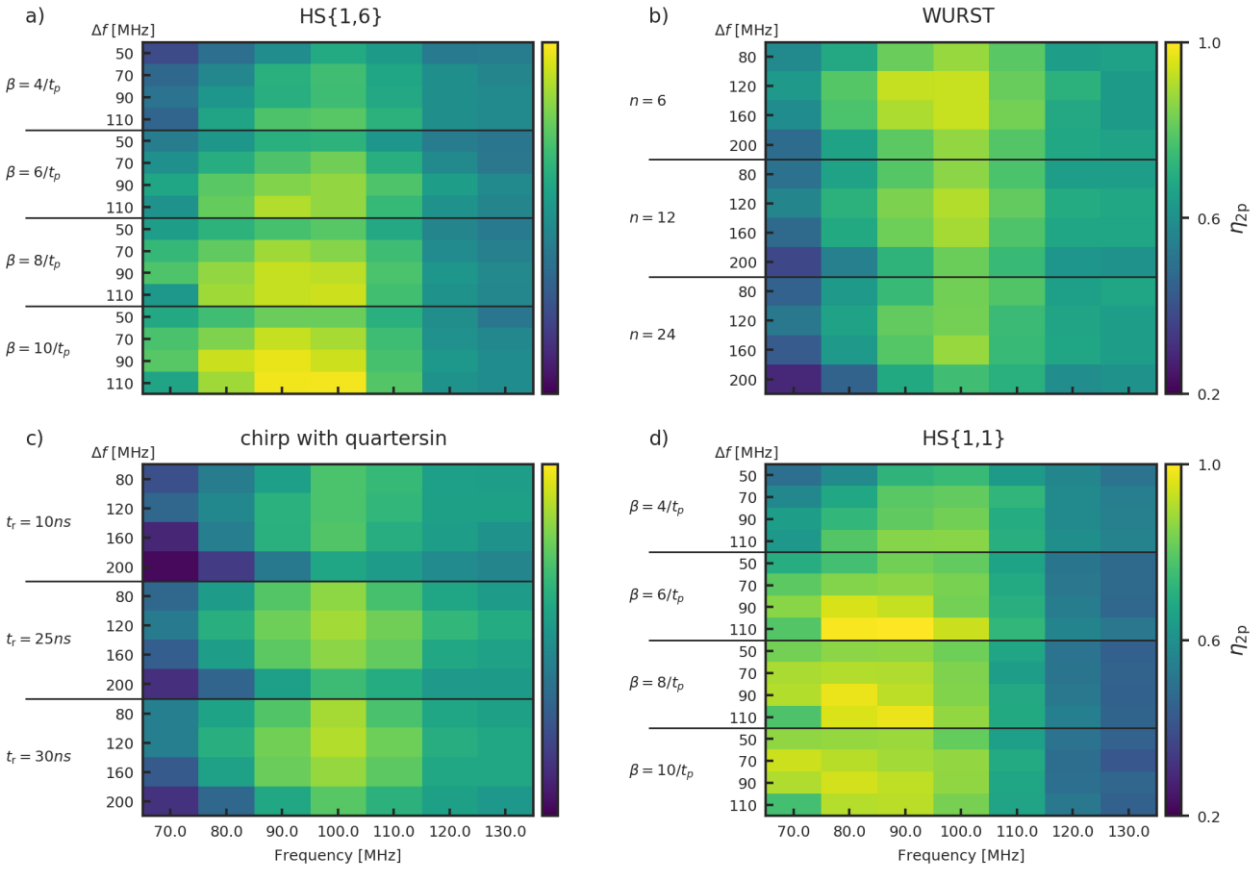

Figure 5: Heat maps with the η_{2p}- values for 4p-DEER measurements with an observer pulse length of 56 ns, Gaussian pulses and an integration window of 56 ns. The observer frequency is at 33.93 GHz. The pump pulse length is 100 ns. Each heat map shows a different pump pulse type:– (a) HS{1,6}, (b)WURST , (c) chirp with quarter sine, and (d) HS{1,1}.

For all observer pulse settings, we identified the best parameter set for each pulse family resulting in a maximised η_{2p}. We then recorded a full DEER trace for each family and compared them by their MNRs. All results for the full DEER traces can be found in Tables S5 and S6. Table 2 shows the parameters and observer pulses that resulted in the best performing chirp, WURST, HS{1,1} and HS{1,6} pulses for the full DEER traces. We found that also for broadband shaped pump pulses Gaussian observer pulses outperform rectangular ones. Again, this hints that Gaussian observer pulses can successfully reduce the frequency overlap with the pump pulse due to their missing sidebands. In all scenarios we found that an observer pulse that is positioned with a 70 MHz offset to the maximum of the resonator profile performs better than an observer pulse position with a 90 MHz offset to the maximum of the resonator profile. The offset to the broadband shaped pump pulse, however, does not change on average, which means that in the former case the observer and pump pulse have a more symmetric positioning around the maximum.

Table 3: The parameters of the observer and pump pulse that gave the best MNR for each pump pulse type. All observer pulses are Gaussian pulses with a pulse length of 74 ns for a 60 % intensity and 56 ns for a 100 % intensity. The observer frequency was 33.93 GHz in all cases. The MNR was evaluated up to 7 µs.

Pump pulse	**Obs. Amp. [%]**	**t_π [ns]**	**Δf [MHz]**	**Offset [MHz]**	**MNR**	**Mod depth λ**
HS{1,6} ($\beta = 10/t_p$)	60	100	110	90	45	0.61

WURST (n=6)	60	100	160	90	40	0.63
Chirp (no smoothing)	100	36	120	80	45	0.49
HS{1,1} ($\beta = 8/t_p$)	100	100	110	90	50	0.52

Broadband shaped pump pulses lead to a larger modulation depth as rectangular and Gaussian pulses. Whereas for non-broadband pulses the modulation depth is limited to around 30 % with our setup, we achieved an increase of up to 63 % with WURST pulses. HS{1,6} pulses also lead to high modulation depths of 61 %. For chirp and HS{1,1} pulses smaller modulation depths of approx. 50 % were observed. However, the highest modulation depth will not necessarily lead to the highest MNR as can be seen in Table 3. This is due to a larger background decay of pulses with a higher inversion efficiency and will be analysed in the next section. Due to a higher bandwidth overlap, broadband shaped pulses will also reduce the echo intensity stronger than rectangular or Gaussian pulses. HS{1,1} pulses seem to be a good compromise between a high modulation depth, a high echo intensity and a background decay that is not too steep. They resulted in the highest MNR of 50 with a pulse length of 100 ns, an offset of 90 MHz, a frequency bandwidth of 110 MHz and $\beta = 8/t_p$ with the observer pulses being Gaussian pulses with an amplitude of 100 % and a frequency of 33.93 GHz. Interestingly, this performance is achieved although the broadband pulse does not achieve a complete inversion (Fig. ~~S6d~~S8d). The modulation depth in that case increased to 52 % (Fig. ~~S8~~S11). This corresponds to an MNR increase of 43 % compared to RR and 22 % compared to GG. To estimate the lower limit of distances that can be determined with such a 100 ns pulse, we performed a simulation to see when the spins are actually flipped during the experiment (see ~~S12). Most~~S7). A visual inspection reveals that most spins are flipped between 20 ns and 80 ns within the pulse duration, making it an effective length of 60 ns where the spins flips occurs, which would correspond to a minimum detectable distance limit of 2.3 nm instead of 2.8 nm for a 100 ns spin flip period.

~~The comparison of pulses with and without bandwidth compensation as suggested by (Doll et al., 2013) showed that a bandwidth compensation does not give a significant advantage in the η_{2p} value under our conditions (S11). This is probably due to the rather flat resonator profile in the region with maximum sensitivity where the pump pulse is applied.~~

~~We have also compared broadband pulses with a length of 100 ns and 200 ns (see SI 12). The 200 ns pulses seem to perform worse for most pulse types than the 100 ns pulses. Particularly, we observed that a longer pump pulse can reduce the echo intensity (see SI 13). As the reason is not absolutely clear to us for now, we decided to stick to 100 ns pulses.~~

Depending on the resonator and the microwave amplifier, different B_1 field strengths are available on different spectrometers. However, as the inversion efficiency of broadband shaped pulses is less dependent on the B_1 field strength as is the case for rectangular and Gaussian pulses, who always require a proper adjustment of the pulse length, we assume the findings here to be rather generalisable. In order to discuss this more quantitatively we simulated inversion profiles of the best performing pulses from Table 3 for B_1 field strengths.

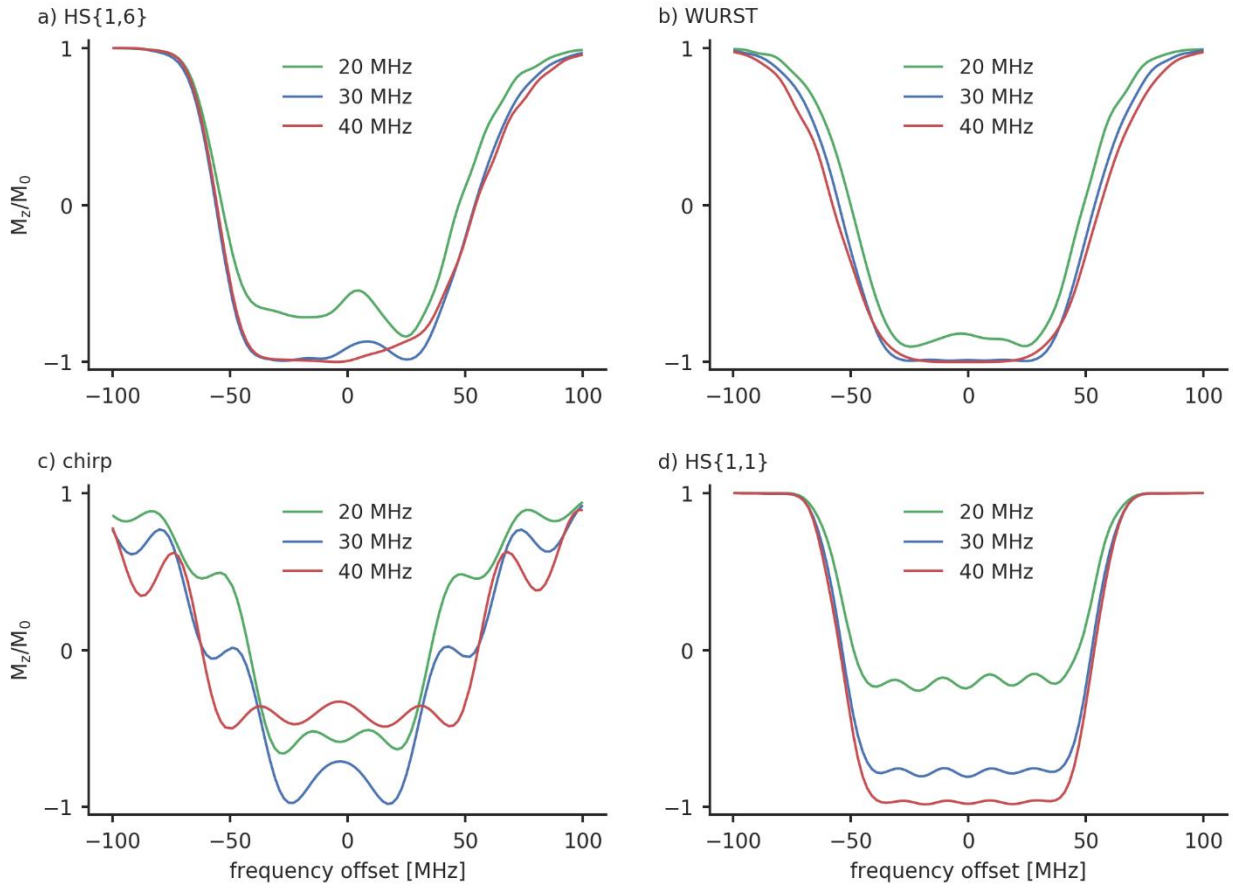

Figure 6: The inversion profiles of the best performing (a) HS{1,6}, (b) WURST, (c) chirp and (d) HS{1,1} pulses with the parameters from Table 3. They were simulated with a B_1 field strength of 20 MHZ (green), 30 MHz (blue) and 40 MHz (red). These field strengths correspond to a π-pulse lengths of 25.0 ns, 16.7 ns (which approximately correspond our setup) and 12.5 ns. The B_1 field here is depicted as the Rabi frequency.

We compare the pulse profiles with B_1 = 30 MHz, which corresponds our setup, with the cases where a lower (B_1 = 20 MHz) or higher (B_1 = 40 MHz) B_1 field strengths are reached. Figure 6 shows how the different pulses behave, when different B_1 field strengths are used. The WURST pulse (Fig. 6b) shows the least variation for different B_1 field strengths. As expected the inversion efficiency drops a little bit for B_1 = 20 MHz. But this drop seems to be rather insignificant and good modulation depths can still be expected. The decrease in inversion efficiency is a bit more significant for the HS{1,6} pulse so that a small

reduction in the modulation depth is possible here. Both pulse profiles do not show significant changes when a higher B_1 field strength is used. The HS{1,1} pulse has a massive drop in inversion efficiency when going to lower B_1 field strengths. This comes not as a surprise as the inversion efficiency is already incomplete at B_1 = 30 MHz. Here, it might be advantageous to reduce the β parameter of the HS{1,1} pulse. As it has been stated earlier this will increase the inversion efficiency. For a higher B_1 field strength of B_1 = 40 MHz the inversion efficiency of this HS{1,1} will increase. Therefore, a higher modulation depth comparable to the HS{1,1} pulse is expected. As this will also increase the background decay, a higher MNR is not guaranteed. The chirp pulse also shows a rather strong decrease in the inversion efficiency for a B_1 = 20 MHz. However, the inversion efficiency also decreased for a higher B_1 field strength of B_1 = 40 MHz. This rather unexpected behaviour is probably caused by an insufficient smoothing of the edges of the chirp pulse. With higher B_1 field strength the initial effective magnetic field vector in the accelerated frame becomes less aligned with the z-axis. Therefore, smoothing becomes more important. In Fig. S10, we compared the inversion profiles of 36 ns and 100 ns chirp pulses with and without quarter sine smoothing. When quarter sine smoothing is applied, chirp pulses can with a length of 36 ns indeed reach a high inversion efficiency with B_1 = 40 MHz. (Fig. S10b). As the width of the inversion profile of this chirp pulse drops significantly for smaller B_1 field strengths, it is only advisable to implement a quarter sine smoothing with chirp pulses of a length of 36 ns when enough microwave power is available. The situation looks different for chirp pulses with a pulse length of 100 ns. Here, the inversion profile looks very similar for all tested B_1 field strengths. Particularly for smaller B_1 field strengths we expect 100 ns chirp pulses to outperform chirp pulses with a length of 36 ns.

Another crucial parameter for DEER measurements that can vary from setup to setup is the width of the resonator profile. Here, we have a FWHM of approximately 200 MHz. Larger widths do not seem to be necessary because they would exceed the width of the spectrum of the nitroxide. If only a smaller width is available, the offset between pump and observer pulses might need to be reduced. This would increase the overlap between the observer and pump pulses. This problem could be overcome by either using longer pump pulses or reducing the frequency width of the broadband shaped pulses. As a narrower resonator profile is also necessarily steeper, it might also be necessary to perform a resonator bandwidth compensation as suggested by (Doll et al., 2013). Performing a resonator bandwidth compensation with our setup does not give a significant advantage in the η_{2p} value (see S15). This is probably due to the rather flat resonator profile in the region with maximum sensitivity where the pump pulse is applied.

3.3 Background behaviour

~~As stated by equation (10) the measured raw data does not only consist of the desired form factor but includes a background contribution emerging from intermolecular interactions. A common way to deal with this, is to fit the background according to equation (11) and divide the raw data by the fit to obtain the form factor that can then be transformed into a distance distribution (Jeschke, 2012; Jeschke et al., 2006).~~ ~~This method, however, leads to an increase in the noise level towards the end of the trace which can significantly disturb the reliability of the distance distribution, as recently shown by (Fábregas Ibáñez and Jeschke, 2020). They suggested alternative methods to correct for the background. We will, however, limit this discussion to a background correction method by division as it is very common.~~

The broader excitation profile of broadband shaped pulses will ~~also~~ increase the background decay which results in a higher noise level of broadband shaped pump pulses compared to rectangular or Gaussian pump pulses. We find an approximately linear relation between the modulation depth and the background decay (~~SI 17~~see S19). To investigate this effect more deeply

we evaluated the MNR of the experimental DEER form factors excluding the later part of the form factor and only taking into account the first part up to a truncation time $\tau_{\mathrm{truncation}}$. Truncation the DEER trace will not change the modulation depth, but due to the background decay, the noise level will be different. Figure ~~6~~7 shows the MNR of broadband pulses as a function of the truncation time $\tau_{\mathrm{truncation}}$. As expected, the MNR decreases with increasing $\tau_{\mathrm{truncation}}$ for all pulses, because of the increase of the noise. However, the rate of the decrease in MNR is different for different pulse types, which means that the relative performance of the pulses also depends on the length of the DEER trace and therefore on the distance between the spin centres that is supposed to be measured.

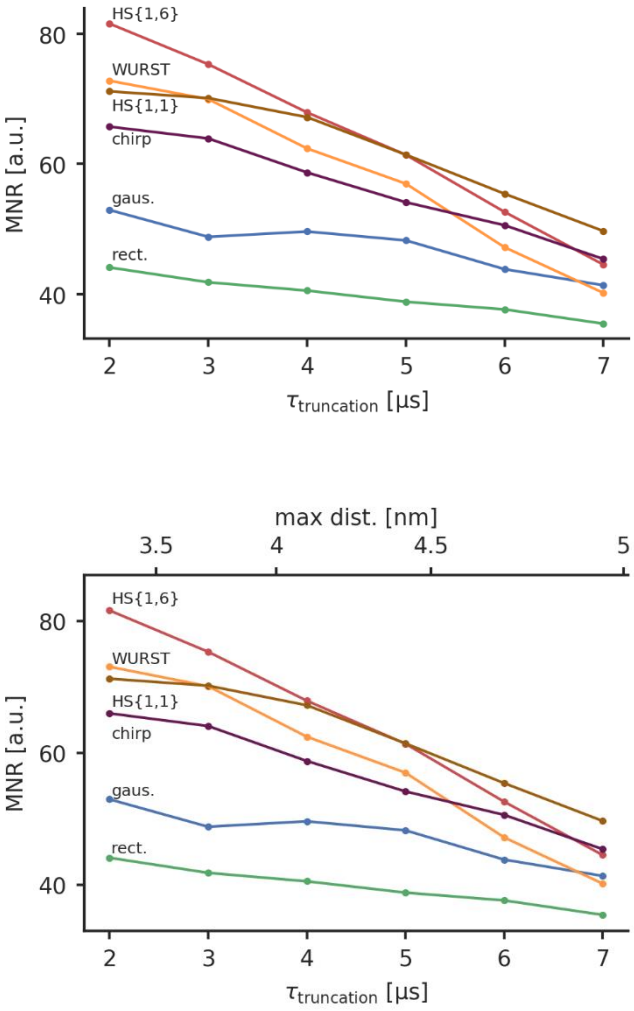

Figure ~~6~~7: The MNR value as a function of the dipolar evolution time up to which the noise has been evaluated, i.e. the truncation time $\tau_{\mathrm{truncation}}$. The sample has a concentration of 80 µM of spin-labelled ligand. The maximum distance according to equation (13) is depicted in the upper x-axis. The line between the points is only a guidance for the eyes.

It turns out that HS{1,6} and WURST pulses with their higher modulation depths have the highest MNR for short DEER traces, whereas for longer traces HS{1,1} and chirp pulses are better. The background decay seems to play a decisive role for the MNR and the pulses resulting in a high modulation depth also have a larger background decay. As the background decay causes the noise level to increase with increasing dipolar evolution time, its influence is less pronounced for short DEER traces,

where the high modulation depth seems to be leading to a high MNR. For longer traces, a high modulation depth is linked to a strong background decay and a high noise level towards the end of the trace. Therefore, the MNR of pump pulses generating a high modulation depth decreases stronger than for pulses effecting a smaller modulation depth. This means that HS{1,1} and chirp pulses perform better for longer traces.

As rectangular and Gaussian pump pulses have rather small modulation depths, the corresponding decrease of the MNR due to the background decay is also rather small, that means that the improvement achievable with broadband shaped pulses is greater for shorter DEER traces. For short truncation times $\tau_{\text{truncation}}$ of 2 µs we observe an increase in MNR from 44 for rectangular pulses (RR) to 82 for the best broadband shaped pulse (RS), which was an HS{1,6} pulse in this case. This corresponds to an increase of 86 %. For long truncation times $\tau_{\text{truncation}}$ of 7 µs, this increase goes down to 43 %. This means that the MNR improvement that can be achieved by broadband shaped pulses can be drastically dependent on the length of the measured DEER trace and therefore on the distance range to be covered by the measurement. For a concentration of 80 µM, a high MNR improvement can be achieved if the maximum distance of interest is below 4 nm with pulse that achieves a high modulation depth. This would correspond to the HS{1,6} and WURST pulse in this case. If longer distances up to 5 nm shall be detected, it seems to be advantageous to use pulses that might not give the highest modulation depth in order to reduce the background decay. An extrapolation for higher truncation times shows that if even longer distances are of interest, broadband shaped pulses will not give a better MNR compared to rectangular pulses. Here, it is necessary to reduce the background decay by using lower concentrations.

The performance of all the pulses at $\tau_{\text{truncation}} = 2$ µs can be found in Tables S7-S10. The chirp, WURST, HS{1,1} and HS{1,6} pulse resulting in the best MNR are summarized in Table 4. For the broadband shaped pulses there were some minor changes in the parameters that gave the MNR when the truncation time was set to a shorter value of $t_{\text{truncation}} = 2$ µs. For RR and GG there were changes in the best parameter settings.

Table 4: The parameters of the observer and pump pulse resulting in the best MNR for each pulse type when the MNR was evaluated up to $\tau_{\text{truncation}}$ ~~= 2µs~~ = 2 µs. All observer pulses are Gaussian pulses with a pulse length of 74 ns for 60 % intensity and 56 ns for 100 % intensity. The observer frequency was 33.93 GHz for all pulses.

Pump pulse	**Obs. Amp. [%]**	t_π **[ns]**	Δf **[MHz]**	**Offset [MHz]**	**MNR**	**Mod depth** λ
HS{1,6} ($\beta = 10/t_p$)	60	100	110	90	82	0.61
WURST (n=6)	100	100	160	90	73	0.63
Chirp (no smoothing)	100	36	120	80	65	0.49
HS{1,1} ($\beta = 8/t_p$)	60	100	110	80	74	0.52

~~The background correction by division is particularly susceptible for a steep background decay and other methods give more reliable distance distributions even if the background decay is high (Fábregas Ibáñez and Jeschke, 2020). Hence, the MNR values determined here cannot be directly converted in the reliability of the determined distance distribution, because this does~~

~~additionally depend on the method that is used for background correction. However, all proposed methods suffer from less reliable distance distributions when the background decay gets higher, so the underlying problem is always present.~~

3.4 Concentration dependence

To check for a concentration dependent performance of broadband shaped pulses we also prepared a sample with a lower concentration of 30 µM ligand and 60 µM WGA and performed DEER measurements with the optimised parameter settings for the short chirp, WURST, HS{1,1} and HS{1,6} pulses. We did, however, not check observer frequencies of 33.91 GHz, since they always performed worse than an observer position of 33.93 GHz. For RR we tested an offset of 70 MHz and 60 % intensity, for GG we tested an offset of 70 MHz as well, but an intensity of 100 %, as these settings performed best before.

This sample showed almost no background for all used pump pulses (see SI ~~18~~12). As the influence of the background is minimised due to the low concentration we expected to find the trends in the MNR as for the case of the high concentrated samples and short truncation times. Figure ~~7~~8 shows the MNR as function of the truncation time point $\tau_{truncation}$ up to which the noise has been evaluated. As expected, no significant decrease of the MNR with higher truncation times $\tau_{truncation}$ was found. Without a significant background the noise towards the end of the background-corrected form factor does not increase significantly. The decrease of the MNR found for the high concentration sample was therefore not observed here. For some pulses there is a slight increase in the MNR with the truncation time, however, we assigned this behaviour to a numerical uncertainty in the analysis.

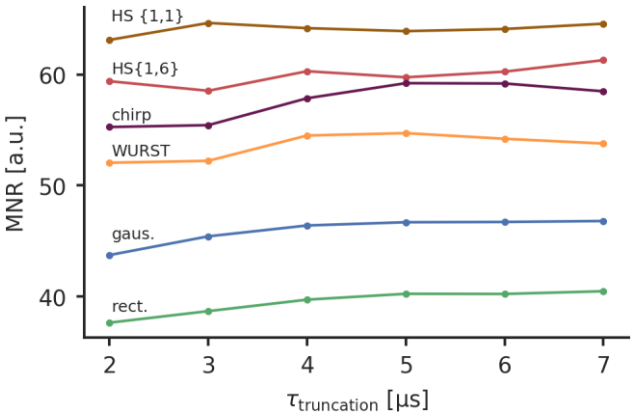

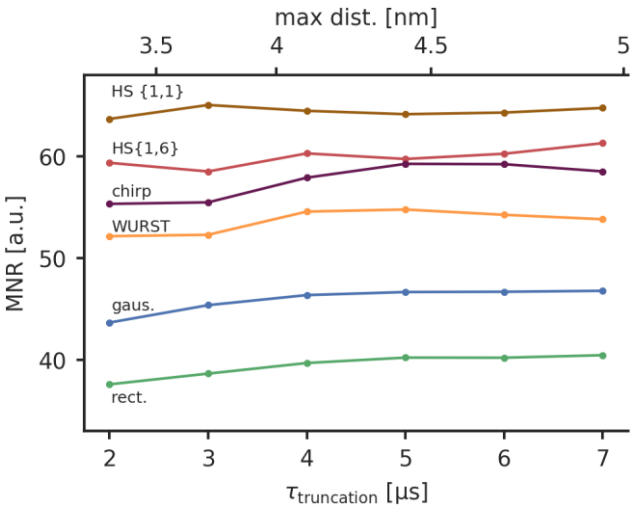

Figure ~~7~~8: The MNR as a function of the dipolar evolution time up to which the noise has been evaluated. The sample has a concentration of 30 µM of spin-labelled ligand. The maximum distance according to equation (13) is depicted in the upper x-axis. The line between the points is only a guidance for the eyes.

Table 5: The parameters of the observer and pump pulse resulting in the best MNR for each pulse type. All observer pulses are Gaussian pulses with pulse lengths of 74 ns for 60 % intensity and 56 ns for 100 % intensity. The observer frequency was 33.93 GHz for all pulses. The MNR was evaluated up to 7 µs.

Pump pulse	**Obs. Amp. [%]**	t_π **[ns]**	Δf **[MHz]**	**Offset [MHz]**	**MNR**	**Mod depth** λ
HS{1,6} ($\beta = 10/t_p$)	100	100	110	90	61	0.55
WURST (n=6)	60	100	160	100	54	0.59
Chirp (no smoothing)	100	36	120	80	58	0.46
HS{1,1} ($\beta = 8/t_p$)	100	100	110	90	65	0.47

With the low concentration sample, we found an MNR of 40 and a modulation depth of 31 % for rectangular pulses, for Gaussian pulses we found an MNR of 47 and a modulation depth of 30 %. Thus, also at lower spin concentrations the Gaussian pulses lead to a similar modulation depth as rectangular pulses, but again to an overall higher MNR. Table 5 shows the results for the different broadband shaped pump pulses in combination with the observer pulse with whom they performed best.

Table 5 shows the optimised parameters for the different pump pulses. All results can be found in Table S11. The parameters found for the observer and pump pulses differ slightly from the parameters identified for the high concentration sample, but lie in a similar range.

The broadband shaped pump pulses resulted in a modulation depth that is a bit lower than for the sample with the high concentration. The MNR was lower as well. Furthermore, the order of performance of the different pulse types changed. While we expected HS{1,6} and WURST pulses with their high modulation depths to perform better than HS{1,1} and chirp pulses for a sample less susceptible to background influence, HS{1,1} pulses were actually performing best and WURST pulses were

the worst broadband shaped pulses. HS{1,1} pulses lead to an increase in the MNR of 60 % compared to rectangular pulses. This is also lower than the 86 % increase that was obtained for the 80 µM ligand concentration. The reason for the change of this behaviour is probably a difference in the resonator profile that we noticed compared to the other sample with the higher concentration (see ~~SI 20~~S22). The achieved B_1 field was a bit lower for this sample which changes the performance of the pulses. However, HS{1,1} and HS{1,6} pulses both give a good MNR with a high concentration as well as with a low concentration.

~~We also performed analytical calculations to get a more quantitative estimate for the MNR increase of broadband shaped pulses depending on the trace length and the spin concentration (see SI 19). They show that the latter two have a significant effect on the performance improvement that can be expected when using a broadband shaped pulse. However, for concentrations typically used in DEER experiments, a sensitivity increase can always be expected when using broadband shaped pulses instead of monochromatic pulses.~~

When the MNR shall be increased by using broadband shaped pulses to detect long distances > 5 nm, lower concentrations are preferable as they reduce the enhancement of the background decay. Here, switching to a concentration of 30 µM of the doubly labelled ligand was enough the significantly reduce the influence of the background. In S19 we performed analytical calculations to estimate the potential MNR increase that can be achieved by switching to broadband shaped pulses for different concentrations and distance ranges. For maximum distances below 4 nm an increase of the MNR can be expected for all concentrations up to approximately 100 µM. The situation is different if distances over 6 nm shall be detected. A significant gain can only be expected for smaller concentrations in the range between 10-30 µM. For higher concentrations the MNR gain drops quickly. For higher concentrations in the range of 80 µM a MNR decrease has to be expected in this distance regime. This is discussed in more detail in S21.

4 Conclusion and Outlook

We have compared various broadband shaped pulses as pump pulses for DEER spectroscopy in Q-band performed on samples with nitroxide spin labels and investigated under which circumstances they perform best. By increasing the inversion profile, broadband shaped pulses can increase the modulation depth from 30 % with rectangular pulses up to 60 %. However, with a larger inversion profile of broadband shaped pulses the overlap with the observer pulse and the background decay will also increase. Both of those effects will tend to reduce the MNR. The overall MNR increase will therefore be a compromise between the increase in the modulation depth and the smaller echo and larger background contribution.

Systematic analysis of a trial-and-error optimisation has yielded that the performance of broadband shaped pulses depends on the dipolar evolution time and the concentration of spin centres. Larger dipolar evolution times mean that the background has decayed stronger by the end of the form factor. Pulses with a higher inversion efficiency will produce a larger background decay and their performance decreases stronger for longer traces than for pulses with a smaller inversion efficiency. We found HS{1,1} and HS{1,6} in combination with Gaussian observer pulses to give a good MNR for high as well as low spin concentrations. HS{1,1} have a lower inversion efficiency and therefore a lower modulation depth but they perform better with longer traces~~.~~ needed for longer distances. The exact parameters depend on the setup, but with values of $\beta = 8/t_p$ or $\beta = 10/t_p$, $t_p = 100$ ns, $\Delta f = 110$ MHz and an offset of 80 MHz or 90 MHz we typically achieved good results. If a high modulation depth which is particularly suitable for short distances should be achieved, HS{1,6} and WURST pulses are the

best pulses. Good parameters are $\beta = 10/t_p$, $t_p = 100$ ns, $\Delta f = 110$ MHz and an offset of 90 MHz for HS{1,6} and $n = 6$, t_p= 100 ns, $\Delta f = 160$ MHz and an offset of 90 MHz or 100 MHz for WURST pulses.

5 Data availability

The raw data can be downloaded at ~~https://doi.org/10.5281/zenodo.3660242 (Scherer et al., 2020)~~https://doi.org/10.5281/zenodo.3726735 (Scherer et al., 2020).

6 Author contribution

AS, ST, SW and MD conceived the research idea and designed the conducted experiments. AS conducted the EPR experiments and analysed the results with ST. The spin labelled ligand was synthesised in the lab of VW. AS prepared all the figures and wrote the draft manuscript. All authors discussed the results and revised the manuscript.

7 Competing interests

The authors declare no conflict of interests.

8 Acknowledgements

We thank Philipp Rohse for the synthesis of the spin labelled ligand. Jörg Fischer is thanked for sample preparation. This project has received funding from the European Research Council (ERC) under the European Union's Horizon 2020 research and innovation programme (Grant Agreement number: 772027 — SPICE — ERC-2017-COG). A.S. gratefully acknowledges financial support from the Zukunftskolleg of the University of Konstanz. A.S., S.T. and S.W. gratefully acknowledge financial support from the Konstanz Research School Chemical Biology (KoRS-CB).

9 References

Abdullin, D., Duthie, F., Meyer, A., Müller, E. S., Hagelueken, G. and Schiemann, O.: Comparison of PELDOR and RIDME for Distance Measurements between Nitroxides and Low-Spin Fe(III) Ions, J. Phys. Chem. B, 119(43), 13534–13542, doi:10.1021/acs.jpcb.5b02118, 2015.

Bahrenberg, T., Rosenski, Y., Carmieli, R., Zibzener, K., Qi, M., Frydman, V., Godt, A., Goldfarb, D. and Feintuch, A.: Improved sensitivity for W-band Gd(III)-Gd(III) and nitroxide-nitroxide DEER measurements with shaped pulses, J. Magn. Reson., 283(Supplement C), 1–13, doi:10.1016/j.jmr.2017.08.003, 2017.

Baum, J., Tycko, R. and Pines, A.: Broadband and adiabatic inversion of a two-level system by phase-modulated pulses, Phys. Rev. A, 32(6), 3435, 1985.

~~Bohlen~~Böhlen, J.-M. and Bodenhausen, G.: Experimental Aspects of Chirp NMR Spectroscopy, J. Magn. Reson. A, 102(3), 293–301, doi:10.1006/jmra.1993.1107, 1993.

Borbat, P. P., Georgieva, E. R. and Freed, J. H.: Improved Sensitivity for Long-Distance Measurements in Biomolecules: Five-Pulse Double Electron–Electron Resonance, J. Phys. Chem. Lett., 4(1), 170–175, doi:10.1021/jz301788n, 2013.

Breitgoff, F. D., Soetbeer, J., Doll, A., Jeschke, G. and Polyhach, Y. O.: Artefact suppression in 5-pulse double electron electron resonance for distance distribution measurements, Phys. Chem. Chem. Phys., 19(24), 15766–15779, 2017.

Breitgoff, F. D., Keller, K., Qi, M., Klose, D., Yulikov, M., Godt, A. and Jeschke, G.: UWB DEER and RIDME distance measurements in Cu(II)–Cu(II) spin pairs, J. Magn. Reson., doi:10.1016/j.jmr.2019.07.047, 2019.

Collauto, A., Feintuch, A., Qi, M., Godt, A., Meade, T. and Goldfarb, D.: Gd(III) complexes as paramagnetic tags: Evaluation of the spin delocalization over the nuclei of the ligand, J. Magn. Reson., 263(Supplement C), 156–163, doi:10.1016/j.jmr.2015.12.025, 2016.

Dalaloyan, A., Qi, M., Ruthstein, S., Vega, S., Godt, A., Feintuch, A. and Goldfarb, D.: Gd(iii)-Gd(iii) EPR distance measurements - the range of accessible distances and the impact of zero field splitting, Phys. Chem. Chem. Phys., 17(28), 18464–18476, doi:10.1039/C5CP02602D, 2015.

Deschamps, M., Kervern, G., Massiot, D., Pintacuda, G., Emsley, L. and Grandinetti, P. J.: Superadiabaticity in magnetic resonance, J. Chem. Phys., 129(20), 204110, doi:10.1063/1.3012356, 2008.

Di Valentin, M., Albertini, M., Zurlo, E., Gobbo, M. and Carbonera, D.: Porphyrin Triplet State as a Potential Spin Label for Nanometer Distance Measurements by PELDOR Spectroscopy, J. Am. Chem. Soc., 136(18), 6582–6585, doi:10.1021/ja502615n, 2014.

Doll, A. and Jeschke, G.: Wideband frequency-swept excitation in pulsed EPR spectroscopy, Spec. Issue Methodol. Adv. EPR Spectrosc. Imaging, 280, 46–62, doi:10.1016/j.jmr.2017.01.004, 2017.

Doll, A., Pribitzer, S., Tschaggelar, R. and Jeschke, G.: Adiabatic and fast passage ultra-wideband inversion in pulsed EPR, J. Magn. Reson., 230, 27–39, doi:10.1016/j.jmr.2013.01.002, 2013.

Doll, A., Qi, M., Wili, N., Pribitzer, S., Godt, A. and Jeschke, G.: Gd(III)–Gd(III) distance measurements with chirp pump pulses, J. Magn. Reson., 259(Supplement C), 153–162, doi:10.1016/j.jmr.2015.08.010, 2015.

Doll, A., Qi, M., Godt, A. and Jeschke, G.: CIDME: Short distances measured with long chirp pulses, J. Magn. Reson., 273, 73–82, doi:10.1016/j.jmr.2016.10.011, 2016.

Edwards, T. H. and Stoll, S.: Optimal Tikhonov regularization for DEER spectroscopy, J. Magn. Reson., 288, 58–68, doi:10.1016/j.jmr.2018.01.021, 2018.

Fábregas Ibáñez, L. and Jeschke, G.: Optimal background treatment in dipolar spectroscopy, Phys. Chem. Chem. Phys., 22(4), 1855–1868, doi:10.1039/C9CP06111H, 2020.

Garwood, M. and DelaBarre, L.: The Return of the Frequency Sweep: Designing Adiabatic Pulses for Contemporary NMR, J. Magn. Reson., 153(2), 155–177, doi:10.1006/jmre.2001.2340, 2001.

Grytz, C. M., Kazemi, S., Marko, A., Cekan, P., Guntert, P., Sigurdsson, S. T. and Prisner, T. F.: Determination of helix orientations in a flexible DNA by multi-frequency EPR spectroscopy, Phys. Chem. Chem. Phys., 19(44), 29801–29811, doi:10.1039/C7CP04997H, 2017.

Hintze, C., Bücker, D., Domingo Köhler, S., Jeschke, G. and Drescher, M.: Laser-Induced Magnetic Dipole Spectroscopy, J. Phys. Chem. Lett., 7(12), 2204–2209, doi:10.1021/acs.jpclett.6b00765, 2016.

Hu, P. and Hartmann, S. R.: Theory of spectral diffusion decay using an uncorrelated-sudden-jump model, Phys. Rev. B, 9(1), 1–13, doi:10.1103/PhysRevB.9.1, 1974.

Hubbell, W. L., Gross, A., Langen, R. and Lietzow, M. A.: Recent advances in site-directed spin labeling of proteins, Curr. Opin. Struct. Biol., 8(5), 649–656, doi:10.1016/S0959-440X(98)80158-9, 1998.

Jassoy, J. J., Meyer, A., Spicher, S., Wuebben, C. and Schiemann, O.: Synthesis of Nanometer Sized Bis-and Tris-trityl Model Compounds with Different Extent of Spin–Spin Coupling, Molecules, 23(3), 682, 2018.

Jeschke, G.: Dipolar Spectroscopy–Double-Resonance Methods, eMagRes, 1459–1476, 2007a.

Jeschke, G.: Instrumentation and experimental setup, in ESR spectroscopy in membrane biophysics, vol. 27, edited by M. A. Hemminga and L. Berliner, pp. 17–47, Springer Science & Business Media., 2007b.

Jeschke, G.: DEER Distance Measurements on Proteins, Annu. Rev. Phys. Chem., 63(1), 419–446, doi:10.1146/annurev-physchem-032511-143716, 2012.

Jeschke, G., Bender, A., Paulsen, H., Zimmermann, H. and Godt, A.: Sensitivity enhancement in pulse EPR distance measurements, J. Magn. Reson., 169(1), 1–12, doi:10.1016/j.jmr.2004.03.024, 2004.

Jeschke, G., Chechik, V., Ionita, P., Godt, A., Zimmermann, H., Banham, J., Timmel, C. R., Hilger, D. and Jung, H.: DeerAnalysis2006—a comprehensive software package for analyzing pulsed ELDOR data, Appl. Magn. Reson., 30(3), 473–498, doi:10.1007/BF03166213, 2006.

Kobzar, K., Ehni, S., Skinner, T. E., Glaser, S. J. and Luy, B.: Exploring the limits of broadband 90° and 180° universal rotation pulses, J. Magn. Reson., 225, 142–160, doi:10.1016/j.jmr.2012.09.013, 2012.

~~Kupce~~Kupče, E. and Freeman, R.: Adiabatic Pulses for Wideband Inversion and Broadband Decoupling, J. Magn. Reson. A, 115(2), 273–276, doi:10.1006/jmra.1995.1179, 1995a.

~~Kupce~~Kupče, Ē. and Freeman, R.: Stretched Adiabatic Pulses for Broadband Spin Inversion, J. Magn. Reson. A, 117(2), 246–256, doi:10.1006/jmra.1995.0750, 1995b.

~~Kupce~~Kupče, Ē. and Freeman, R.: Optimized Adiabatic Pulses for Wideband Spin Inversion, J. Magn. Reson. A, 118(2), 299–303, doi:10.1006/jmra.1996.0042, 1996.

Kuzhelev, A. A., Akhmetzyanov, D., Denysenkov, V. P., Krumkacheva, O., Shevelev, G., Bagryanskaya, E. and Prisner, T. F. F.: High-frequency pulsed electron-electron double resonance spectroscopy on DNA duplexes using trityl tags and shaped microwave pulses, Phys. Chem. Chem. Phys., doi:10.1039/C8CP03951H, 2018.

Lovett, J. E., Lovett, B. W. and Harmer, J.: DEER-Stitch: Combining three- and four-pulse DEER measurements for high sensitivity, deadtime free data, J. Magn. Reson., 223, 98–106, doi:10.1016/j.jmr.2012.08.011, 2012.

Mahawaththa, M., Lee, M., Giannoulis, A., Adams, L. A., Feintuch, A., Swarbrick, J., Graham, B., Nitsche, C., Goldfarb, D. and Otting, G.: Small Neutral Gd(III) Tags for Distance Measurements in Proteins by Double Electron-Electron Resonance Experiments, Phys. Chem. Chem. Phys., doi:10.1039/C8CP03532F, 2018.

Mentink-Vigier, F., Collauto, A., Feintuch, A., Kaminker, I., Tarle, V. and Goldfarb, D.: Increasing sensitivity of pulse EPR experiments using echo train detection schemes, J. Magn. Reson., 236, 117–125, doi:10.1016/j.jmr.2013.08.012, 2013.

Milikisiyants, S., Voinov, M. A., Marek, A., Jafarabadi, M., Liu, J., Han, R., Wang, S. and Smirnov, A. I.: Enhancing sensitivity of Double Electron-Electron Resonance (DEER) by using Relaxation-Optimized Acquisition Length Distribution (RELOAD) scheme, J. Magn. Reson., 298, 115–126, doi:10.1016/j.jmr.2018.12.004, 2019.

Milov, A. D., Ponomarev, A. B. and Tsvetkov, Y. D.: Electron-electron double resonance in electron spin echo: Model biradical systems and the sensitized photolysis of decalin, Chem. Phys. Lett., 110(1), 67–72, doi:10.1016/0009-2614(84)80148-7, 1984.

Milov, A.D., Salikhov, K.M. and Shirov, M.D.: Use of the double resonance in electron spin echo method for the study of paramagnetic center spatial distribution in solids., Fiz Tverd Tela, 23(1), 975–982, 1981.

O'Dell, L. A.: The WURST kind of pulses in solid-state NMR, Solid State Nucl. Magn. Reson., 55–56, 28–41, doi:10.1016/j.ssnmr.2013.10.003, 2013.

Pannier, M., Veit, S., Godt, A., Jeschke, G. and Spiess, H. .: Dead-Time Free Measurement of Dipole–Dipole Interactions between Electron Spins, J. Magn. Reson., 142(2), 331–340, doi:10.1006/jmre.1999.1944, 2000.

Polyhach, Y., Bordignon, E., Tschaggelar, R., Gandra, S., Godt, A. and Jeschke, G.: High sensitivity and versatility of the DEER experiment on nitroxide radical pairs at Q-band frequencies, Phys. Chem. Chem. Phys., 14(30), 10762–10773, doi:10.1039/C2CP41520H, 2012.

Pribitzer, S., Sajid, M., Hülsmann, M., Godt, A. and Jeschke, G.: Pulsed triple electron resonance (TRIER) for dipolar correlation spectroscopy, J. Magn. Reson., 282, 119–128, doi:10.1016/j.jmr.2017.07.012, 2017.

Robotta Marta, Gerding Hanne R., Vogel Antonia, Hauser Karin, Schildknecht Stefan, Karreman Christiaan, Leist Marcel, Subramaniam Vinod and Drescher Malte: Alpha-Synuclein Binds to the Inner Membrane of Mitochondria in an α-Helical Conformation, ChemBioChem, 15(17), 2499–2502, doi:10.1002/cbic.201402281, 2014.

Scherer, A., Tischlik, S., Weickert, S., Wittmann, V. and Drescher, M.: Raw data for "Optimising broadband pulses for DEER depends on concentration and distance range of interest," , doi:10.5281/zenodo.3726735, 2020.

Schwefel, D., Maierhofer, C., Beck, J. G., Seeberger, S., Diederichs, K., Möller, H. M., Welte, W. and Wittmann, V.: Structural Basis of Multivalent Binding to Wheat Germ Agglutinin, J. Am. Chem. Soc., 132(25), 8704–8719, doi:10.1021/ja101646k, 2010.

Spindler, P. E., Schöps, P., Kallies, W., Glaser, S. J. and Prisner, T. F.: Perspectives of shaped pulses for EPR spectroscopy, J. Magn. Reson., 280(Supplement C), 30–45, doi:10.1016/j.jmr.2017.02.023, 2017.

Spindler Philipp E., Glaser Steffen J., Skinner Thomas E. and Prisner Thomas F.: Broadband Inversion PELDOR Spectroscopy with Partially Adiabatic Shaped Pulses, Angew. Chem. Int. Ed., 52(12), 3425–3429, doi:10.1002/anie.201207777, 2013.

Tait, C. E. and Stoll, S.: Coherent pump pulses in Double Electron Electron Resonance spectroscopy, Phys. Chem. Chem. Phys., 18(27), 18470–18485, doi:10.1039/C6CP03555H, 2016.

Tannús, A. and Garwood, M.: Improved Performance of Frequency-Swept Pulses Using Offset-Independent Adiabaticity, J. Magn. Reson. A, 120(1), 133–137, doi:10.1006/jmra.1996.0110, 1996.

Teucher, M. and Bordignon, E.: Improved signal fidelity in 4-pulse DEER with Gaussian pulses, J. Magn. Reson., 296, 103–111, doi:10.1016/j.jmr.2018.09.003, 2018.

Wort, J., Ackermann, K., Giannoulis, A., Stewart, A., Norman, D. and Bode, B. E.: Sub-micromolar pulse dipolar EPR spectroscopy reveals increasing CuII-labelling of double-histidine motifs with lower temperature., Angew. Chem., 0(ja), doi:10.1002/ange.201904848, 2019.

Supporting Information of

Optimising broadband pulses for DEER depends on concentration and distance range of interest

Andreas Scherer, Sonja Tischlik, Sabrina Weickert, Valentin Wittmann, Malte Drescher

Department of Chemistry and Konstanz Research School Chemical Biology, University of Konstanz, Konstanz, Germany

Correspondence to: Malte Drescher (malte.drescher@uni–konstanz.de)

Contents

S1 Additional materials and methods

All experiments have been performed on a Bruker Elexsys E580 spectrometer at Q-band (34 GHz). The spectrometer is equipped with a SpinJet-AWG unit (Bruker) and a 150 W pulsed travelling-wave tube (TWT) amplifier (Applied Systems Engineering, Fort Worth, USA). All samples were measured in 3 mm outer diameter sample tubes in an overcoupled ER5106QT-2 resonator (Bruker). The quality factor Q of the overcoupled resonator is approximately 200.

The samples were cooled to 50 K with a Flexline helium recirculation system (CE-FLEX-4K-0110, Bruker Biospin, ColdEdge Technologies) comprising a cold head (expander, SRDK-408D2) and a F-70H compressor (both SHI cryogenics, Tokyo, Japan), controlled by an Oxford Instruments Mercury ITC.

S1.1 EDFS

The echo-detected-field sweep spectra were recorded with a Hahn echo sequence ($\frac{\pi}{2}$ - τ - π - τ − echo) pulse-sequence with τ = 1.5 µs, a sweep width of 200 G and 10 shots per point, 3 scans and rectangular pulses. The length of the π-pulse was 16 ns at a frequency of 34 GHz.

S1.2 Nutation experiments

Pulse lengths of rectangular and Gaussian pulses were determined with nutation experiments with the pulse sequence (inversion pulse $-\tau_1-\frac{\pi}{2}-\tau_2-\pi-\tau_2-$ echo). τ_1 was set to 1 µs.

S1.3 Resonator profile

The resonator profile was measured by a series of nutation experiments at different frequencies as described in the literature (Doll and Jeschke, 2014). It was measured over 300 MHz with a step size of 10 MHz. The magnetic field was co-stepped. The nutation frequencies were calculated by a Fourier transformation of the nutation traces.

S1.4 DEER

All DEER experiments were measured with the standard four pulse DEER sequence:

$$\frac{\pi}{2_{obs}}-\tau_1-\pi_{\text{obs}}-t-\pi_{\text{pump}}-\tau_1+\tau_2-t-\pi_{\text{obs}}-\tau_2-\text{echo}$$

The delay between the $\pi/2$ and the π pulse in the observer channel τ_1 was 400 ns. The dipolar evolution time τ_2 was 8 µs. For all DEER experiments with rectangular and Gaussian pump pulses the pump frequency was set to 34.00 GHz. The magnetic field was chosen such that the pump lies on the maximum of the nitroxide spectrum. We used the phase cycling ((x) [x] x_p x) as suggested by (Tait and Stoll, 2016) and nuclear modulation averaging as suggested by (Jeschke, 2012).

S1.5 DEER optimisation

For the optimisation measurements we used a python script that can automatically perform several DEER experiments after another. We shifted the magnetic field from 1.2090 T to 1.2113 T for an observer pulse of 33.91 GHz and from 1.2097 T to 1.2119 T for an observer position of 33.93 GHz to ensure that the pump pulse is on the maximum of the nitroxide spectrum. Figure S1 illustrates the idea with a fixed observer frequency of 33.93 GHz.

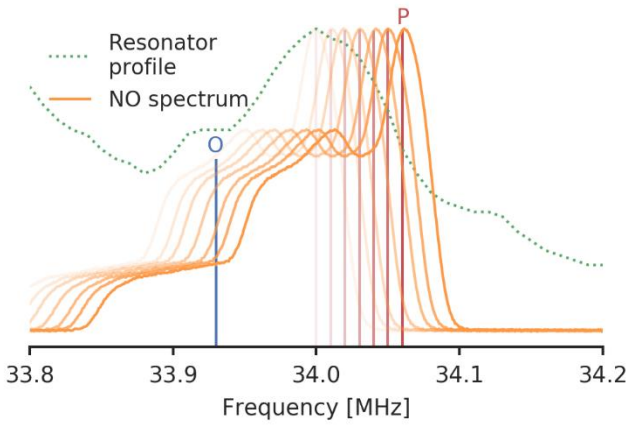

Figure S1: The resonator profile (green dots) with the different offsets during an optimisation measurement. The nitroxide spectrum (orange) is shifted with the offset. The observer frequency stays fixed at 33.93 GHz and is indicated by a blue line. The shift of the pump spin is indicated by the red line.

S1.6 Pulse calculations

For rectangular and Gaussian pulses, we used the pulses that are generated by Bruker Xepr software. For Gaussian pulses the FWHM is defined by FWHM $= \frac{t_{\mathrm{p}}}{2\sqrt{2\ln(2)}}$. All other pulses were calculated with the *pulse* function from the *easyspin* (Version 5.2.21) package for MATLAB R2018b (Stoll and Schweiger, 2006). The resulting pulse shapes were normalised to amplitude values between -1 and 1 and loaded into Xepr.

S1.7 Integration window

The integration window was determined by recording a series of 300 Hahn echoes in transient mode. We evaluated the signal-to-noise (SNR) with different integration windows and determined the integration window with the maximum SNR.

S1.8 Inversion profiles

Inversion profiles for broadband shaped pulses were measured with the pulse sequence.

$$\text{broadband shaped pulse} - \tau_1 - \frac{\pi}{2}_{obs} - \tau_2 - \pi_{\mathrm{obs}} - \tau_2 - \text{echo}$$

The inversion profiles were measured as the echo intensity as function of the frequency offset of the initial broadband shaped pulses. The $\pi/2$ and π pulses were rectangular pulses with a fixed frequency of 34 GHz.

~~S2~~S2 The MNR as the function of merit

Here, we want to discuss whether the MNR is a suitable function of merit for the determination of distance distributions and up to which time point in the DEER trace, the MNR needs to be evaluated to serve this purpose. Therefore, we performed simulations with a model distance distribution p_0 that is based on the narrow distance distribution of the model system used in this study. We approximated the experimentally obtained distance distribution with a Gaussian with a mean at 5.08 nm and a standard deviation of 0.08 nm. We varied the background density in ten steps from k = 0.01 1/µs to k = 0.3 1/µs in combination with a low, medium and high noise level (noise σ_0 = 0.02, 0.05 and 0.1) that was added to the DEER trace. The background dimension was set to d = 3 and a modulation depth of 0.5 was used. The DEER traces were simulated in the time domain up to 8 µs. For each parameter set we generated ten different traces. To compare the background correction by division (Jeschke et al., 2006) with the kernel inclusion approach as described in (Fábregas Ibáñez and Jeschke, 2020) we analysed all simulated DEER traces with both methods. We did not fit the background but used the true background function. The regularisation parameter was chosen according to the generalised cross-validation method. The quality of the resulting distance distributions p was estimated by the Euclidian distance D from the true distance p_0:

$$D(p, p_0) = \|p - p_0\|_2 \quad (1)$$

The MNR of the form factor F was calculated as described in the main text up to a limit of 7 µs according to equation (13) of the main text.

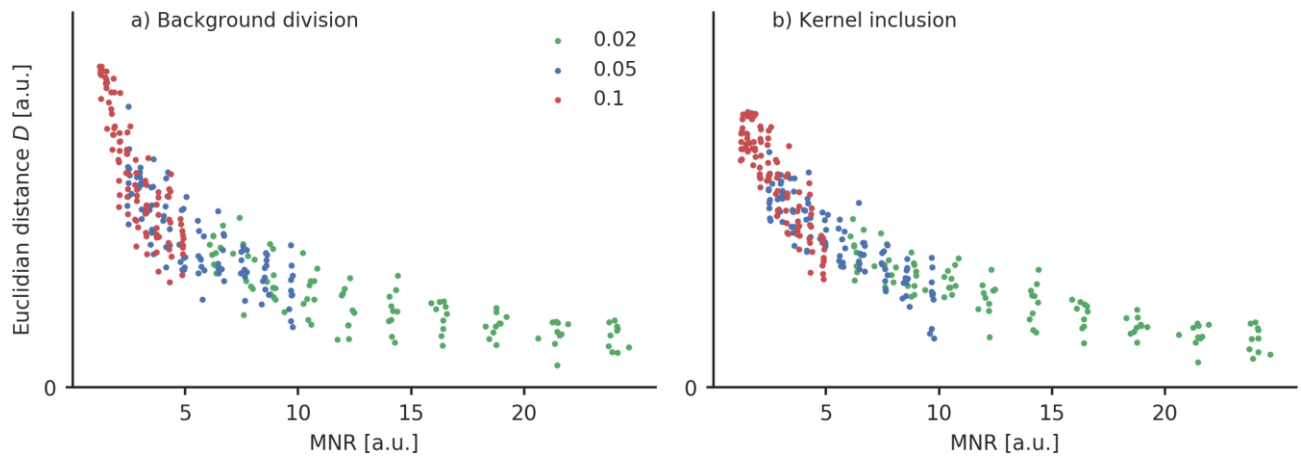

Figure S2: The Euclidian distance D of the real and calculated distance distribution as defined in equation (1) is plotted as a function of the MNR. Each dot represents a simulated DEER trace with either low (σ_0 = 0.02, green), medium (σ_0 = 0.05, blue) and high (σ_0 = 0.1, red) noise. The background correction was performed by (a) dividing the DEER trace by the background and (b) including the background in the kernel.

In Fig. S2, the quality of the determined distance distribution was plotted as a function of the determined MNR for both a background correction by division (Fig. S2a) and a kernel inclusion approach (Fig. S2b). For each noise level the MNR only depends on the density of the background as all other parameters are kept constant and only the background density is varied. So a lower MNR corresponds to a higher background density rate and vice versa. For the low noise level (σ_0 = 0.02), the quality of the determined distance distributions only varies a little for different background density rates. For medium (σ_0 = 0.05) and high (σ_0 = 0.1) noise levels, however, the dependency of the quality of the determined distance distribution decreases significantly with a decreasing MNR. If the MNR is only evaluated up to an early point of the form factor, the information of the background decay rate is lost in this case and is not properly included in the MNR as the MNR would then depend nearly exclusively on the given noise level.

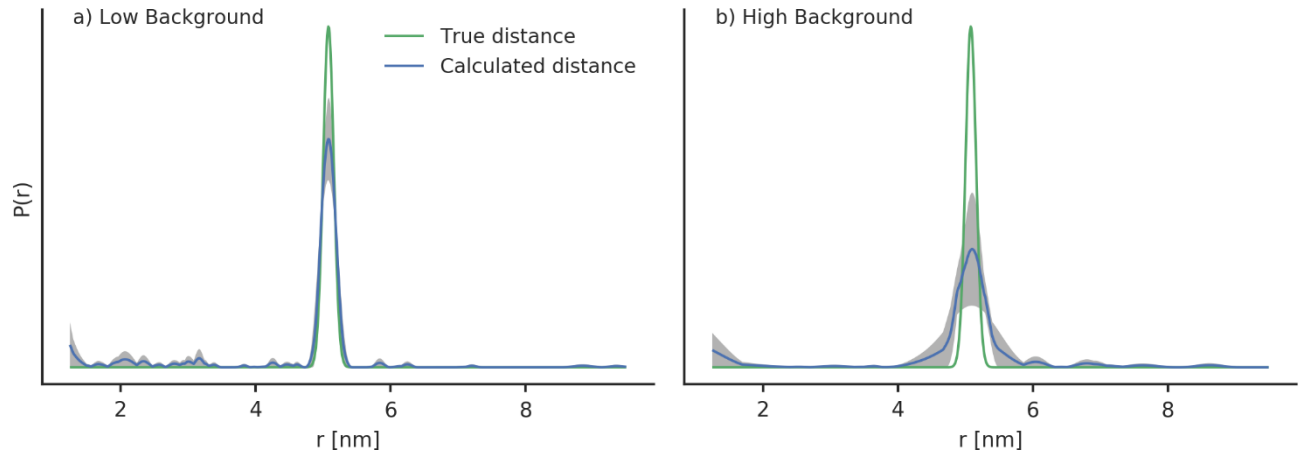

Figure S3: An exemplary distance distribution obtained for a medium noise level (σ_0 = 0.02) with (a) a low background density (k = 0.01 MHz) and (b) a high background density (k = 0.3 MHz). The grey area shows the area that is covered by the

calculated distance distribution for ten exemplary DEER traces. The mean of the shaded area is drawn in blue and the true distance is drawn in green.

A closer inspection reveals that whereas the obtained distance distributions for high background densities reproduce the mean of the distance distribution correctly, they overestimate the width of the distribution and the distance appears to be broader as it is (see Fig. S3 for an exemplary data set). Depending on the information that shall be obtained by the DEER measurements, the mean of the distance distribution might suffice. However, if high resolution distance distributions shall be obtained, it seems to be important to optimise the MNR up to the limit which is given by equation (13) of the main text. The comparison of both background correction methods shows that the kernel inclusion gives better results particularly for a high noise and a high background decay. It should therefore be considered as the superior method. However, the correlation between the quality of the determined distance distribution and the MNR is still valid. This is why, we consider the MNR as a proper function of merit, even if the kernel inclusion approach is used.

For a more comprehensive study, the effect of the MNR on the quality of the obtained distance distribution could also be tested for distance distributions with different distance ranges and widths. Such a detailed study was, however, beyond the scope of the this manuscript.

S3 Determination of the integration window

To determine the ideal integration window we recorded a series of Hahn echoes and calculated the SNR ratio for different integration window lengths. The results show that for rectangular pulses the ideal integration window is typically longer than the π-pulse length (Fig. ~~S2~~S4). An improvement of up to 14 % for a π-pulse length of 28 ns and an ideal integration window of 44 ns was achieved.

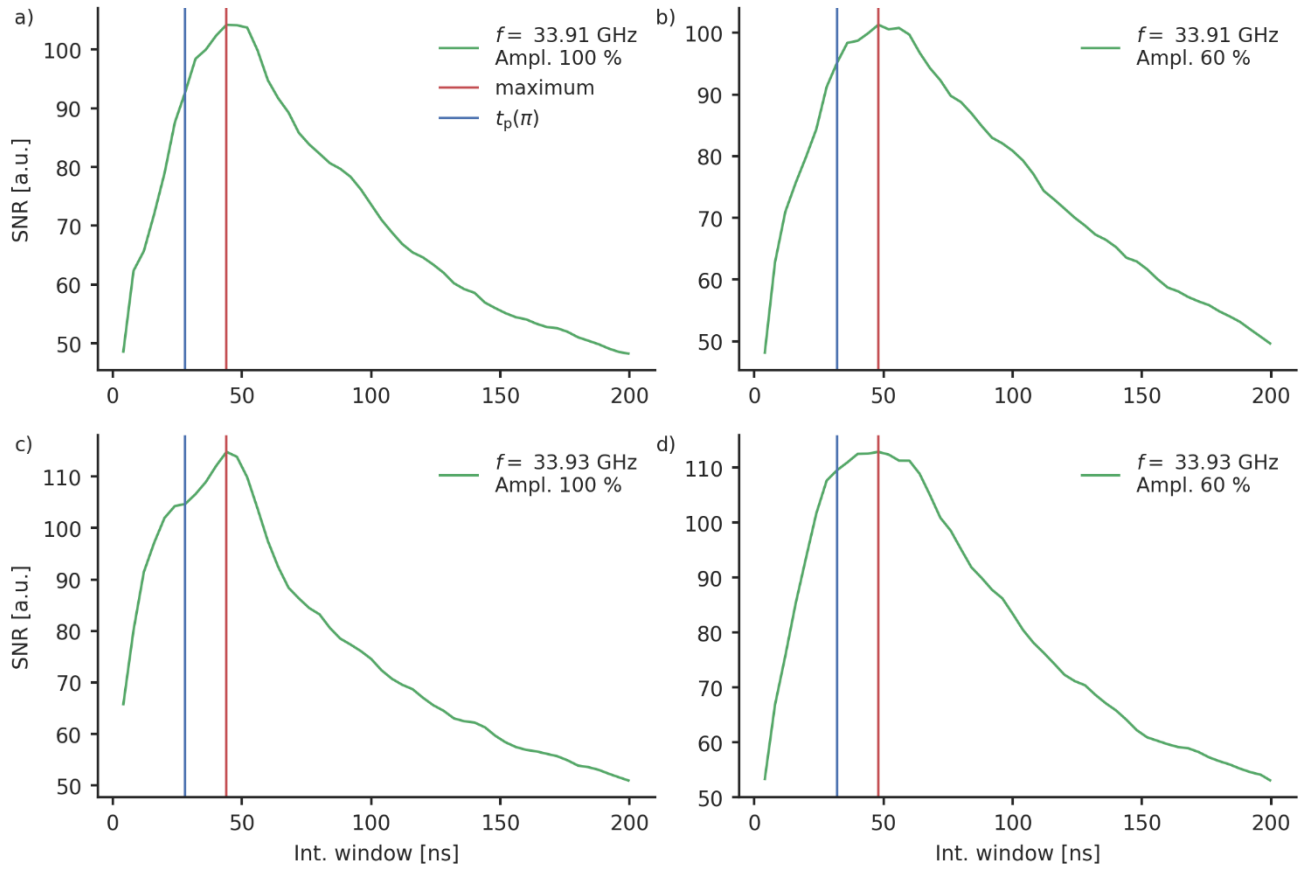

Figure ~~S2~~S4: The SNR for rectangular pulses of a series of transient Hahn echoes is shown as a function of the integration window length. The red lines indicate the integration window with the maximum SNR, the blue lines indicate an integration window that has the length of the π-pulse. The pulses have the following settings: a) frequency: 33.91 GHz, amplitude: 100 %. b) frequency: 33.91 GHz, amplitude: 60 %. c) frequency: 33.93 GHz, amplitude: 100 %. d) frequency: 33.93 GHz, amplitude: 60 %.

For Gaussian pulses the ideal integration window is typically smaller than the π-pulse length (~~figure S3~~Fig. S5).

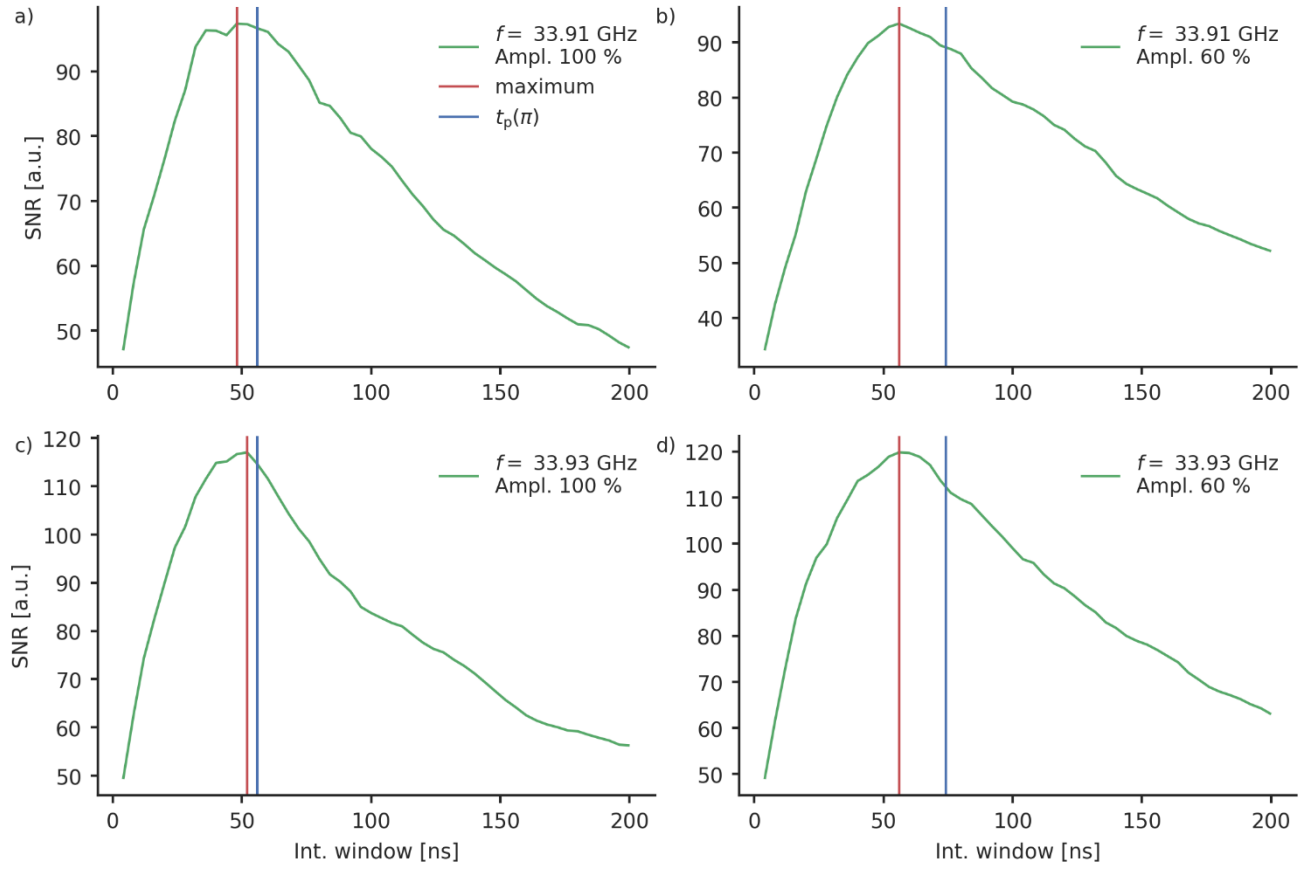

Figure ~~S3~~S5: The SNR for Gaussian pulses of a series of transient Hahn echoes is shown as a function of the integration window length. The red lines indicate the integration window with the maximum SNR, the blue lines indicate an integration window that has the length of the π-pulse. The pulses have the following settings: a) frequency: 33.91 GHz, amplitude: 100 %. b) frequency: 33.91 GHz, amplitude: 60 %. c) frequency: 33.93 GHz, amplitude: 100 %. d) frequency: 33.93 GHz, amplitude: 60 %.

~~S3~~S4 Parameters for the observer pulse

Table S1: Parameters for the rectangular observer pulses. The pulse length is referring to the π-pulse.

f_{obs} [GHz]	Obs. Amp. [%]	t_π [ns]	Length of integration window [ns]
33.91	100	28	44
	60	32	48
33.93	100	28	44
	60	32	48

Table S2: Parameters for the Gaussian observer pulses. The pulse length is referring to the π-pulse.

f_{obs} [GHz]	Obs. Amp. [%]	t_π [ns]	Length of integration window [ns]
33.91	100	56	48
	60	74	56
33.93	100	56	52
	60	74	56

~~S4~~S5 The MNR for rectangular and Gaussian pump pulses evaluated up to 7 µs

Table S3: MNR for a rectangular pump pulse and different rectangular observer pulses. The pump pulses had a length of 16 ns. The MNR has been evaluated up to 7 µs.

f_{obs} [GHz]	Obs. Amp. [%]	t_π [ns]	MNR	Mod depth λ
33.91	100	28	30	0.32
	60	32	32	0.32
33.93	100	28	32	0.31
	60	32	35	0.31

Table S4: MNR for a Gaussian pump pulse and different Gaussian observer pulses. The pump pulses had a length of 34 ns. The MNR has been evaluated up to 7 µs.

f_{obs} [GHz]	Obs. Amp. [%]	t_π [ns]	MNR	Mod depth λ
33.91	100	56	36	0.31
	60	74	32	0.29
33.93	100	56	41	0.31
	60	74	38	0.31

~~S5~~S6 Inversion profiles for rectangular and Gaussian pulses

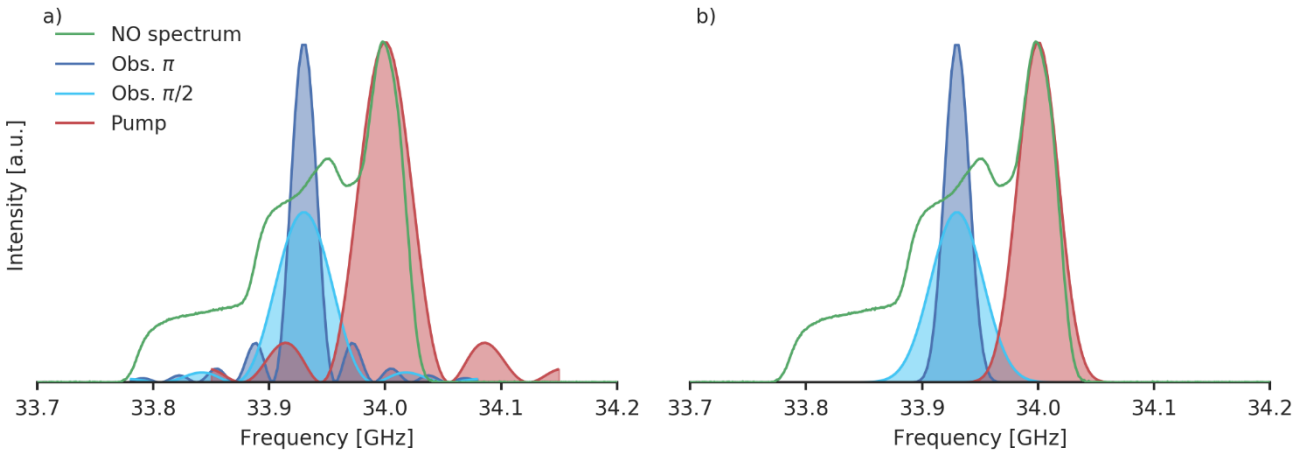

Figure ~~S4~~S6: The excitation profiles of the observer (blue) and pump pulses (red) of (a) rectangular and (b) Gaussian pulses. The light blue profiles are for the $\pi/2$ observer pulses and the dark blue profiles for the π observer pulse. The rectangular observer pulses have an amplitude of 60 %, a pulse length of 32 ns (π on observer) and 16 ns (pump), and the Gaussian have an amplitude of 100 %, a length of 56 ns (π on observer) and 34 ns (pump). It can be seen that the spectral overlap can be reduced with Gaussian pulses. The pulse amplitudes of the pump pulse are always 100 %.

~~S6~~S7 Simulations of spin inversion trajectories

We simulated the effect of an HS{1,1} pulse with a pulse length of 100 ns, a truncation parameter of $\beta = 8/t_p$, a frequency sweep range from -55 MHz and 55 MHz. We performed the numerical simulation in the density operator framework with MATLAB R2018b. The maximum of the B_1-field was set to 30 MHz, which corresponds to the maximum of the resonator profile. This pulse shows a good inversion between a frequency range of approximately -40 MHz and 40 MHz (~~figure~~Fig. S7a). In ~~figure~~Fig. S7b, the inversion of a spin packet with an offset of -40 MHz and 40 MHz are shown. It can be seen that the spins are inverted in a time window between roughly 20 ns and 80 ns, making an effective pulse length of 60 ns. This ~~corresponds~~would correspond to a minimum distance of 2.32 nm. Note that these numbers were only obtained by visual inspection, so this should only be considered as a qualitative discussion. The spin flip behaviours is also different for different pulses.

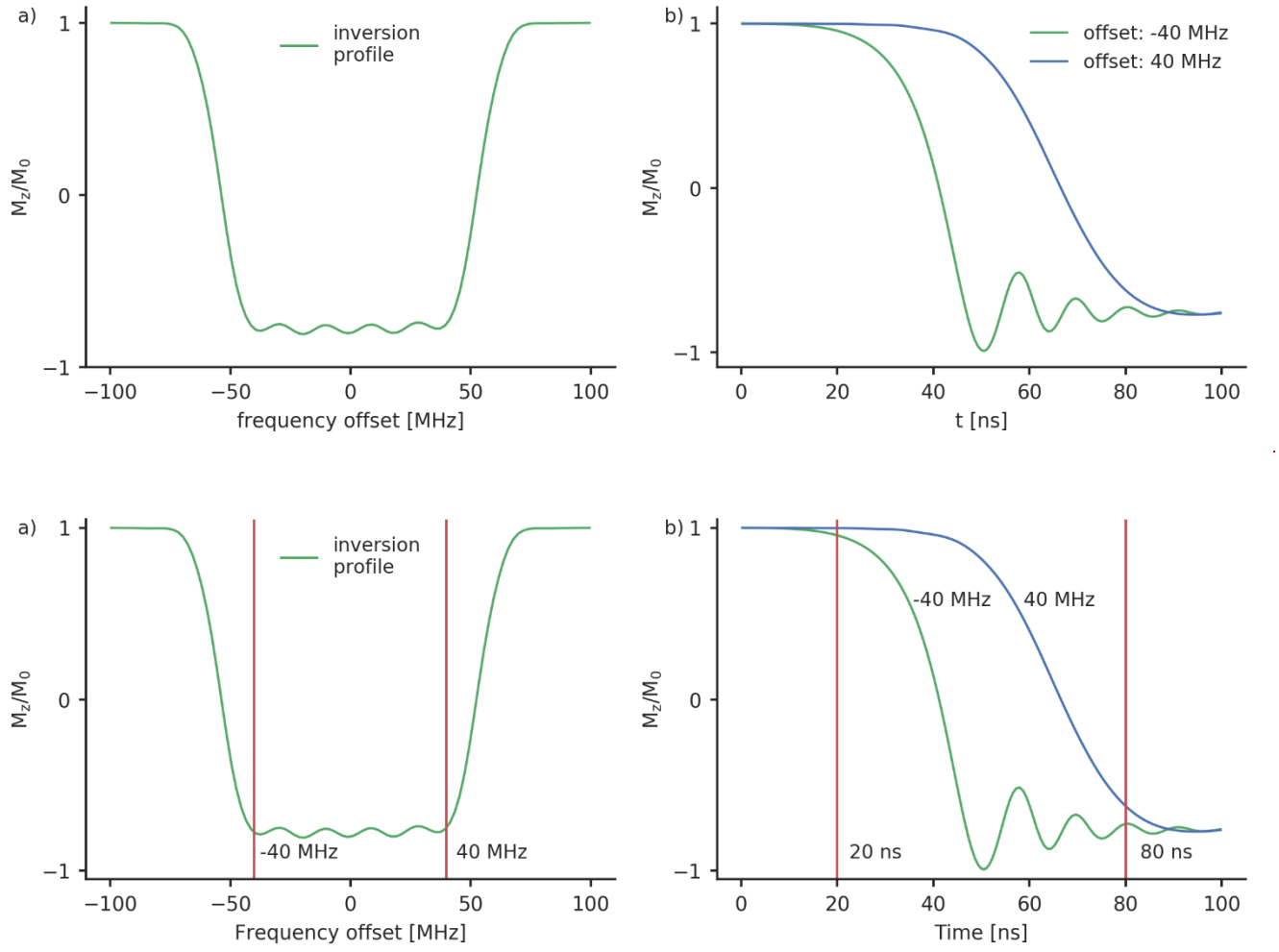

Figure ~~S5~~S7: a) The excitation profile of HS{1,1} with a pulse length of 100 ns, a truncation of $\beta = 8/t_p$ and a frequency range from -55 MHz and +55 MHz. b) The inversion of a spin packet with an offset of -40 MHz (blue) and +40 MHz (green).

~~S7~~S8 The MNR for broadband pump pulses evaluated up to 7 µs

Table S5: MNR for the different broadband shaped pulses with a rectangular observer pulse. The MNR has been evaluated up to 7 µs.

f_{obs} [GHz]	Obs. Amp. [%]	Pump pulse	t_π [ns]	Δf [MHz]	Offset [MHz]	MNR	Mod. depth λ
33.91	100	HS{1,6} ($\beta = 8/t_p$)	100	110	90	32	0.63
		WURST (n=6)	100	160	90	37	0.64
		Chirp ($t_r = 30$ ns)	36	120	90	33	0.50
		HS{1,1} ($\beta = 6/t_p$)	100	110	90	41	0.57
	60	HS{1,6} ($\beta = 10/t_p$)	100	110	90	31	0.62
		WURST (n=6)	100	160	90	30	0.64
		Chirp ($t_r = 30$ ns)	100	160	90	32	0.67
		HS{1,1} ($\beta = 6/t_p$)	100	110	90	34	0.57
33.93	100	HS{1,6} ($\beta = 10/t_p$)	100	110	100	39	0.57
		WURST (n=6)	100	160	100	39	0.62
		Chirp ($t_r = 10$ ns)	36	120	90	38	0.47
		HS{1,1} ($\beta = 6/t_p$)	100	110	90	43	0.53
	60	HS{1,6} ($\beta = 10/t_p$)	100	110	90	40	0.60
		WURST (n=6)	100	120	100	36	0.57
		Chirp ($t_r = 10$ ns)	36	120	90	38	0.47
		HS{1,1} ($\beta = 8/t_p$)	100	90	80	43	0.48

Table S6: MNR for the different broadband shaped pulses with a Gaussian observer pulse. The MNR has been evaluated up to 7 µs.

f_{obs} [GHz]	Obs. Amp. [%]	Pump pulse	t_π [ns]	Δf [MHz]	Offset [MHz]	MNR	Mod. depth λ
33.91	100	HS{1,6} ($\beta = 10/t_p$)	100	90	90	36	0.60
		WURST (n=6)	100	160	90	30	0.64
		Chirp ($t_r = 10$ ns)	36	120	80	37	0.50
		HS{1,1} ($\beta = 6/t_p$)	100	110	90	40	0.58
	60	HS{1,6} ($\beta = 8/t_p$)	100	110	90	38	0.63
		WURST (n=6)	100	160	100	34	0.48
		Chirp ($t_r = 10$ ns)	100	120	90	38	0.48
		HS{1,1} ($\beta = 6/t_p$)	100	110	90	37	0.58
33.93	100	HS{1,6} ($\beta = 10/t_p$)	100	90	90	39	0.57
		WURST (n=6)	100	160	100	38	0.62
		Chirp (no smoothing)	36	120	80	45	0.49
		HS{1,1} ($\beta = 8/t_p$)	100	110	90	50	0.52
	60	HS{1,6} ($\beta = 10/t_p$)	100	110	90	45	0.61
		WURST (n=6)	100	160	90	40	0.63
		Chirp ($t_r = 9$ ns)	36	120	80	45	0.47
		HS{1,6} ($\beta = 8/t_p$)	100	110	80	47	0.52

~~S8~~S9 Inversion profiles for the broadband shaped pulses

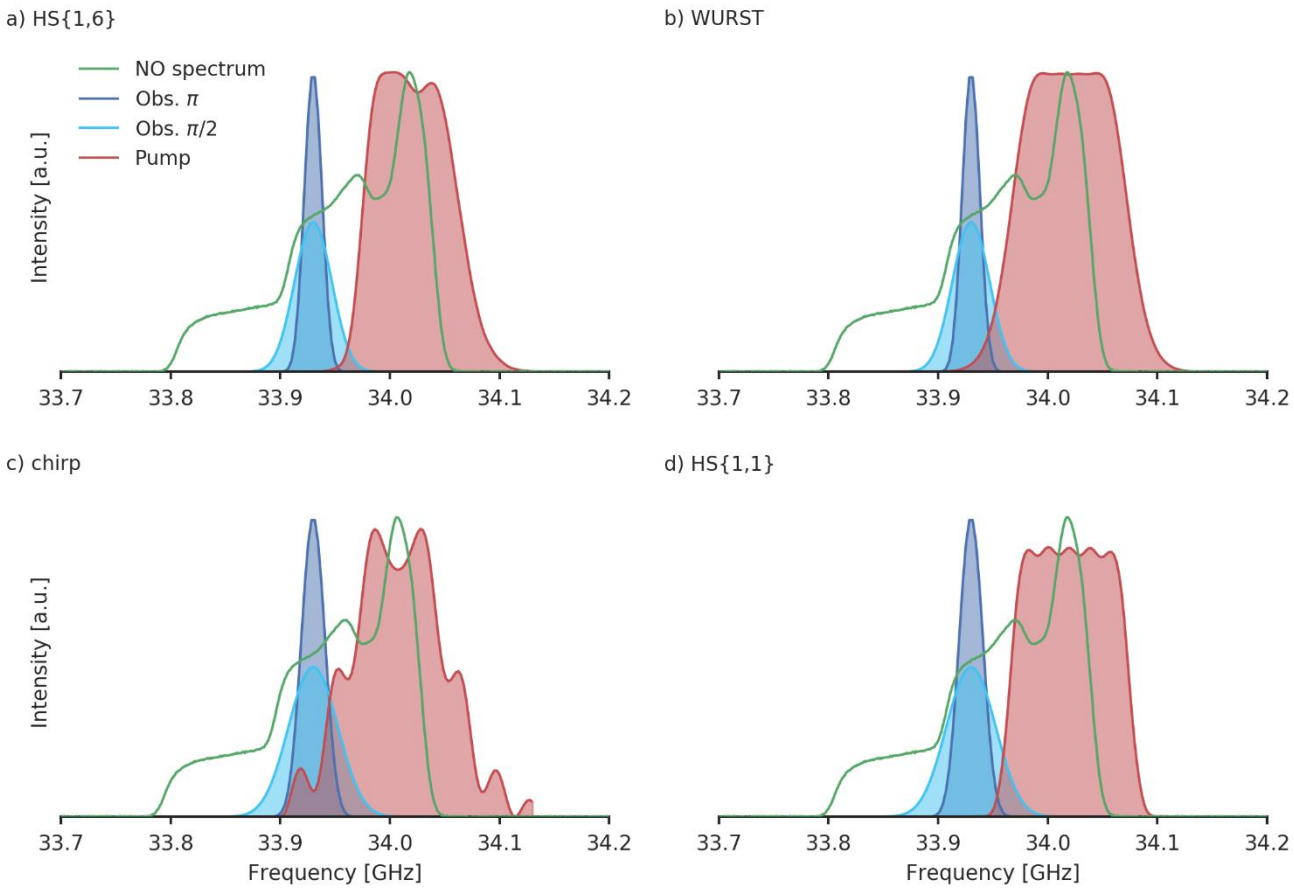

Figure ~~S6~~S8: The ~~inversion~~excitation profiles of ~~a~~the best performing (a) HS{1,6}, (b) WURST, (c) chirp and (d) HS{1,1} pulse. The parameters of the pump and observer pulses can be found in table 3 of the main text.

~~S9~~S10 Pulse ~~shaped~~shapes of the broadband shaped pulses

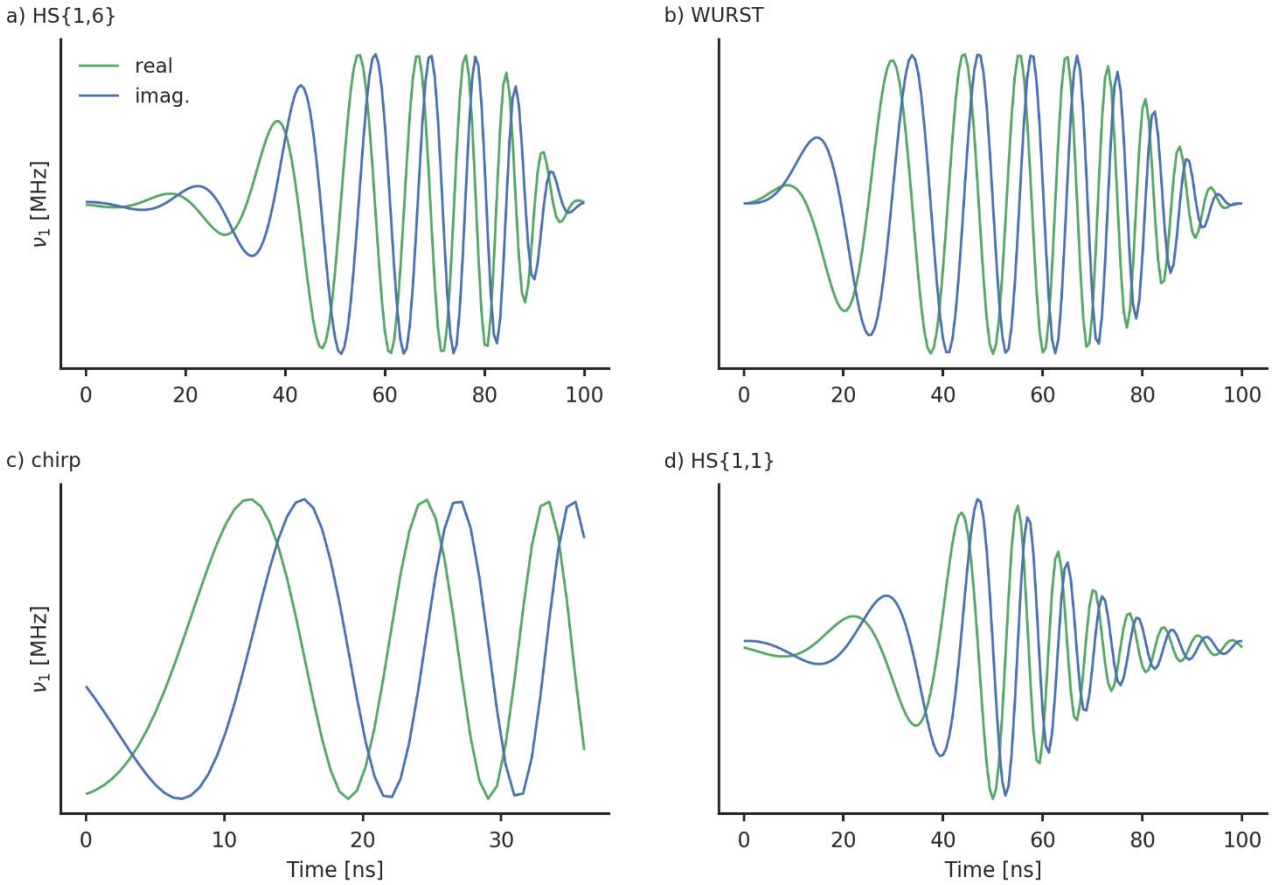

Figure ~~S7~~S9: The pulse ~~shaped~~shapes of ~~an~~the best performing (a) HS{1,6} , (b) WURST , (c) chirp and (d) HS{1,1} pulse with the real part (green) and imaginary part (blue). The parameters broadband shaped pulses can be found in table ~~2~~3 of the main text.

~~S10~~S11 Comparison of ~~full~~simulated and experimental inversion profile

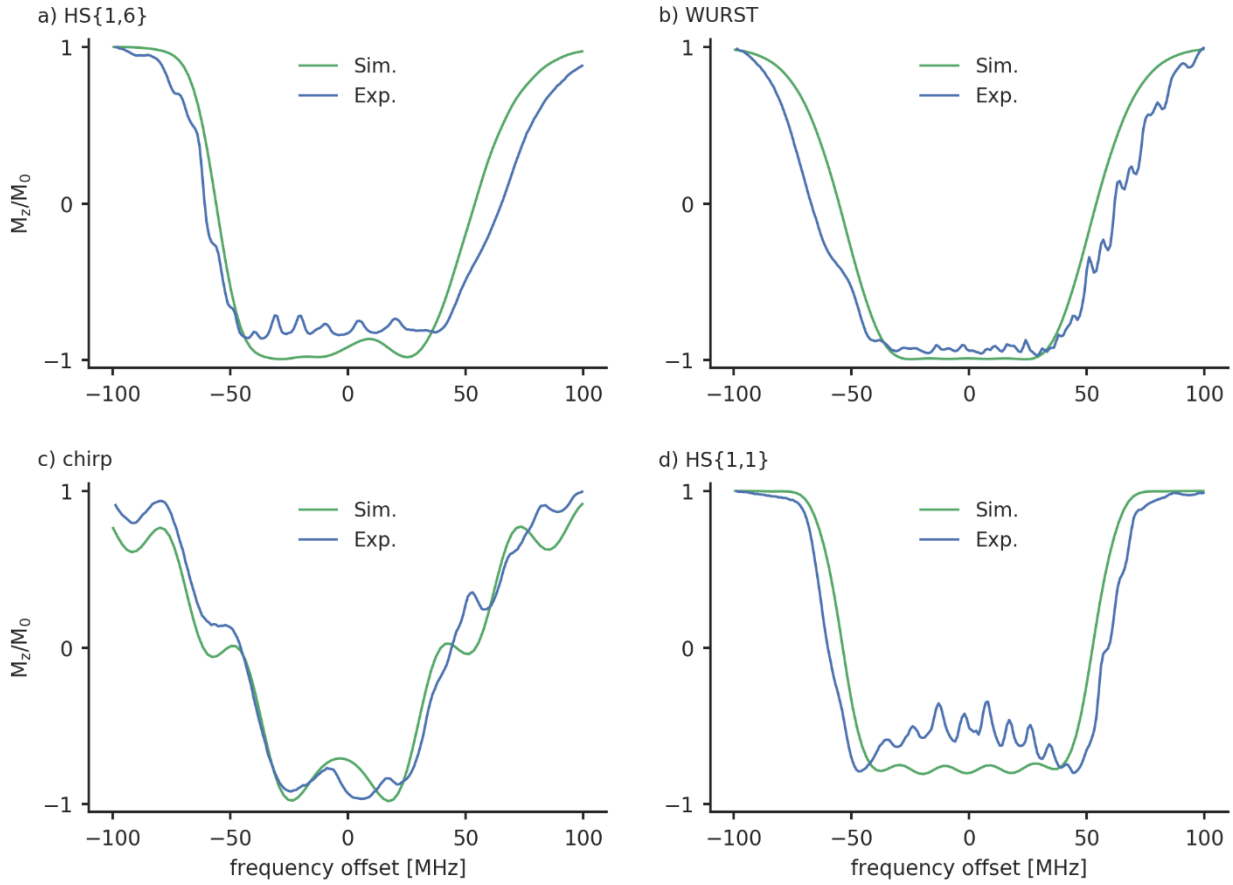

Figure S10: The simulated (green) and experimentally recorded (blue) inversion profiles of the best performing (a) HS{1,6}, (b) WURST, (c) chirp and (d) HS{1,1} pulse. The parameters of the pump and observer pulses can be found in table 3 of the main text.

We recorded the inversion profiles of the best performing pulses and compared them with the simulations in order to detect potential deviations. The results in Fit. S10 shows that the experimentally recorded inversion profiles reproduce the general trends of the simulations. Nonetheless, there are some deviations that are probably caused by the spectromeer and that shall be discussed here.

It can be noticed that for HS{1,6} and HS{1,1} pulses the measured inversion profiles do not reach the inversion profile of the simulation. For HS{1,6} the overall inversion efficiency is a bit lower than expected and for HS{1,1} pulses a bump in the centre of the frequency sweep was found. The simulations can, however, predict the fact that HS{1,6} have a higher inversion efficiency than HS{1,1} pulses. For WURST and chirp pulses the experimentally recorded inversion profiles reach the inversion efficiency of the simulation.

The experimental inversion profiles of HS{1,6}, HS{1,1} and chirp pulses have a larger inversion range than what is predicted by the simlations. This can increase the overlap with the observer pulse and therefore reduce the echo intensity. But as the inversion range is only a little bit larger, we consider this not to be particularly worrysome. For HS{1,6} and HS{1,1} pulses, the larger inversion range could compensate the reduced inversion efficiency

For the chirp pulses the frequency range as well as the inversion efficiency of the experimental and simulated inversion profiles agree. There are some minor deviations in the pattern of the oscillations that are present in the inversion profile, which we do not expect to have a large effect on the performance of the pulse.

S12 Full DEER traces

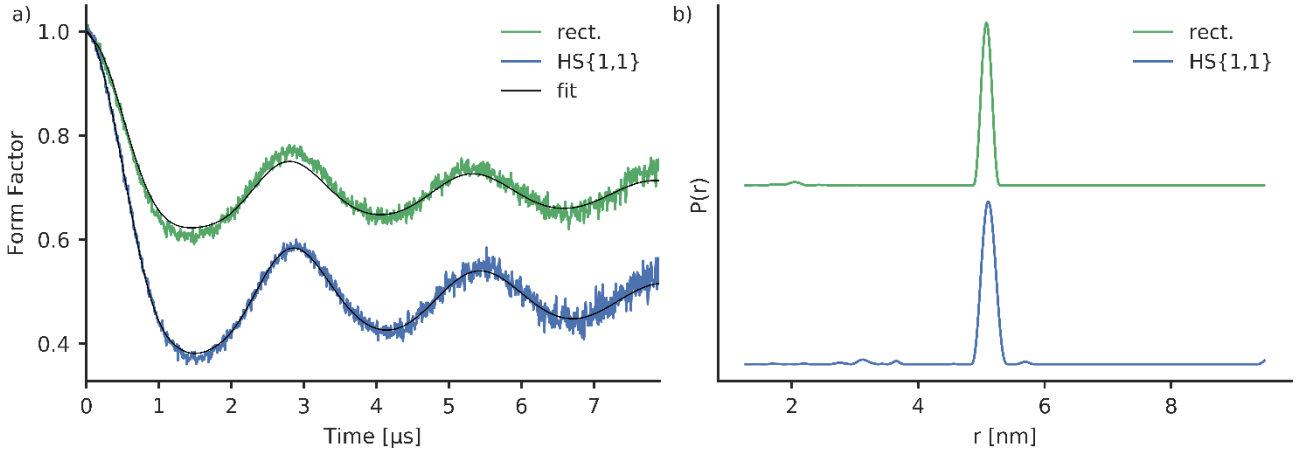

Figure ~~S8~~S11: Comparison of the performance of DEER with rectangular pulses (green) and with Gaussian observer pulses and the HS{1,1} pulse from table 1 that yielded the best MNR (blue). The form factors are shown in (a) and the corresponding distance distributions in (b). One 10 minute scan was recorded for both experiments. The corresponding DEER traces are depicted in Fig. S17.

S13 ~~S11~~The influence of the length of broadband shaped pump pulses

Tests with broadband shaped pump pulses with pulse lengths of 200 ns and 400 ns showed that they do not lead to an overall performance increase. This is shown here exemplary by comparing the performance of HS{1,1} pump pulses and Gaussian observer pulses (Fig. S12). There are indeed some pump pulses (for example a HS{1,1} pulse with $\beta = 10/t_p$ and $\Delta f =$ 110 MHz) that show an improvement with a longer pulse length, however there is no overall gain by using a pump pulse length of 200 ns.

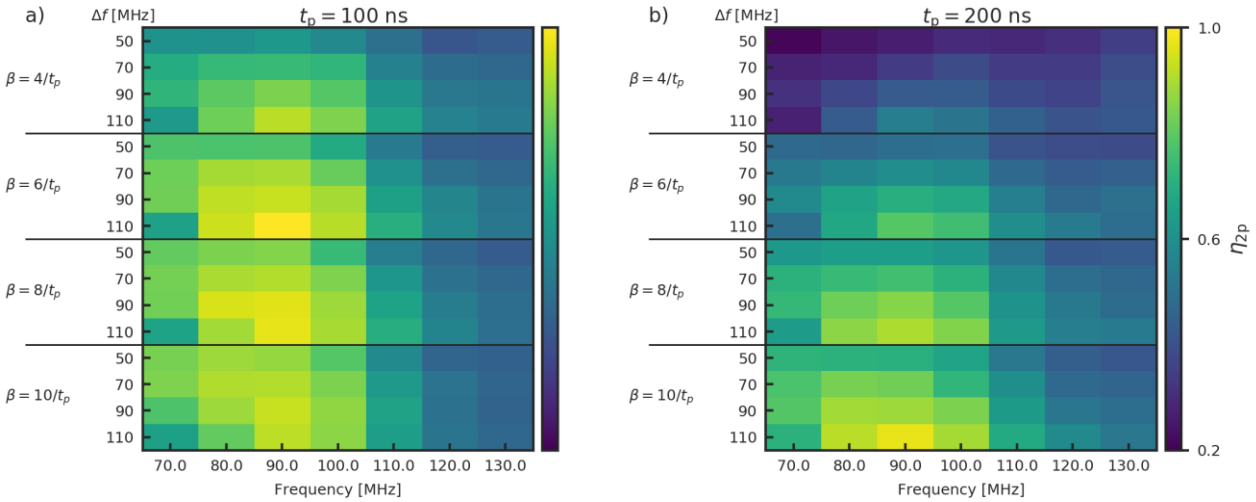

Figure S12: HS{1,1} pump pulses of (a) 100 ns and (b) 200 ns length. The observer pulses were Gaussian pulses with 100 % intensity at an observer position with a 90 MHz offset from the centre of the resonator profile and a pulse length of 56 ns for the π pulse. The colour bars are normalised to the same value so that both heat maps are comparable.

We noticed that a major problem with longer broadband shaped pump pulses is that the intensity of the echo can be reduced (Fig. S13a). For a pump pulse offset of 90 MHz, the echo intensity at the zero time of the DEER trace is reduced significantly when increasing the pump pulse lengths from 100 ns over 200 ns to 400 ns.

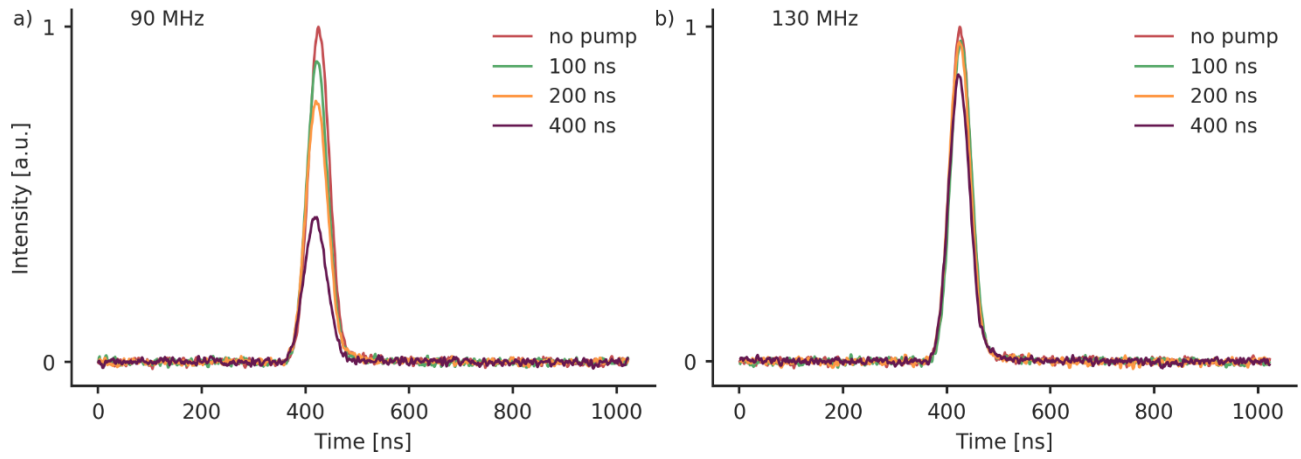

Figure S13: The echo at the zero time of the DEER trace. The observer pulses were Gaussian pulses with 100 % intensity at an observer position with a 70 MHz offset from the centre of the resonator profile and a pulse length of 56 ns for the π pulse. The pump pulses were HS{1,1} pulses with $\beta = 8/t_p$ and $\Delta f = 110$ MHz. The offset between the pulses is (a) 90 MHz and (b) 130 MHz.

A comparison of the calculated inversion profiles of the respective pulses (Fig. S14a-c) shows that, whereas the 100 ns pulse should lead to an incomplete inversion, a nearly complete inversion can be expected for the longer pulses. Furthermore, the longer pulses should have slightly steeper excitation flanks. Those trends can indeed be found for the measured inversion profiles. There are some deviations of the measured and calculated inversion profiles. The measured inversion profile of the 100 ns pulse shows an increased frequency width compared to the calculated profile. Furthermore, there is bump in the centre of the frequency sweep. The measured inversion profiles of the longer pulses show the expected steep frequency flanks that can also be seen in the simulation. The inversion profiles of the 200 ns and the 400 ns pulses show a small asymmetry around the centre of the frequency sweep. We assign these deviations to instrumental pulse distortions caused by the spectrometer.

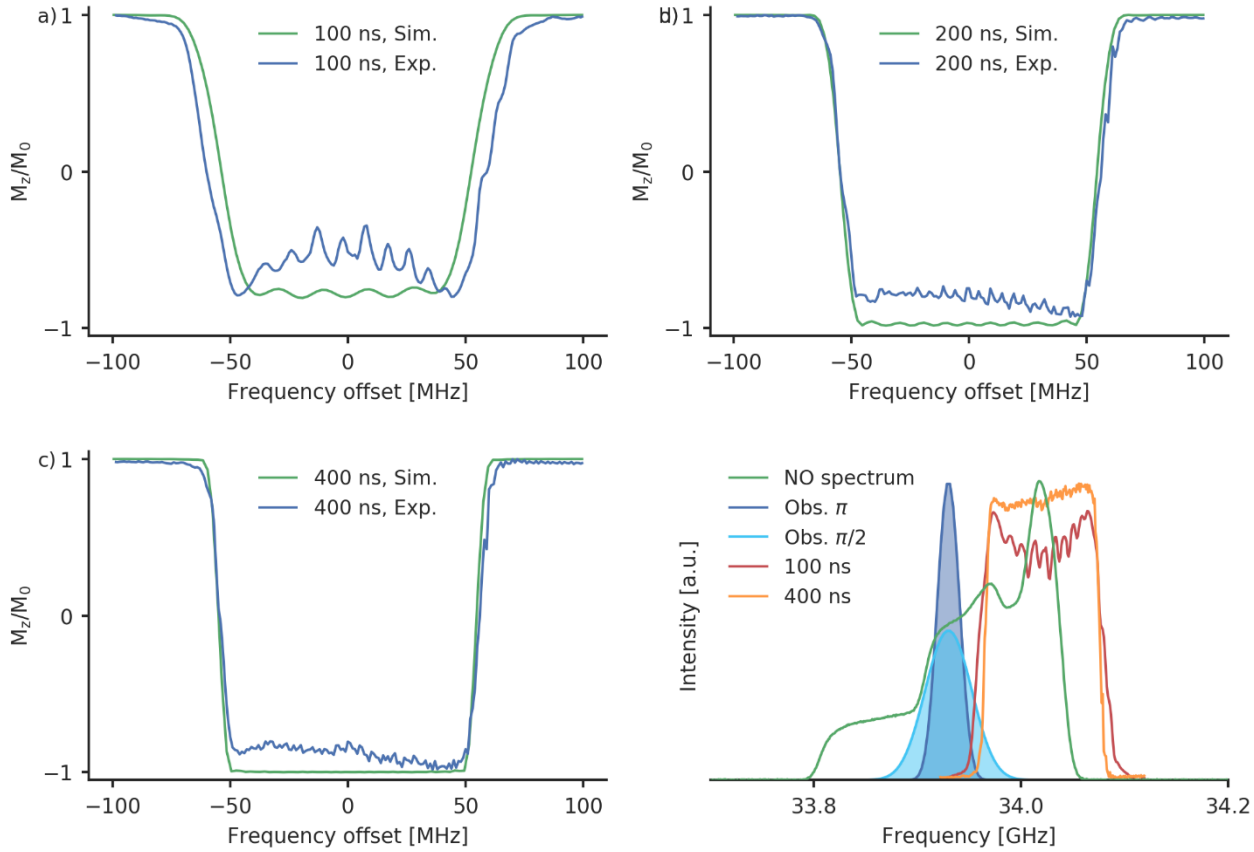

Figure S14: Calculated and measured inversion profiles of a HS{1,1} pulse with $\beta = 8/t_p$ and $\Delta f = 110$ MHz and a pulse length of (a) 100 ns, (b) 200 ns and (c) 400 ns. A 400 ns calculated pump excitation profiles next to the observer pulse excitation profiles is shown in (d).

It is expected that steeper excitation flanks lead to a smaller overlap with the observer pulses and therefore a smaller effect on the echo intensity. Despite this is the case here as well (Fig. 14d), the overlap is not reduced completely and 400 ns pulse still

has some remaining spectral overlap with the observer pulses. We assume that the contradictive findings concerning the echo intensity here are caused by this remaining small overlap. It could become more perturbing for longer pulses as the overall energy of the pulses increases with the pulse length and therefore potential disturbances might be enhanced. A measurement with an larger offset between the pulses at 130 MHz shows that the echo decrease is indeed reduced (Fig. S13b) when the overlap gets smaller. Despite leading to a higher echo intensity, such a high offset is not favourable for nitroxode-nitroxide DEER, because of the limited width of the nitroxide spectrum.

S14 The influence of the B_1 field strength on chirp pulses

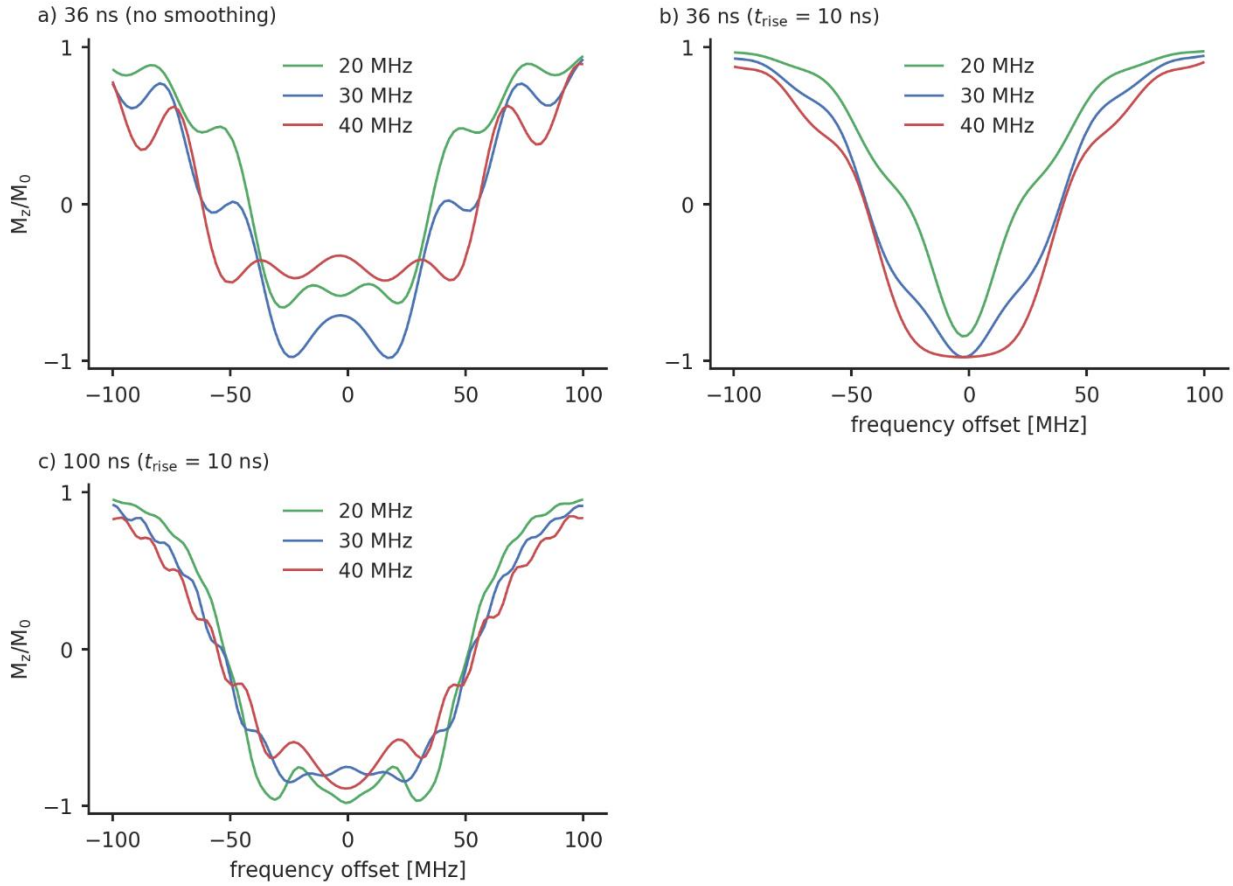

Figure S15: The inversion profiles of different chirp pulses with (a) a pulse length of 36 ns and no quarter sine smoothing, (b) a pulse length of 36 ns and a quarter sine smoothing with t_r = 10 ns and (c) a pulse length of 100 ns and a quarter sine smoothing with t_r = 10 ns. The frequency width of all pulses is Δf = 120 MHz.

S15 Comparison of bandwidth compensated and non-bandwidth compensated pulses

We tested the performance of a bandwidth compensation for HS{1,6}, WURST, chirp and HS{1,1} pump pulses. The observer pulses were rectangular with an offset of 90 MHz and an observer π pulse length of 28 ns. We estimated the effect of bandwidth

compensation with the help of the η_{2p} parameter. For WURST and chirp pulses, a bandwidth compensation lead to an improvement of 3.0 % and 3.2 %. However, for HS{1,6} and HS{1,1} pulses, we observed a decrease of 10.5% and 2.6% (data not shown). As a bandwidth compensation requires a measurement of the resonator profile before each DEER measurement and did not always result in an increase in performance, we decided to stick to pulses without bandwidth compensation.

~~S12 Comparison of 100 ns and 200 ns pulse lengths~~

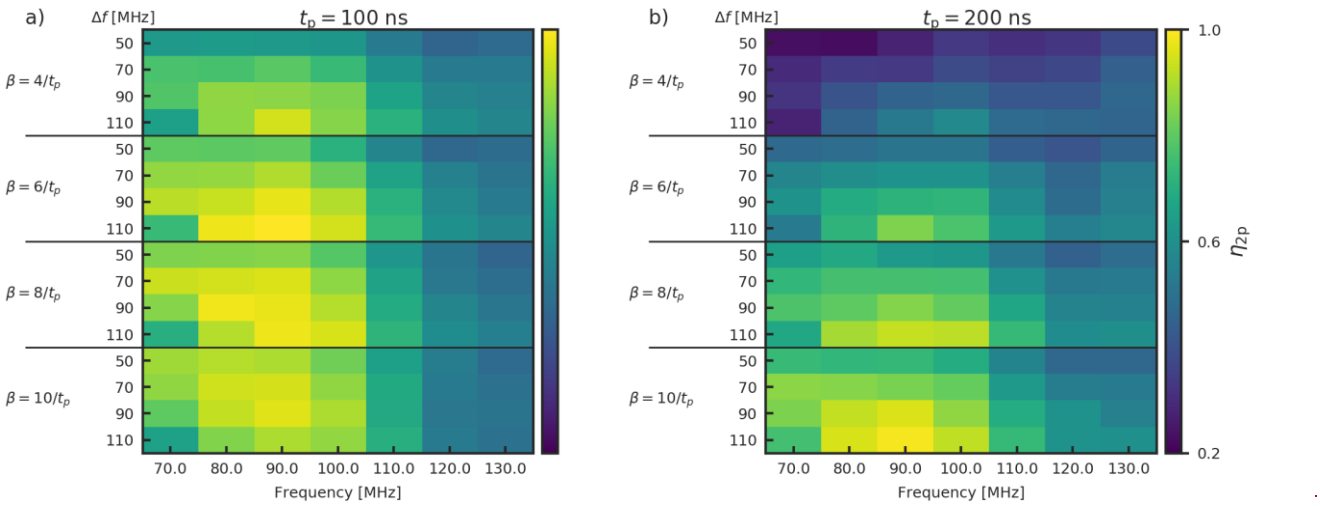

~~Figure S9:~~ ~~HS{1,1} pump pulses of (a) 100 ns and (b) 200 ns length. The observer pulses were rectangular with 100 % intensity at an observer position of 33.91 GHz and a pulse length of 28 ns for the π pulse.~~**S16**

~~S13 Echo decrease with long broadband shaped pump pulses~~

~~We have checked the echo intensity at the zero time of the DEER trace with different pump pulses. There is always a slight decrease of the echo intensity in the presence of a pump pulse (Fig. S8a). It is, however, negligible for rectangular pump pulses. With a 100 ns HS{1,1} pulse there is a stronger decrease of the echo, which gets even worse for 200 ns and 400 ns pulses. In the last case, nearly the whole echo has disappeared. The reason for this behaviour is not entirely clear to us as the excitation profiles do not change significantly with the pulse length (Fig. S8 b). However, we chose not to investigate 200 ns and 400 ns pulses.~~

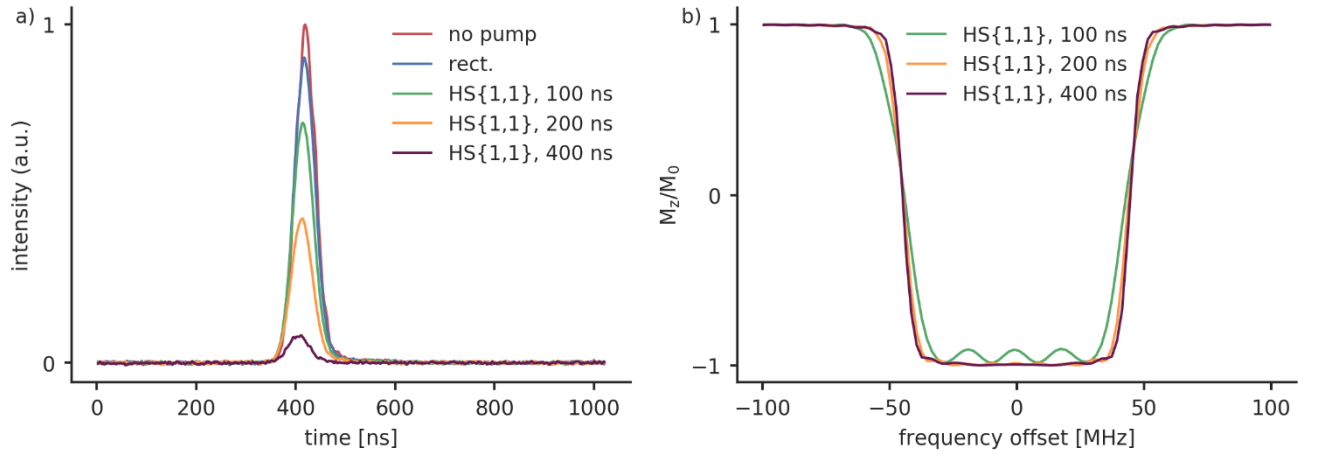

~~**Figure S10:** a) The echoes are at the zero time of the DEER trace. The echoes are recorded without a pump pulse (red), with a rectangular pump pulse (blue), with a 100 ns (green), 200 ns (yellow) and 400 ns (purple) HS{1,1} pump pulse (b) shows the excitation profile of the respective HS{1,1} pump pulses. Their parameters are $\beta = 6/t_p$, $\Delta f = 90$ MHz, offset to observer: 80 MHz and a pulse length of 100 ns (green), 200 ns (yellow) and 400 ns (purple).~~

~~S14~~ The MNR for rectangular and Gaussian pump pulses evaluated up to 2 µs

Table S7: MNR for a rectangular pump pulse and different rectangular observer pulses. The pump pulses had a length of 16 ns. The MNR has been evaluated up to 2 µs.

f_{obs} [GHz]	Obs. Amp. [%]	t_π [ns]	MNR	Mod. depth λ
33.91	100	28	41	0.32
	60	32	41	0.32
33.93	100	28	40	0.31
	60	32	44	0.31

Table S8: MNR for a Gaussian pump pulse and different Gaussian observer pulses. The pump pulses had a length of 34 ns. The MNR has been evaluated up to 2 µs.

f_{obs} [GHz]	Obs. Amp. [%]	t_π [ns]	MNR	Mod. depth λ

33.91	100	56	50	0.31
	60	74	42	0.29
33.93	100	56	53	0.31
	60	74	48	0.31

~~S15~~S17 The MNR for broadband pump pulses evaluated up to 2 µs

Table S9: MNR for the different broadband shaped pulses with a rectangular observer pulse. The MNR has been evaluated up to 2 µs.

f_{obs} [GHz]	Obs. Amp. [%]	Pump pulse	t_π [ns]	Δf [MHz]	Offset [MHz]	MNR	Mod. depth λ
33.91	100	HS{1,6} ($\beta = 8/t_p$)	100	110	90	58	0.63
		WURST (n=6)	100	160	90	60	0.64
		Chirp ($t_r = 30$ ns)	36	120	90	52	0.50
		HS{1,1} ($\beta = 6/t_p$)	100	110	90	64	0.57
	60	HS{1,6} ($\beta = 10/t_p$)	100	110	90	59	0.62
		WURST (n=6)	100	160	90	63	0.63
		Chirp ($t_r = 30$ ns)	100	160	90	57	0.66
		HS{1,1} ($\beta = 6/t_p$)	100	110	90	53	0.57
33.93	100	HS{1,6} ($\beta = 10/t_p$)	100	110	100	60	0.57
		WURST (n=6)	100	160	100	63	0.62
		Chirp ($t_r = 10$ ns)	36	120	90	57	0.47
		HS{1,1} ($\beta = 6/t_p$)	100	110	90	65	0.53
	60	HS{1,6} ($\beta = 10/t_p$)	100	110	90	64	0.60
		WURST (n=6)	100	120	100	59	0.57
		Chirp ($t_r = 10$ ns)	36	120	90	58	0.47
		HS{1,1} ($\beta = 8/t_p$)	100	90	80	58	0.48

Table S10: MNR for the different broadband shaped pulses with a Gaussian observer pulse. The MNR has been evaluated up to 2 µs. The chirp pulse where no t_r time is specified is a pulse without the quartersine smoothing.

f_{obs} [GHz]	Obs. Amp. [%]	Pump pulse	t_π [ns]	Δf [MHz]	Offset [MHz]	MNR	Mod. depth λ
33.91	100	HS{1,6} ($\beta = 10/t_p$)	100	90	90	65	0.60
		WURST (n=6)	100	160	90	64	0.64
		Chirp ($t_r = 10$ ns)	36	120	80	59	0.50
		HS{1,1} ($\beta = 6/t_p$)	100	110	90	68	0.58
	60	HS{1,6} ($\beta = 8/t_p$)	100	110	90	71	0.63
		WURST (n=6)	100	160	100	67	0.63
		Chirp ($t_r = 10$ ns)	100	120	90	59	0.48
		HS{1,1} ($\beta = 6/t_p$)	100	110	90	63	0.58
33.93	100	HS{1,6} ($\beta = 10/t_p$)	100	90	90	73	0.57
		WURST (n=6)	100	160	100	72	0.62
		Chirp (no smoothing)	36	120	80	65	0.49
		HS{1,1} ($\beta = 8/t_p$)	100	110	90	71	0.52
	60	HS{1,6} ($\beta = 10/t_p$)	100	110	90	82	0.61
		WURST (n=6)	100	160	90	73	0.63
		Chirp ($t_r = 9$ ns)	36	120	80	63	0.47
		HS{1,1} ($\beta = 8/t_p$)	100	110	80	74	0.52

~~S16~~S18 The MNR of the diluted sample evaluated up to 7 µs

Table S11: MNR for the different broadband shaped pulses with a Gaussian observer pulse. The MNR has been evaluated up to 2 µs. The chirp pulse where no t_r time is specified is a pulse without the quartersine smoothing.

f_{obs} [GHz]	Obs. Amp. [%]	Pump pulse	t_π [ns]	Δf [MHz]	Offset [MHz]	MNR	Mod. depth λ
33.93	100	HS{1,6} ($\beta = 10/t_p$)	100	90	90	61	0.55
		WURST (n=6)	100	160	100	54	0.59
		Chirp (no smoothing)	36	120	80	58	0.46
		HS{1,1} ($\beta = 8/t_p$)	100	110	90	65	0.47
	60	HS{1,6} ($\beta = 10/t_p$)	100	110	90	59	0.56
		WURST (n=6)	100	160	90	53	0.58
		Chirp (t_r = 9 ns)	36	120	80	54	0.43
		HS{1,1} ($\beta = 8/t_p$)	100	110	80	55	0.46

~~S17~~S19 Correlation between the background density and the modulation depth

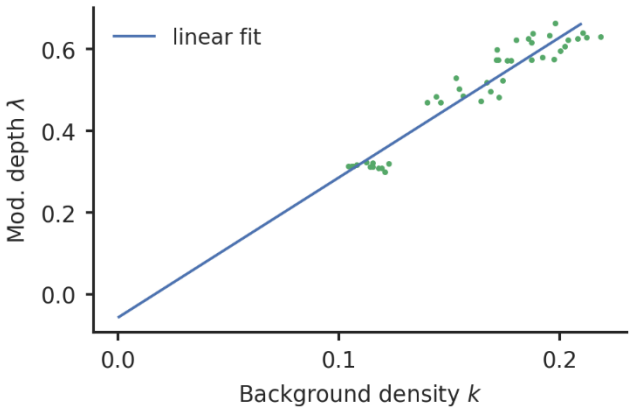

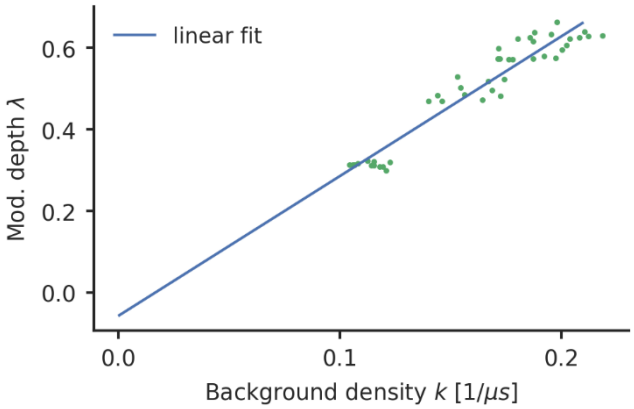

Figure ~~S11~~S16: The correlation between the modulation depth and the background. Each dot represents a DEER trace that has been measured in the course of this study. Theoretically, the modulation depth and the background density should lie on a line through the origin. This is in fact roughly the case. The determination of the background density k seems to give a rather large error, which causes the deviations from the expected result. The fitted line has a slope of 3.43 µs and an x-axis distance of -0.06.

~~S18~~S20 Background ~~of diluted sample with 30 µM ligand concentration~~decay of the DEER traces

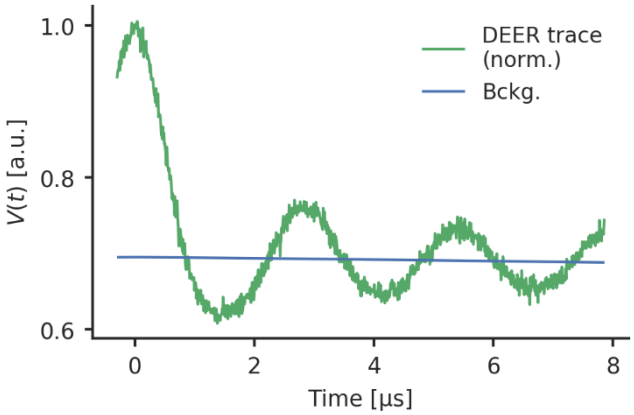

~~**Figure S12:** The (normalised) raw data of the sample with a ligand concentration of 30 µM spin concentration and rectangular pulses. It can be seen that there is almost no background decay (blue).~~

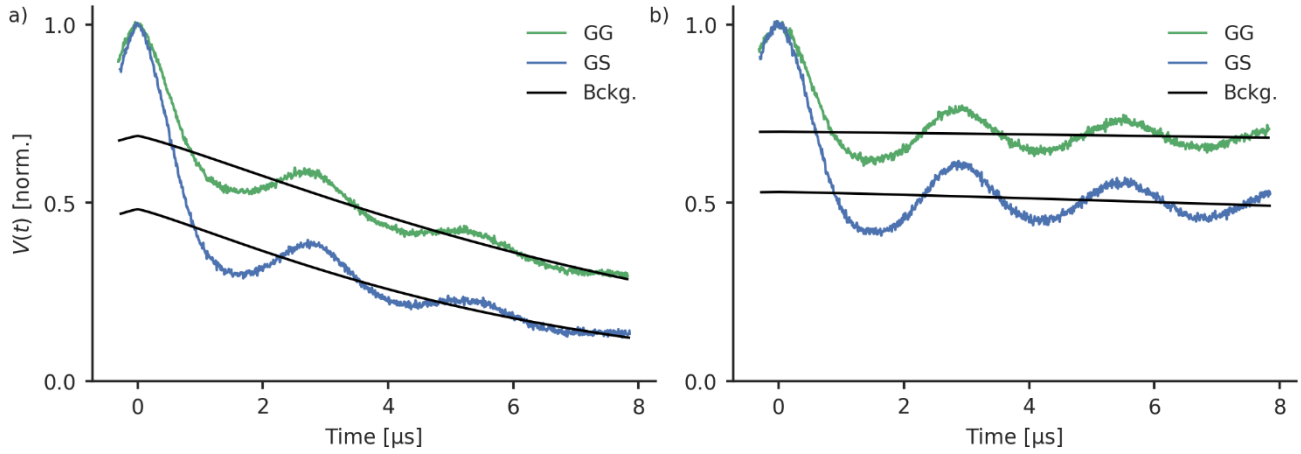

Figure S17: The (normalised) experimental raw data of the sample with a 80 µM (a) and 30 µM (b) ligand concentration. The settings for GG (green) were performed with a 100 %pulse amplitude and a 70 MHz offset. For GS (blue), the observer pulses were at a frequency of 70 MHz offset from the centre of the resonator. The pump pulses were HS{1,1} pulses, with the parameters $\beta = 8/t_p$, $t_p = 100$ ns, $\Delta f = 110$ MHz and an offset from the observer pulse of 90 MHz. Note that the acquisition time for the sample with lower concentration was longer in order to reach a similar noise level for both cases. The corresponding form factors are depicted in Fig. S11.

S21 Calculation of the background-dependent performance of broadband shaped pulses

To ~~quantify~~estimate the ~~effect~~influence of ~~the~~ broadband shaped pulses ~~on the background decay~~for different maximum distances and concentrations, we performed some analytical calculations. The background decay reduces the echo-intensity and therefore decreases the signal-to-noise ratio towards the end of the DEER trace. Whereas the measured trace $V(t)$ has a constant noise level σ_0, the background corrected form factor has an increasing noise level towards the end:

$$\sigma(t) = \sigma_0 \exp(kt),$$

(~~1~~2)

where $\sigma(t)$ is the noise of the form factor and k is the background ~~decay factor~~density. Here, we assumed a 3D background. As discussed in the main text, the form factor is truncated at a time $t_{\text{truncation}}$ to exclude the later part. An integration from $t = 0$ to $t = \tau_{\text{truncation}}$, with $\tau_{\text{truncation}}$ as the dipolar evolution time, yields the average noise in the form factor

$$\sqrt{<\sigma^2>} = \sigma_0 \sqrt{\frac{1}{2k\tau_{\text{truncation}}}(\exp(2k\tau_{\text{truncation}}) - 1)}.$$

(~~2~~3)

The modulation-to-noise (MNR) as the ratio of the modulation depth λ and the average noise is then described by:

$$\mathrm{MNR} = \frac{\lambda}{\sigma_0}\sqrt{\frac{2k\tau_{\mathrm{truncation}}}{\exp(2k\tau_{\mathrm{truncation}})-1}}.$$

(~~3~~4)

As both the modulation depth λ and the background density k directly depend on the inversion efficiency, a linear dependence can be expected between them. Indeed, we experimentally found an approximately linear correlation between them (Fig. ~~S11~~S16). Whereas the η_{2P} value captures a decrease in echo intensity it will miss the effect of a larger background decay. We chose exemplary parameters that resembled our experimental findings. For the modulation depth, we assumed an increase from 30 % to 50 ~~%.~~%, which corresponds to the modulation depths that we found for rectangular and the best HS{1,1} pump pulse. For the density of the background we assumed an increase about the same factor: $k_{\mathrm{S}} = \frac{5}{3}k_{\mathrm{R}}$ with k_{S} as the background density for the broadband shaped pulse and k_{R} as the background density for the rectangular ~~pulse. According to equation (4~~pulses. As the sample with a concentration of 80 µM of doubly-labelled ligand had a background density k_{R} of approximately 0.1 with rectangular pulses, we tested k_{R} –values from 0 to 0.15 1/µs to keep it in a realistic range. According to equation (5) this will give an MNR increase of

$$\mathrm{MNR}_{\mathrm{increase}} = \frac{5}{3}\sqrt{\frac{5\,(\exp(2\mathrm{k_R}\tau_{\mathrm{truncation}})-1)}{3\,(\exp\left(\frac{10}{3}\mathrm{k_R}\tau_{\mathrm{truncation}}\right)-1)}}.$$

(~~4~~5)

~~The heat map in Fig. S13 gives the result of this equation for different values of k_{R} and $\tau_{\mathrm{truncation}}$.~~

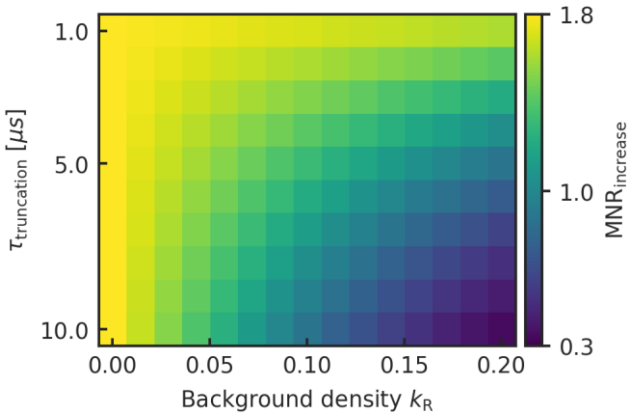

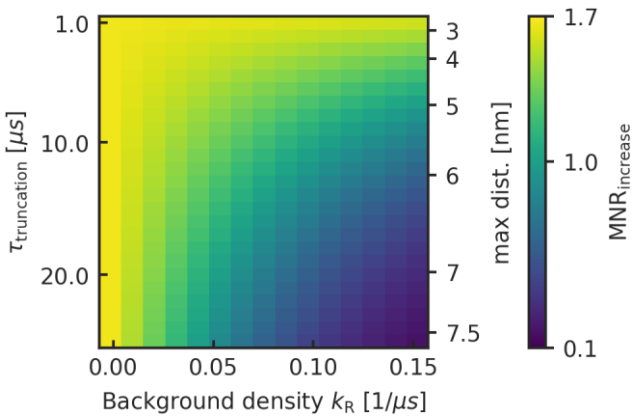

Figure ~~S13~~S18: The MNR-ratio of adiabatic and rectangular pulses as a function of the background density (with rectangular pulses) and the $\tau_{truncation}$ ~~time.~~time. The corresponding maximum distance according to equation (13) of the main text is also depicted. As the background density reflects the concentration the x-axis is a measure for the concentration of the spin centres. In our sample with 80 µM, we had a background density k_R of 0.1 with rectangular pulses.

~~Our results hint that the performance of shaped pulses can heavily depend on the circumstances of the measurement. For long traces and high concentrations, where a strong background decay has to be expected, broadband shaped pulses can further increase this decay and therefore increase the noise level. For short traces and low concentration on the other hand the increase in modulation depth due to broadband shaped pulses outperform the steeper background decay. Note that for our measurements, we typically had a k_R of about 0.1 at a concentration of 80 µM with rectangular pulses. This means that a value of 0.2 would correspond to a concentration of 160 µM which is a lot larger than what is needed for most practical applications (Jeschke, 2012). This means that in all relevant cases a sensitivity increase can be expected when broadband shaped pulses are used. Particularly, broadband shaped pulses perform better for lower concentrations and for shorter distances who allow to pick a shorter dipolar evolution time. For practical applications, a sensitivity increase due to adiabatic pulses is mostly desirable for samples with large distances and low concentrations who typically suffer the most from a low sensitivity. Our results hint that whereas for small concentrations a MNR improvement owing to broadband shaped pulses can be expected, however, this increase gets worse for longer dipolar evolution times.~~

Figure S18 shows that the performance of shaped pulses can heavily depend on the circumstances of the measurement. For a maximum distance below 4 nm ($\tau_{truncation} \approx 5$ µs), a MNR increase can be expected for all realistic concentration ranges. This is not the case if a longer distance shall be detected. For maximum distances around 5 nm, the MNR increase goes to 1 for high background densities of $k_R = 0.15$ 1/µs, which corresponds to very high concentrations > 100 µM. Typical concentrations for DEER measurements are around 50 µM, which here corresponds to a $k_R \approx 0.06$ 1/µs. For this concentration, a significant increase in the MNR can only be expected up to a truncation time of $\tau_{truncation} = 10$ µs, which is equal to a maximum distance of approximately 6 nm.

As broadband shaped pulses are particularly interesting for long distances, the calculations were performed up to a rather long truncation time of 25 µs (maximum distance of approximately 7.5 nm). For distances in the range > 6 nm, only with concentrations in the range of 10-30 µM ($k_R \approx 0.01$-0.04 1/µs) a significant increase in the MNR due to broadband shaped pump pulses can be expected. The MNR increase drops quickly when higher concentrations are used. For a maximum distance of 7.5 nm and for concentrations over approximately 40 µM no increase can be expected any more due to broadband shaped pulses. If a concentration of 80 µM is used, the MNR is about to decrease to roughly 40 % when switching to broadband shaped pulses. It is known that diluting the sample is favourable if long distances shall be detected because it increases the phase memory time of the echo (Schmidt et al., 2016). When broadband shaped pump pulses, the higher background decay adds an additional point for carefully choosing the concentration of the sample and it seems to be advisable to avoid high concentrations.

S22 Comparison of the resonator profiles

Figure ~~S14~~S19 shows the resonator profiles of the measurement of the sample with the high and the low concentration. The B_1 strengths that have been achieved for the sample with the low concentration were a bit lower.

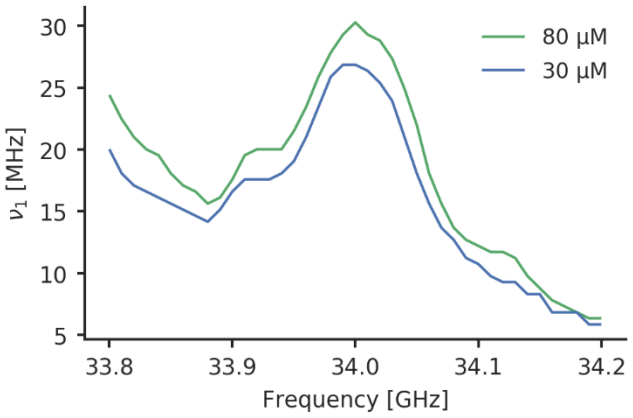

Figure ~~S14~~S19: Resonator profiles for samples with an 80 µM concentration (green) where all optimisation measurements have been performed and for the sample with a 30 µM concentration (blue).

S21 Supporting Information References

Doll, A. and Jeschke, G.: Fourier-transform electron spin resonance with bandwidth-compensated chirp pulses, J. Magn. Reson., 246, 18–26, doi:10.1016/j.jmr.2014.06.016, 2014.

Fábregas Ibáñez, L. and Jeschke, G.: Optimal background treatment in dipolar spectroscopy, Phys. Chem. Chem. Phys., 22(4), 1855–1868, doi:10.1039/C9CP06111H, 2020.

Jeschke, G.: DEER Distance Measurements on Proteins, Annu. Rev. Phys. Chem., 63(1), 419–446, doi:10.1146/annurev-physchem-032511-143716, 2012.

Jeschke, G., Chechik, V., Ionita, P., Godt, A., Zimmermann, H., Banham, J., Timmel, C. R., Hilger, D. and Jung, H.: DeerAnalysis2006—a comprehensive software package for analyzing pulsed ELDOR data, Appl. Magn. Reson., 30(3), 473–498, doi:10.1007/BF03166213, 2006.

Schmidt, T., Wälti, M. A., Baber, J. L., Hustedt, E. J. and Clore, G. M.: Long Distance Measurements up to 160 Å in the GroEL Tetradecamer Using Q-Band DEER EPR Spectroscopy, Angew. Chem. Int. Ed., 55(51), 15905–15909, doi:10.1002/anie.201609617, 2016.

Stoll, S. and Schweiger, A.: EasySpin, a comprehensive software package for spectral simulation and analysis in EPR, J. Magn. Reson., 178(1), 42–55, doi:10.1016/j.jmr.2005.08.013, 2006.

Tait, C. E. and Stoll, S.: Coherent pump pulses in Double Electron Electron Resonance spectroscopy, Phys. Chem. Chem. Phys., 18(27), 18470–18485, doi:10.1039/C6CP03555H, 2016.